**PAUL SCHERRER INSTITUT**

PSI

Laboratory for Electrochemistry

Annual Report 2002

http://ecl.web.psi.ch

Cover Photo
Enlargement of a 10 x 10 x 2 mm
platinum electrode inserted in a Kel-F
holder and the hanging electrolyte
meniscus. The main advantage of this
arrangement for electroanalytical
measurements is that it allows
easy handling of the electrode for
different treatments.

PAUL SCHERRER INSTITUT

Laboratory for Electrochemistry

Annual Report 2002

With excerpts from the 2002 Annual Scientific Report of
the PSI Research Department General Energy (ENE)

TABLE OF CONTENTS

EDITORIAL

Günther G. Scherer

The Electrochemistry Laboratory is dedicated to research in various areas of advanced electrochemical energy storage and conversion processes. In addition, the Electrochemistry Laboratory provides expertise and innovative solutions in the fields of batteries, fuel cells, supercapacitors, electrolysis, electrocatalysis, electrochemical material science, and modern methods for electrochemical interface analysis. With this particular research effort Paul Scherrer Institut's Electrochemistry Laboratory, as the leading institution in this area in Switzerland, will contribute to the long term development of zero emission converters and energy storage systems in the context of a sustainable development.

Currently, the laboratory is organized into the following six research groups: Fuel Cells (G.G. Scherer), Fuel Cell Systems (F. Büchi), Batteries (P. Novak), Capacitors (R. Kötz), Materials I (T. Lippert), Materials II (HP Brack). Within this Annual Report each of the research groups is represented by several contributions, highlighting their research efforts and their results of the past year.

The successful operation of a fuel cell – supercapacitor hybrid power train in a VW Bora passenger car has demonstrated the potential of the laboratory to conduct research at the utmost forefront in this area while leading a team of collaborators including partners from academia and industry. Results on the development of components for this power train where described in the Scientific Report of 2001, now results concerning the automobile in operation either "on the street" or under the test conditions of a driving cycle on a dynamic test bench are presented. The results described give convincing proves of the energy saving potential of this power train configuration.

The know-how in polymer electrolyte fuel cells and supercapacitors, built up in the past over several years, laid the sound basis to carry out the above described car project. As can be seen from the various contributions in these two areas, we still continue to broaden and deepen our knowledge in these areas. Concerning polymer electrolyte fuel cells, various aspects of electrocatalysis, proton-conducting polymers, novel aspects of cell design including modelling, *in situ* diagnostic methods, and stack development were in the continuous focus of our research efforts. Concerning supercapacitors, our research efforts concentrate on the characterization and modification of highly porous carbon materials and the understanding of the fundamentals of the electrochemical double layer on these materials.

The lithium-ion battery is a most promising candidate for numerous applications of electrochemical power sources. Considerable progress could be achieved in materials development projects in collaboration with industrial partners in this research area. Among others, carbon electrodes developed in house for high current density discharge (10C) could be demonstrated. Further, new electrolyte compositions were evaluated which lead to advantages in the production process of the battery and in an extended temperature window of battery operation. Finally, with an industrial partner, two patent applications concerning a new ceramic separator for lithium-ion batteries were filed.

Many of our projects are materials development oriented. Surface, interface, and interphase aspects of materials play an important role, according to the processes occurring in electrochemical conversion and storage systems. Emphasis is also given to develop the necessary tools of thin film preparation, surface modification, and surface analysis. These tools are applied to a vast variety of materials, among others to polymers and glasses for non-electrochemical applications.

Communication to our partners in research projects, within the Paul Scherrer Institut, and to the scientific community outside of PSI is of utmost importance to us. For this reason, the laboratory organized four successful events with international participation. On January 23, a scientific colloquium was held to honour Dr. Otto Haas on the occasion of his 60th birthday (see separate page). On June 11 and 12 a workshop on *Modelling of the Polymer Electrolyte Fuel Cell* jointly organized by PSI, Research Center Jülich, and Imperial College London took place at PSI. Further, in a successful tradition we continued our series of Electrochemistry One-Day Symposia at PSI with the topic of *Carbons in Electrochemical Systems*. The international participation gave proof that a relevant theme of modern electrochemistry was chosen. Finally, together with our Research Department General Energy and our Laboratory for Combustion Research we organized the 3rd International Meeting in our series Energy Technologies for a Sustainable Future (ETSF3, November 29 at PSI), addressing the topic *Fuel Cells and Combustion Engines in Competition for the Future*.

Many of our current projects will continue and some new will be started in the course of the year 2003. Collaboration with industry is expressed in many projects. This gives us great confidence to further contribute successfully to the field of Electrochemistry and transfer our know-how to industrial partners as well as to support education of students in these areas in the wider context of a sustainable energy development.

OTTO HAAS
60TH BIRTHDAY, JANUARY 23, 2002

Elisabeth and Otto Haas

On the occasion of his 60th birthday, January 23, 2002, a scientific colloquium was held to honour Dr. Otto Haas. Dr. Haas had served as the head of the laboratory for many years and until the end of 2001. During this time, he guided the development of the laboratory from a "single person enterprise" to its current state as an internationally recognized landmark in electrochemistry.

**SCIENTIFIC CONTRIBUTIONS FROM
THE LABORATORY FOR ELECTROCHEMISTRY
FOR THE PSI SCIENTIFIC REPORT 2002
VOLUME V, GENERAL ENERGY**

HARD CARBON AS ANODE MATERIAL IN LITHIUM BATTERIES: SYNTHESIS AND CHARACTERIZATION

M.C. Baertsch, L. Schmid (ETH Zürich), A. Baiker (ETHZ), P. Novák

Hard carbon is a possible alternative as negative electrode material for rechargeable lithium-ion batteries. A fast production of hard carbon can be reached if the curing time of the precursor is short. Due to the promising results from literature regarding epoxy resin as precursor we produced hard carbon from a commercially available fast-setting epoxy resin. The surface area and pore structure properties of the carbon powder were investigated with gas adsorption methods. The carbon particle size distribution was analysed with a laser diffraction instrument.

1 INTRODUCTION

Modern electronic devices, like laptops, digital cameras and mobile phones, demand more and more energy and power. At the same time electronic devices are getting smaller and smaller in size. This signifies that the power and energy density of the current sources will be a key factor of choice of the future energy sources. In comparison to other rechargeable batteries, the lithium-ion battery stands out because it possesses excellent specific energy and power and shows good cycling stability. These crucial properties are the reason why rechargeable lithium-ion batteries are the leading power source in laptops.

In today's commercially available secondary lithium-ion batteries, one of the main negative electrode materials is graphite. The development of graphites has been so successful that long-term cycleability near the theoretical specific energy limit of 372 Ah/kg has been achieved. This means that scientists have to look for alternative electrode materials if higher specific energies are demanded. One alternative is hard carbon which consists of a porous non-graphitisable carbon structure. First experiments with hard carbons, showing the suitability of this kind of carbon as negative electrode material, go back to the early nineties [1,2]. Dahn and co-workers obtained first cycle specific capacities of more than 500 Ah/kg using epoxy resin as precursor [3]. To minimise the time consuming curing process of a standard epoxy resin we tested a fast-setting one as precursor.

2 EXPERIMENTAL

The fast-setting, paste-like two component epoxy resin AW 2101 was purchased from Ciba (Switzerland). The two components (resin and hardener) were thoroughly mixed in equal amounts (volume or weight) and distributed as a 300 μm layer onto a Teflon surface within five minutes after mixing. The curing took about two hours at ambient temperature. The cured epoxy layer was then cut into small pieces and 5 g amounts were pyrolysed under argon gas in a special furnace. The heating rate was 5 °C/min and the final temperature (700 °C, 750 °C, 800 °C and 850 °C) was maintained for two hours. The furnace was opened when the temperature was below 100 °C. The pyrolysed epoxy pieces were ground in a planetary ball mill to a fine black or dark grey carbon powder.

The particle size distribution was analysed with a Horiba LA-500 laser diffraction instrument using a He-Ne laser as the light source. The measurable particle size range lies between 0.1 and 200 μm. Only a few milligrams of hard carbon powder were necessary to measure the particle size distribution. The surface area and pore structure properties were determined with gas adsorption methods like adsorption and desorption isotherms, BET theory and BJH calculation. The measurements were performed with a Micromeritics ASAP 2010 instrument. In order to guarantee the reproducibility of the measurements the samples had to be evacuated over night at 250 °C until the pressure fell below 6 μmHg.

3 RESULTS

After pyrolysis the particle size shape of the hard carbon is too irregular to be used as electrode material. After dry milling in the planetry ball mill the carbon powder has a defined size distribution appropriate to optimal electrolyte wetting. Figure 1 shows the typical partical size distribution of the hard carbon after milling.
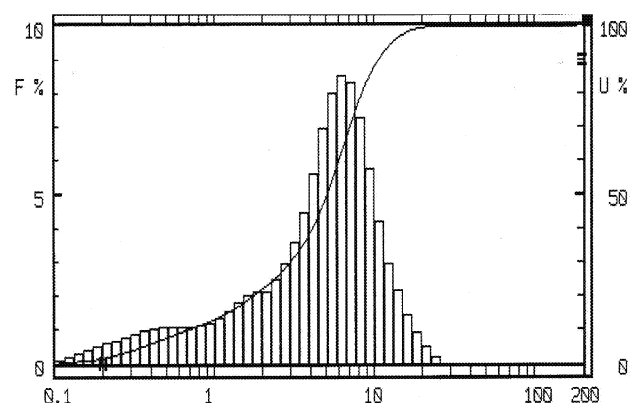
Fig. 1: Fraction (%) vs. diameter (μm) plot of hard carbon particles after milling. Fast-setting epoxy resin was used as the precursor for the hard carbon.

Most of the carbon particles have diameter between 2 and 20 μm. The highest fraction of particles has a diameter of 7 μm. The distribution does not show a Gauss curve because of the large amount of particles smaller than 2 μm.

The surface area of the four samples heat treated at 700 °C, 750 °C, 800 °C and 850 °C was measured using the (nitrogen) gas adsorption method (BET-method). The surface area of the first three samples yields 77 m^2/g, 45 m^2/g and 18 m^2/g, respectively. Contrary to the trend, the 850 °C sample shows a value of 38 m^2/g.

The analysis of the adsorption and desorption isotherms allows the interpretation of the pore distribution of the hard carbon powder.
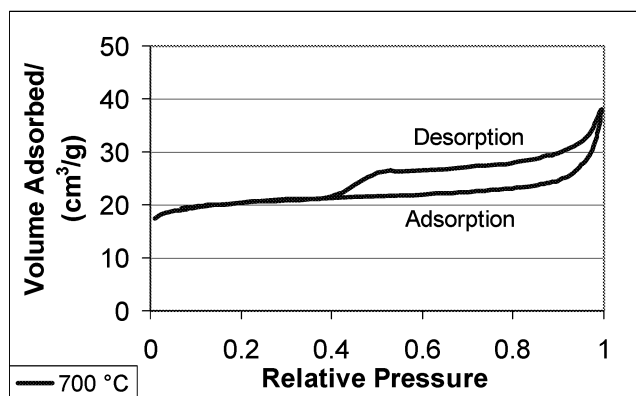
Fig. 2: Adsorption and desorption isotherms of the epoxy sample heat treated at 700 °C.
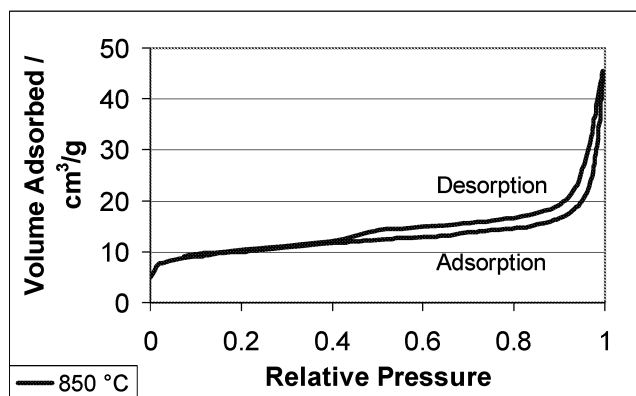
Fig. 3: Adsorption and desorption isotherms of the epoxy sample heat treated at 850 °C.

Adsorption isotherms generally follow one of six forms [4]. The flat adsorption isotherms in Figure 2 and 3 are characteristic of an adsorbent having extremely small pores (micropores). Nevertheless, the hysteresis loop resulting from the non-congruent trace of adsoption and desorption isotherm indicates that the carbon powder also possesses pores in the mesopore and macropore range. The flat adsorption curve of the 700 °C sample shows a much higher amount of adsorbed nitrogen gas than the 850 °C sample. This fact is in agreement with the BET results. The reason of the decreasing amount of adsorbed gas with higher heat treatment temperatures is due to the change from open to closed pores.

Figure 4 shows the pore size distribution of the 700 °C and 850 °C samples. The calculation is based on the BJH method [5], which uses the Kelvin equation on the assumption of a straight cylindrical pore model. The BJH method is only valid for mesopores and macropores, i.e. interpretations of the pore distribution below 2 nm are not possible. The two curves show the same shape below 20 nm but differ clearly in the macropore region. One possible explanation could be that a slight activation of the sample occurred due to the non-perfect sealing ring in the pyrolysis furnace (diffusion of oxygen).
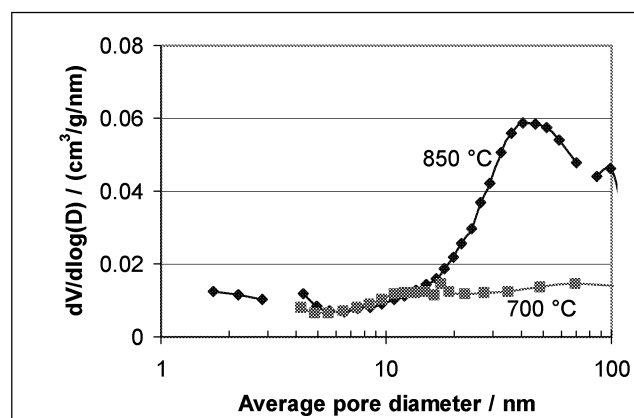
Fig. 4: Pore size distribution of the samples heat treated at 700 °C and 850 °C.

4 CONCLUSION

Fast-setting epoxy resin precursor is a good alternative for the fast production of carbon as negative electrode material. The nitrogen gas adsorption measurements show that the hard carbon powder consists not only of micropores but also of mesopores and macropores. The higher heat treatment temperature seems to favour the macropores at the expense of the micropores. Electrochemical experiments will definitely show whether the fast-setting epoxy resin is suitable for future application in lithium-ion batteries.

5 REFERENCES

[1] A. Omaru et al., ECS Meeting Abstracts **92-2**, 34 (1992).

[2] S. Yata et al., Synth. Met. **62**, 153 (1994).

[3] J.R. Dahn et al., Carbon **34**, 193 (1996).

[4] P.A. Webb and C. Orr, Analytical Methods in Fine Particle Technology, ISBN 0-9656783-0-X

[5] E.P. Barrett et al., J. Am. Chem. Soc. **73**, 373 (1951).

THE INFLUENCE OF GRAPHITE SURFACE MODIFICATION ON THE EXFOLIATION DURING ELECTROCHEMICAL LITHIUM INSERTION

H. Buqa, D. Goers, L. Hardwick, M.E. Spahr (TIMCAL SA), P. Novák

For graphites as negative electrode materials in lithium ion batteries, the chemistry and morphology of their surface play a major role in chemical and electrochemical reactivity and interaction with the solid electrolyte interphase (SEI). To understand more about the key material parameters influencing the electrochemical performance of highly crystalline graphites, the synthetic TIMREX® SLX 50 graphite was modified and the influence on its electrochemical lithium insertion properties was studied.

1 INTRODUCTION

Graphitic carbons are the first choice as negative electrode materials in lithium-ion cells for the reasons of performance and cost. It is now well known that in lithium-ion cells a protective thin solid film called the Solid Electrolyte Interphase (SEI) always covers the carbon surface [1]. The SEI formation mechanism is rather complex and not yet completely understood. Lithium ions are consumed for the formation of this protective film. This decreases the maximum possible charge and energy density of the battery. Thus, losses have to be minimized [2, 3]. In order to obtain the most effective SEI formation, the graphite material must be carefully selected and its surface morphology should be optimised. It is also necessary to understand the individual influence of structural defects (rhomboedral stacking faults) and surface defects on the irreversible capacity. The identification of the material parameters, that have roles in the SEI formation, will be an important development for facilitating further improvements of carbon negative electrode materials for lithium ion batteries.

In this contribution, we report on the effects of graphite surface modification on its exfoliation (i.e., on the irreversible lithium consumption) during electrochemical lithium intercalation into the graphite electrode. The surface of graphite particles can be modified by, e.g., heat treatment and/or oxidation. For the best negative electrode performances, heat treatment conditions have to be carefully selected with respect to the electrochemical behaviour of graphite.

2 EXPERIMENTAL

The oxidation of graphite material (TIMREX® SLX 50, TIMCAL SA, Bodio) was performed for one hour at different temperatures using a muffle furnace (Nabertherm, Switzerland AG). The stream of dry air over the sample (about 5 g) was set to 100 l/h, and the heating rate 20 °C/min. The reaction time was 1 hour.

Electrochemical charge/discharge measurements were carried out at 25 °C in a temperature controlled box in laboratory cells described elsewhere [4]. Metallic lithium was used as the reference and counter electrode. 1 M $LiPF_6$ in DMC/EC 1:1 (w/w) (E. Merck, Darmstadt, Germany) was used as the electrolyte solution. The graphite electrodes were prepared by blade coating of the graphite materials on to a copper foil current collector. PVDF was used as binder material. For the galvanostatic electrochemical charge/discharge measurements we chose relatively low cur-

rent densities of 10 mA/g of carbon to complete the solid electrolyte interphase formation in the first Li^+ insertion cycle. After a potential of 5 mV vs. Li/Li^+ was reached in the first galvanostatic Li^+ insertion, the discharging was continued potentiostatically until the specific current dropped below 5 mA/g.

The graphite was characterised by scanning electron microscopy (SEM), X-ray diffraction (XRD) and Raman spectroscopy. The XRD and Raman spectroscopy studies of these graphite materials will be presented in a different paper contained in this Scientific Report by D. Goers et al. [5].

3 RESULTS

Figure 1 shows a more detailed study of the treatment temperature applied to a TIMREX® SLX 50 graphite material. The Figure highlights where the critical temperature which leads to the deterioration of the electrochemical insertion properties occurs.
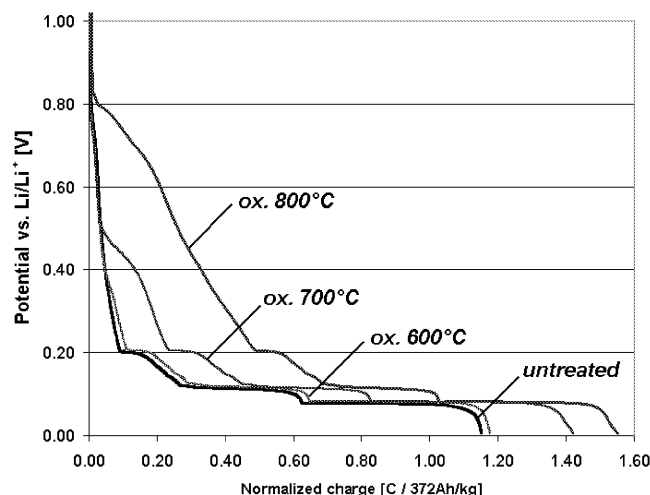
Fig. 1: First electrochemical insertion of Li^+ in TIMREX® SLX 50 graphite before and after oxidation in air at different temperatures.

The potential plateau at 0.45 V vs. Li/Li^+ describes the electrochemical exfoliation of the graphite structure. During the exfoliation process of the graphite electrode, the electrode surface area increases. The SEI-layer must be formed on a larger surface area compared to the non-exfoliated electrode which explains the significant increase of the irreversible capacity during the exfoliation process.

The exfoliation of the graphite structure during electrochemical lithium intercalation, strongly depends on

the oxidation temperature. At 700 °C, the characteristic potential plateau at about 0.45 V *vs.* Li/Li$^+$ could be observed in galvanostatic Li$^+$ insertion experiments using a 1 *M* LiPF$_6$ EC/DMC 1:1 (w/w) electrolyte. This plateau increased in size and plateau potential (0.8 V *vs.* Li/Li$^+$) when the temperature was further increased at to 800 °C. A negative electrode, which consisted of a graphite material treated at lower temperatures, did not show this potential plateau.

From the electrochemical we conclude that the oxidation treatment of graphite can result in different anode performance in terms of graphite exfoliation. The oxidation temperature has an influence on the electrochemical properties, particularly on the formation of the SEI layer.
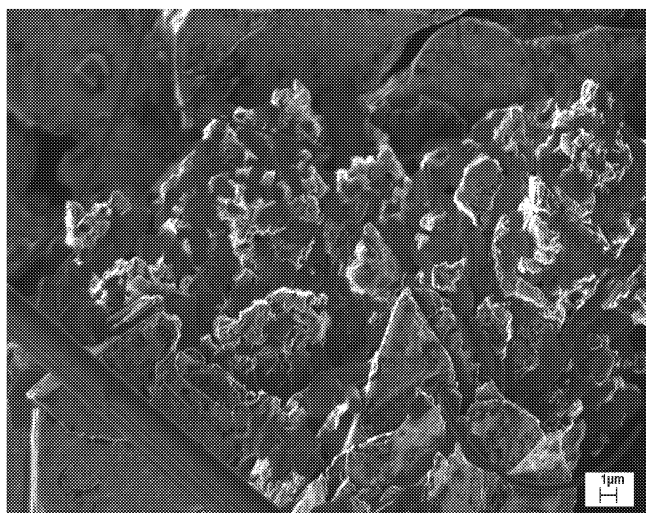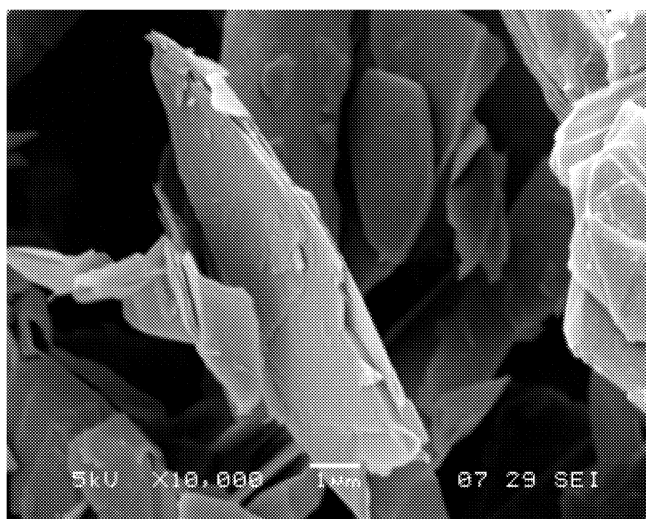
Fig. 2: SEM pictures of untreated TIMREX® SLX 50 graphite (top) and oxidised SLX 50 graphite at 800 °C (1h) and subsequently stabilized potentiostatically at 0.3 V *vs.* Li/Li$^+$ (bottom).

Figure 2 (top) shows, as an example, the SEM picture of untreated TIMREX® SLX 50 graphite powder. To further investigate the origin of the potential plateau, we performed *post-mortem* SEM studies of oxidised SLX 50 graphite at 800 °C electrodes which were galvanostatically discharged to 0.3 V *vs.* Li/Li$^+$ and

subsequently stabilized potentiostatically at this potential. The same cells were used for the scanning electron microscopy studies. The cells were dismantled, the negative electrodes were washed thoroughly with DMC and dried in argon.

The *post-mortem* SEM - analysis is presented in Figure 2 (bottom). From the SEM picture, exfoliation of the graphene layers could not be clearly observed. The X-ray diffraction patterns of the graphite materials indicated no significant change of the crystallinity and texture of the graphite during oxidation up to 800 °C (see D. Goers et al. [5]). The graphite crystal structure, i.e., the amount of rhombohedral stacking faults does not show a direct influence on the electrochemical phenomenon of graphite exfoliation. Surface defects, superficial disordered carbon or the crystallinity near the graphite surface do not seem to be responsible for an effective SEI-formation, which avoids the graphite exfoliation in ethylene-carbonate based electrolyte. No significant change of the graphite surface areas could be also detected up to this temperature. Due to very low oxygen concentration on the graphite surface, it is difficult to apply even modern surface analytical methods (e.g. DRIFT, XPS) on graphite materials to detect changes of the surface functional groups which could explain the electrochemical behavior of the of the heat-treated graphite before and after the extended exposure to air [6]. Therefore, we assume that the treatments affected the surface morphology and surface chemistry of the graphite and, thus, influenced its electrochemical properties.

The only factors which decide whether or not the quality of the SEI-layer is sufficient to suppress the exfoliation of graphene layers during the electrochemical insertion of lithium ions into the graphite, are the surface chemistry of the graphite and the choice of electrolyte solution.

4 ACKNOWLEDGEMENT

5 REFERENCES

[1] M. Winter, J. O. Besenhard, M. E. Spahr, P. Novák, Adv. Mater. **10**, 725 (1998).

[2] M. E. Spahr, H. Wilhelm, F. Joho, J.-C. Panitz, J. Wambach, P. Novák, N. Dupont-Pavlovsky, J. Electrochem. Soc., in press (2002).

[3] H. Buqa, P. Golob, M. Winter, J. O. Besenhard, J. Power Sources **97-98**, 122 (2001).

[4] F. Joho, B. Rykart, A. Blome, P. Novák, H. Wilhelm, M. E. Spahr, J. Power Sources **97-98**, 78 (2001).

[5] D. Goers, H. Buqa, L. Hardwick, A. Würsig, P. Novák, PSI Scientific Report 2002, **V**, 69-70 (2003).

[6] H. P. Boehm, Carbon **40**, 145, (2002).

SYSTEMATIC INVESTIGATIONS ON ACYCLIC ORGANIC CARBONATE SOLVENTS FOR LITHIUM-ION BATTERIES

J. Vetter, S. Peter, P. Novák

Electrochemical cycling tests on cells with graphite electrodes and several alkyl methyl carbonates were performed. Experiments with mixed binary solvent electrolytes with ethylene carbonate (EC) showed that the alkyl methyl carbonates $H_3CO(CO)O(CH_2)_nH$ (n = 3–5) are suitable as co-solvents in lithium-ion batteries. Ternary mixtures of EC, BMC, and propylene carbonate (PC) showed better overall performances than EC/PC electrolytes. The branched isobutyl methyl carbonate (i-BMC) outperforms its linear isomer (BMC) in terms of electrochemical performance. $LiPF_6$ is superior to $LiClO_4$ as conducting salt in both EC/BMC and EC/i-BMC mixtures in terms of electrolyte conductivity, rate capability, and cycling stability.

1   INTRODUCTION

State-of-the-art lithium-ion batteries consist of a carbon-based negative electrode, a positive lithium metal mixed oxide electrode, and a separator soaked in an organic electrolyte. The electrolyte is usually composed of a lithium salt dissolved in an organic solvent mixture. Among the solvents used is a variety of cyclic and non-cyclic carbonates. Since these solvents are not thermodynamically stable at the potential of metallic lithium or lithiated carbon, they decompose during the first charge/discharge cycles. On the surface of the negative electrode, they form an electrically insulating, lithium-ion conducting protective film, called the solid electrolyte interphase (SEI). The stability of the SEI is essential for safe and effective functioning of the whole battery. Since the formation of the SEI is associated with irreversible charge consumption, which lowers the usable charge density of the cell, a quick and charge-effective formation, along with a good long-term stability of the SEI is desirable.

Since the SEI is built up of decomposition products of the electrolyte, the performance of the cell depends to a great extent on the composition of the electrolyte solution and the electrochemical behaviour of every single electrolyte component. Nevertheless, since only a few of the compounds of interest are commercially available, systematic investigations on the topic have seldom been made.

In this paper we report on a systematic study of the electrochemical behaviour of some compounds of the homologous series of the alkyl methyl carbonates of interest for lithium-ion batteries, both as single solvents and co-solvents in binary and ternary mixtures with EC and PC. Electrochemical cycling experiments have been performed to compare the first cycle irreversible charge capacity and long-term cycling stability of graphite electrodes in these various electrolytes.

2   EXPERIMENTAL

The organic carbonates butyl methyl carbonate (BMC), *iso*butyl methyl carbonate (*i*-BMC), and methyl pentyl carbonate (MPentC) were synthesized from the corresponding alcohols and methyl chloroformate. After purification, the compounds were obtained in high yield and purity (>99.5% GC). Together with commercially available methyl propyl carbonate

(MPC), the electrochemical behaviour of the compounds was investigated in half cells against lithium in mixtures with ethylene carbonate (EC) and propylene carbonate (PC). $LiClO_4$ or $LiPF_6$ served as conducting salts for the measurements.

3   RESULTS

For a given graphite and salt, the quality of the SEI formed during the first cycles depends mainly on the composition of the solvent mixture and its electrochemical behaviour. Ethylene carbonate (EC) is known as a good film-forming compound, while propylene carbonate (PC), shows a rather poor behaviour, especially with most synthetic graphites in the carbon electrode. Unfortunately, EC cannot be used as a single solvent for room temperature applications due to its high freezing point of 36°C. It has to be mixed with some co-solvents to ensure sufficient low-temperature electrolyte conductivity. Among the co-solvents tested for the purpose, non-cyclic organic carbonates have shown the best performance to date.

Various binary mixtures of the non-cyclic carbonates with ethylene carbonate (EC) were investigated to find the best carbonate and an optimum composition. Mixtures with an EC content of 50, 40, and 20 wt.% and 1M $LiClO_4$ as the conducting salt were tested. The results are shown in Figure 1 and summarized in table 1. Data are also given for EC/diethyl carbonate (DEC) mixtures as a reference.
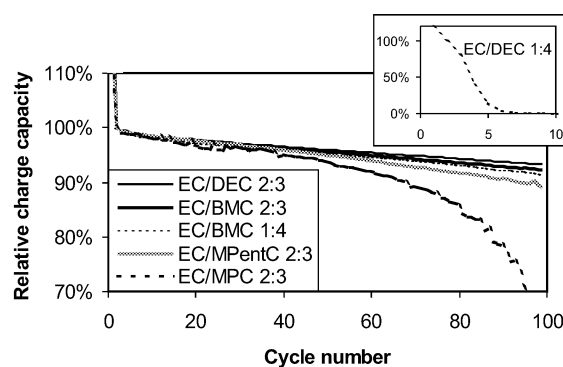
Fig. 1: Cycling behaviour of graphite electrodes in cells with alkyl methyl carbonate / EC mixtures), normalized to the 3rd cycle charge capacity (1M $LiClO_4$, natural graphite vs. Li metal).

Despite the still high charge capacity, mixtures of MPC and MPentC with EC build up high internal resistances upon prolonged cycling leading to slow lithium insertion into the graphite. Figure 1 gives the cycling data normalized to the second cycle to eliminate differences in 1st cycle charge losses. Since all 1:1 mixtures behave virtually the same in this graph, data are shown for lower EC content only.

EC/	DEC	MPC	BMC	*i*-BMC	MPentC
1:1 50%	16.5%	17.2%	18.2%	18.5%	16.2%
2:3 40%	16.0%	14.8%	18.7%	17.0%	18.0%
1:4 20%	16.4%	12.8%	20.4%	21.2%	17.4%

Table 1: 1st cycle charge losses of graphite electrodes in binary mixtures of alkyl methyl carbonates with EC (1M LiClO$_4$, natural graphite vs. Li metal).

In mixtures containing BMC, as for DEC, sufficiently high reversible capacities can be obtained even after prolonged cycling (above 340 Ah/kg after 100 cycles), whereas a slow capacity fading is observed for both MPC and MPentC. Furthermore, while the mixed solvent EC/DEC 1:4 exhibits rapid capacity fading leading to premature cell death after only a few cycles (Figure 1, insert), both EC/BMC mixtures, 1:4 and 2:3 by weight, show high reversible capacities.

Based on the higher cycling rates in binary mixtures compared to the other solvents, BMC was chosen for further examination in ternary mixtures with EC and propylene carbonate (PC). Using natural graphite as intercalation material, for both EC/BMC 2:3 and all ternary EC/PC/BMC mixtures, 1st cycle charge losses are significantly lower than for EC/PC 2:3. Despite slightly higher fading rates in the subsequent cycles, the BMC containing mixtures still outperform EC/PC 2:3 in terms of overall charge capacity during the first 100 cycles (Figure 2).
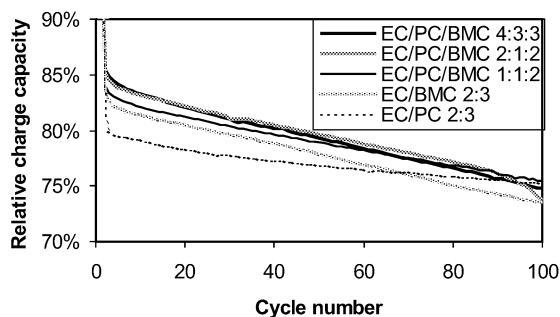
Fig. 2: Cycling behaviour (intercalation half-cycle) of graphite electrodes in various binary and ternary EC/PC/BMC mixtures (40 % EC content), normalized to the 1st cycle charge capacity (1M LiClO$_4$, natural graphite vs. Li metal).

In comparison of the linear compound BMC with its branched isomer *i*-BMC, a slightly lower conductivity is observed for solutions containing *i*-BMC. Despite this fact, in electrochemical cycling experiments EC/*i*-

BMC mixtures show a better performance than the corresponding EC/BMC mixtures in terms of cycling stability (Figure 3). Also, EC/*i*-BMC mixtures are less sensitive to the mixing ratio. This is especially the case with LiClO$_4$ as the conducting salt. In mixtures containing LiPF$_6$ the effect is much less noticeable.
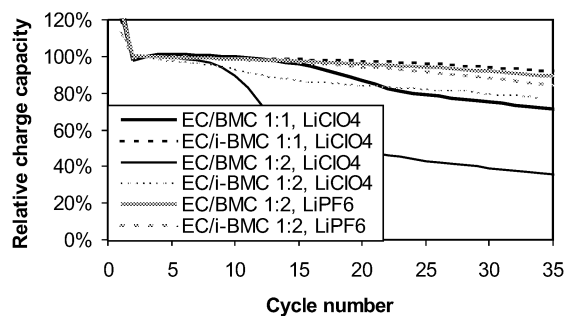
Fig. 3: Cycling behaviour of graphite electrodes in cells with EC/BMC and EC/*i*-BMC mixtures, with LiClO$_4$ or LiPF$_6$, normalized to the 3rd cycle charge capacity (1M solution, synthetic graphite vs. Li metal).

A closer investigation of the influence of the conductive salt shows that in mixtures containing LiPF$_6$ both EC/BMC and EC/*i*-BMC electrolytes have a performance close to that of commercially available electrolytes. With LiClO$_4$ as the conductive salt, a reduced cycleability is observed. The effect is larger with BMC, but still significant in the case of *i*-BMC (Figure 3).

In Figure 4, charge capacities during galvanostatic charging at C/5 rate ("galvanostatic charge") of cells with 1:1 mixtures and both conducting salts are plotted relative to the total charge capacity vs. cycle number. In this graph, a lower galvanostatic charge indicates slower kinetics of the lithium insertion into the graphite electrode due to higher SEI resistance and lower electrolyte conductivity. The results show a lower rate capability of cells with LiClO$_4$ as the conducting salt.
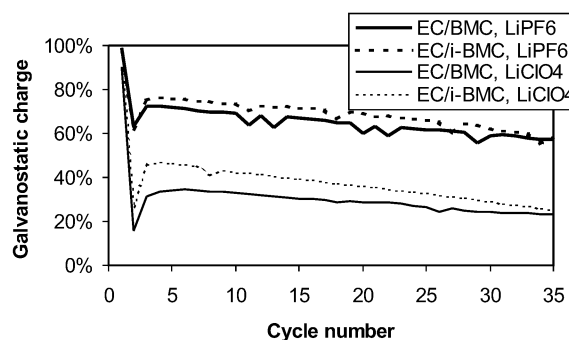
Fig. 4: Relative galvanostatic charge in various 1:1 solvent mixtures with two conductive salts (1M solutions, synthetic graphite vs. Li metal).

4 ACKNOWLEDGEMENTS

ANALYTICAL INVESTIGATIONS ON THE SOLID ELECTROLYTE INTERPHASE (SEI) FILM ON GRAPHITE ELECTRODES IN LITHIUM-ION BATTERIES

J. Vetter, P. Novák

In order to investigate the organic decomposition products of the electrolyte forming the solid electrolyte interphase (SEI) on carbon electrodes in lithium-ion batteries, pre-cycled graphite electrodes were extracted. The extracts were analysed by gas chromatography (GC) and Fourier transform infrared spectroscopy (FTIR). A method for the separation of the compounds by high performance liquid chromatograpy (HPLC) was developed, and the SEI extracts were classified by comparison with reference substances. The results suggest that the SEI components have a molecular weight of several hundred mass units and a polyethylene oxide (PEO) like structure.

1 INTRODUCTION

The solid electrolyte interphase (SEI) layer, i.e., the passivation layer formed on the surface of the carbonaceous negative electrode material, is the key component in the negative electrode, determining the electrochemical performance and safety of the whole lithium-ion battery. Common models assume that the SEI is formed by electrolyte reduction during the first few lithium insertion/extraction cycles. But it is obvious from Figure 1 that the SEI formation is not completed before 20-40 deep cycles when the irreversible charge capacity reaches its final value.
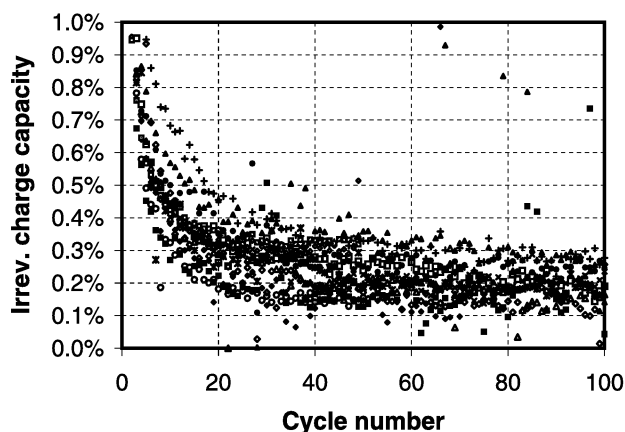
Fig. 1: Irreversible charge capacity for natural and synthetic graphites, vs. Li, in a number of carbonate electrolytes (salts $LiClO_4$ and $LiPF_6$, rates C/7-C/30).

A clear identification of all components of the SEI is an important factor for thorough understanding and further improvements of lithium-ion batteries. The SEI layer is considered to consist of decomposition products of salt and solvent, such as Li_2CO_3, LiF, lithium alkoxides, lithium alkyl carbonate, and polymers thereof. Models assume that the SEI is composed of two major constituents described as inorganic and organic interpenetrating layers. The composition of the inorganic layer is fairly well understood. But, after a decade of research, the understanding of the organic layer is still a challenge: the inevitable exposure of the SEI film to vacuum, which occurs when using common surface analytical methods, results in a loss of volatile (organic) components, shrinkage of the film, and even chemical changes.

Zhang et al. [1] hypothesized from ac impedance measurements that, in ethylene carbonate (EC) based electrolytes, the SEI formation takes place through two major stages. The first stage (before lithiation of graphite) is the formation of a loose, highly resistive film. The film formation proceeds via a nucleation and growth mechanism, as we have demonstrated by *in-situ* scanning probe microscopy [2]. According to Zhang et al. a stable and highly conductive SEI film is formed in the second stage. On a molecular level, this type of behaviour can be explained if we assume that a porous, rather thick, and insulating organic layer is formed first. Then, this organic layer rearranges and/or further reacts to a lithium-ion conducting, polyethylene oxide (PEO) like layer as suggested by Ogumi et al. [3].

2 EXPERIMENTAL

We have performed various analyses of the organic SEI constituent. First, standard graphite electrodes were charged and then discharged at a C/37 rate in cells with an EC/ DMC/$LiPF_6$ electrolyte (Merck, LP30) and a Li counter electrode. Then, the graphite electrodes were extracted using moist acetonitrile (AN), the SEI extract was concentrated, and analysed.

Various chromatographic and analytical methods were used to separate and identify the SEI compounds. Good results were obtained with FTIR, GC, and HPLC in combination with an evaporative light scattering detector (ELSD).

3 RESULTS

The FTIR spectra (Figure 2) revealed that, next to EC, there are SEI components in the extract. Signals attributed to SEI components are marked in the graph with an asterisk. Using *in-situ* mass spectrometry, ethylene and hydrogen were the only volatile components we detected during SEI formation. Gas chromatography analyses of the SEI extract confirmed that there are no volatile SEI components, i.e., no organic molecules with short chains.
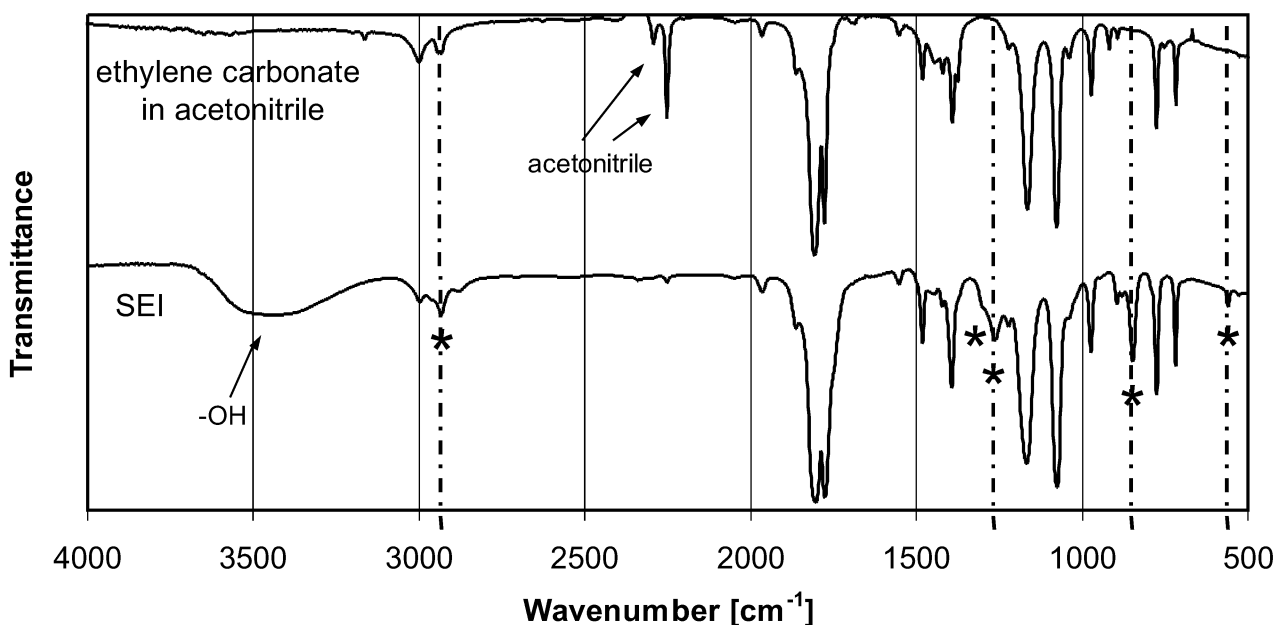
Fig. 2: FTIR spectra of (bottom trace) an SEI extract concentrate in moist acetonitrile and (top trace) EC in ace-tonitrile. The asterisks indicate features assigned to the SEI.

An analytical procedure was developed in order to separate the SEI extracts into its compounds. Poly-ethylene glycol mixtures of different average chain length were used as a standard to optimise the method and to evaluate the quality of the separation. Results obtained with the developed method are shown in Figure 3 (upper part). Good separation of the compounds of different chain length could be ob-tained.
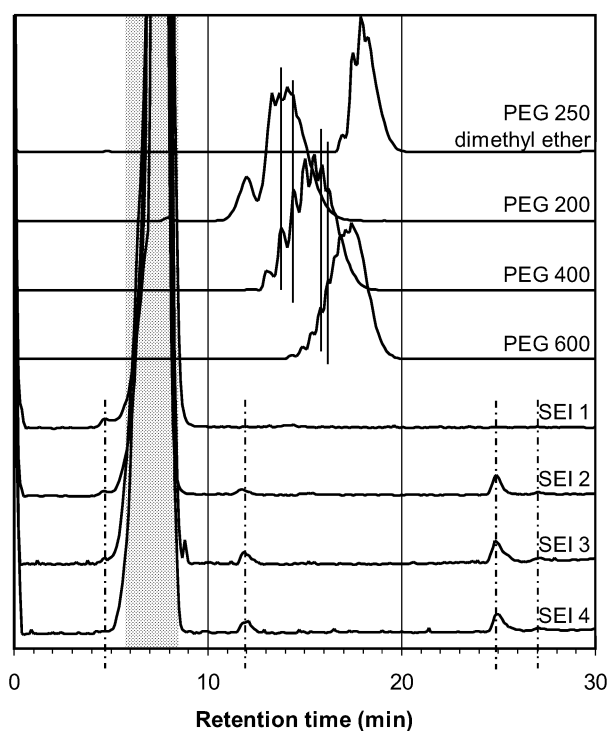
Analysis of the SEI compounds, on the other hand, turned out to be a challenging task. Since the SEI compounds are only present in trace amounts in the extract, a sufficient amount of material could not yet be collected to perform a full structural analysis of the compounds. Nevertheless, results of the HPLC analy-ses (Figure 3) and comparison with reference sub-stances show that the organic part of the SEI consists of compounds having a molecular mass of several hundred mass units. Our findings strongly support the hypothesis of Ogumi et al. [3]. In HPLC, the com-pounds behave very similar to polyethylene glycol.

With the procedure for the separation of the compounds at hand, the next step of investigation will be the accumulation of a sufficient amount of the substances for structural analysis. This will lead to a deeper understanding of the formation mechanisms of the SEI and allow the rational design of electrolytes for lithium-ion batteries with improved energy density and performance.

4   REFERENCES

[1]   S.S. Zhang, M.S. Ding, K. Xu, J. Allen, T.R. Jow; *Understanding solid electrolyte interface film for-mation on graphite electrodes;* Electrochem. Solid-State Lett. **4**, A206 (2001).

[2]   P. Novák, F. Joho, M. Lanz, B. Rykart, J.-C. Panitz, D. Alliata, R. Kötz, O. Haas; *The complex electrochemistry of graphite electrodes in lithium-ion batteries;* J. Power Sources **97-98**, 39 (2001).

[3]   Z. Ogumi, A. Sano, M. Inaba, T. Abe; Pyroly-sis/gas chromatography/mass spectroscopy analysis of the surface film formed on graphite negative electrode; J. Power Sources **97-98**, 157 (2001).

Fig. 3: HPLC evaporation light scattering detector traces for various polyethylene glycols and four SEI extract concentrates. The shadow area marks fea-tures assigned to inorganic compounds.

RAMAN SPECTROSCOPIC AND STRUCTURAL STUDIES OF HEAT-TREATED GRAPHITES FOR LITHIUM-ION BATTERIES

D. Goers, H. Buqa, L. Hardwick, A. Würsig, P. Novák

Standard graphite TIMREX® SLX 50 was oxidised at 500-800 °C under air atmosphere. Scanning Electron Microscopy (SEM), Raman spectroscopy and X-ray Powder Diffraction (XRD) were used to study the changes in morphology and crystallinity. The results show a slight increase of the L_a value and a decrease of the rhombohedral fraction with increased heat-treatment temperature (HTT). Above 700 °C SEM images of graphite reveal holes and cavities.

1 INTRODUCTION

Lithium-ion batteries often contain graphite as the electroactive material for the negative electrode. Graphite material parameters like particle size distribution, particle shape, crystallinity, and the composition of surface groups can affect the performance of lithium-ion batteries. One of the most important parameters of graphite is the crystallite size in the basal plane L_a. It corresponds to the reciprocal amount of disordered regions. Raman spectroscopy has evolved as a sensitive detection tool as it is receptive to the symmetry of structure near surface regions. With Raman spectroscopy and the use of Tuinstra and Koenig's equation, L_a can be obtained from the intensities of the G-band at 1580 cm^{-1} and the D-band at 1355 cm^{-1} [1]. From the calculation of L_a values of graphites, their investigation using XRD and SEM, it is possible to study the effect of heat treatment modification.

2 EXPERIMENTAL

Oxidation of Graphite

The oxidation of graphite material (TIMREX® SLX 50, TIMCAL SA, Bodio) was performed for one hour using a muffle furnace (Nabertherm Switzerland AG). The stream of dry air over the sample (about 5 g) was set to 100 l/h and the heating rate to 20 °C/min.

Raman Microscopy

A confocal Raman microscope (Labram, Jobin Yvon, earlier DILOR Instruments SA) was used to acquire Raman spectra of graphite samples. The light source used was an external Kr$^+$ laser (Coherent Inc.) at 530.9 nm, which excites the sample with approximately 10 mW of power. The Raman spectra were recorded in the spectral range of 1000-2000 cm^{-1} with a resolution of 4 cm^{-1}. Raman band positions were calibrated against the spectrum of a neon lamp (Penray, Oriel). Raman maps of the electrodes were created, using a rectangle of 40x40 µm located on a selected surface point of the electrode. Within this area 12x12 Raman spectra were recorded.

For carbons a relationship exists between the correlation length L_a (derived by analysis of X-ray data) and the spectroscopically derived ratio I(D)/I(G), $L_a = 4.4 / [I(D)/I(G)]$ nm, where I(D) and I(G) are the integrated band intensities of the D- and G-band re-

spectively [1]. For comparison different positions on the electrode were selected and measured. For each spectrum the L_a values were calculated leading to the creation of 2D contour maps.

X-Ray Diffraction

Powder X-Ray Diffraction (XRD) measurements were performed using a STOE Stadip diffractometer working with Cu K$_{\alpha 1}$ radiation (1.5418 Å) and a Ge monochromator. All measurements were accomplished in a range of 6° < θ < 100° with a mea-surement time of 30 minutes.

The coherent length of the graphite crystallite in the basal plane L_a and the crystallite size along the c-axis L_c were determined from the full-width-at-half-maximum (FWHM) of (110) and (002) carbon Bragg peaks using the Scherrer equation [2, 3].

$$L_a = \frac{1.84\lambda}{B\cos\theta} \qquad L_c = \frac{0.89\lambda}{B\cos\theta}$$

From the above equations: λ is the wavelength of the X-Ray beam, B is the angular width of the respective diffraction peak at half-maximum intensity after correction for instrumental line broadening and θ is the Bragg angle. To obtain B the FWHM (B_{exp}) was first measured and then the instrumental broadening B_{inst} was subtracted [4].

$$B = \sqrt{B_{exp}^{\,2} - B_{inst}^{\,2}}$$

The rhombohedral fraction was derived by the comparison of intensities of the (101) hexagonal and rhombohedral peaks.

Electrochemical investigations of the heat-treated graphites will be presented in a different article contained in this scientific report by H. Buqa et al.

3 RESULTS

The SEM picture of heat-treated graphite at 700 °C (Figure 1) reveals the presence of holes or cavities within the prismatic planes. Changes on the edge planes are only visible on graphites treated at 700 °C or above. On certain positions cavities where also observed on the basal planes of the graphite, probably due to the reaction of surface impurities. At lower temperatures no structural changes are observed.
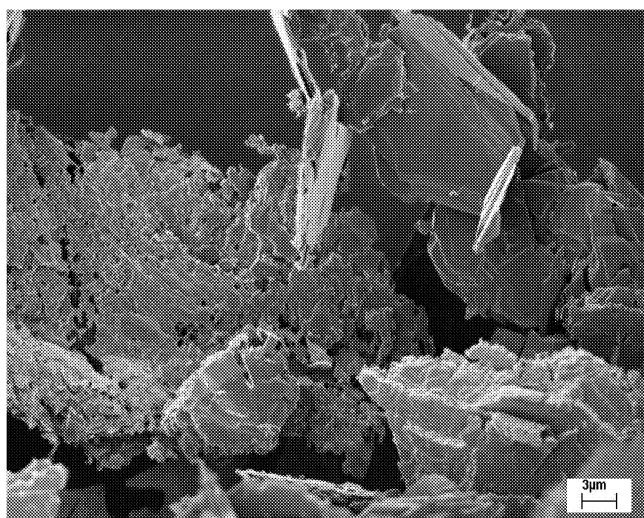
Fig. 1: Scanning electron microscope image of TIM-REX® SLX 50, oxidised in air for 1 hour at 700 °C.

Raman spectroscopy provides a lateral spatial distribution of the L_a values on the electrode surface. This gives the possibility of the creation of 2D contour maps (Figure 2). The surface of the graphite electrode consists mainly of a sea of disorder with islands of highly ordered graphite.
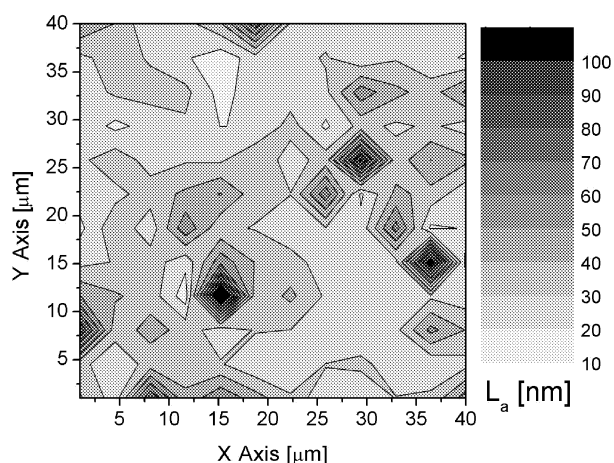
Fig. 2: Contour map of the selected region of untreated TIMREX® SLX 50

Figure 3 shows the Raman spectra of various heat-treated graphites. The G-Band was observed at 1577 cm^{-1}, no shift in this band is observed with increasing HTT. Due to the high crystallinity of the graphite samples used, the D-band has a very low prominence. The L_a values are in the range of 30 - 80 nm indicating a small increase with HTT (Table 1). However the L_a values obtained by XRD do not indicate any significant increase and are in a different order range. This may be due to the surface sensitivity of Raman spectroscopy and the limited effect of tem-

perature modification upon the bulk during the short heat treatment time of 1 hour. The variation of L_a values obtained by different techniques is not yet fully understood. Furthermore a decrease in the rhombohedral fraction with increased HTT was observed.
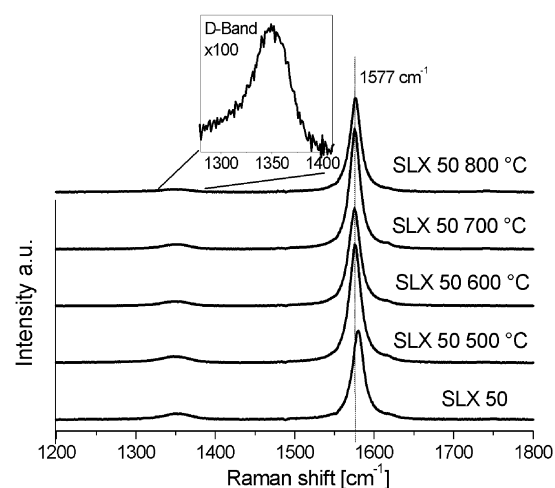
Fig. 3: Average spectra of heat-treated graphite TIMREX® SLX 50. In the case of HTT = 800 °C the D-band was enlarged by a factor of 100.

Treatment	Rhombohedral fraction [%]	XRD L_c [nm]	XRD L_a [nm]	Raman spectroscopy L_a [nm]
untreated	16	71	150	30
500 °C	16	60	152	48
600 °C	15	63	167	60
700 °C	11	76	162	68
800 °C	11	78	156	72

Table 1: Results of Raman and XRD analysis of heat-treated graphite TIMREX® SLX 50.

4 ACKNOWLEDGEMENT

5 REFERENCES

[1] F. Tuinstra, J. L. Koenig, J. Chem. Phys. **53**, 1126 (1970).

[2] K. Kinoshita, *Carbon*, Wiley Interscience Publication (1988).

[3] F. Cao, I. Barsukov, H. J. Bang, P. Zaleski, J. Prakash , J. Electrochem. Soc. **147,** 3579-3583 (2000).

[4] C.S. Wang, G.T. Wu, W.Z. Li, J. Power Sources **76,** 1-10 (1998).

CHARACTERIZATION OF CARBONACEOUS MATERIALS TO BE USED FOR BIFUNCTIONAL AIR-ELECTRODES IN RECHARGEABLE ZINC-AIR BATTERIES

R. Richner, M. Brüsewitz (ZOXY AG, Oberderdingen), M.Spahr (Timcal, Bodio), O.Haas

Graphitized carbon blacks were investigated in terms of their stability in bifunctional air-electrodes. The long-term stability can be considerably enhanced by an appropriate graphitization of the original carbon black. Activation of the graphitized carbon blacks in air at elevated temperatures can improve the overpotential but may lead to a lower stability.

1 INTRODUCTION

The electrically rechargeable Zn/air battery is a competitive energy storage device, which is due to its high specific energy. In addition, it has considerable economical and ecological advantages[1]. The cycle life of this battery depends very much on the lifetime of the bifunctional air electrode. This is a gas-diffusion electrode consisting of an active layer and a diffusion layer [1,2,3], the active layer being the critical part for the function and life of bifunctional air electrodes. The most important components in the active layer are the carbon black and the catalyst. Their chemical and electrochemical stability strongly influences the lifetime of the bifunctional electrode.

In the present work we investigated the influence of carbon black pretreatments on the electrochemical activity and cycling behavior of the bifunctional air electrodes.

2 EXPERIMENTAL

The active layer of the bifunctional air electrodes was prepared with 35 % graphitized Vulcan XC72 carbon black as the carrier and 50 % $La_{0.6}Ca_{0.4}CoO_3$ perovskite as the catalyst. These components are bonded with 15 % PTFE. The diffusion layer was made of 85 % acetylene black and 15 % PTFE. The electrodes were rolled as described in [1], where the two layers are rolled together, then dried and sintered using petroleum-based doughs of the layer components.

As an alternative, electrodes were made from dry powders in a process where the two layers are spread as dry powders, then hot-pressed together at 340 °C in order to sinter the binder and form the composite electrode.

The cycle life of the rolled, bifunctional carbon electrodes was measured in cycles consisting of 3 h of a cathodic current of 6 mA/cm^2 followed by 3 h of an anodic current having the same current density.

For the cycle life data of the pressed electrodes shown in Figure 2, the cathodic current density in each cycle was 48 mA/cm^2 during 4 h, and the anodic current density was 12 mA/cm^2 during 16 h.

3 RESULTS AND DISCUSSION

Several bifunctional air electrodes were produced using different graphitized carbon blacks. The carbons used are described in Table 1 in terms of xylene den-

sity (according to DIN 12797, which gives a measure of the degree of graphitization), BET surface area (which is important for the activity of the carbon), and cycle life obtained with rolled electrodes prepared from these carbons.

Carbon	Xylene density / (g/ml)	Surface area / (m²/g BET)	Cyle life* (n)
0	-	250	475
A	1.856	72	629
A1	-	92	203
B	1.891	60	1037
B1	-	75	-
C	1.974	49	-
C1	-	53	-

Table 1: Properties of carbon Vulcan XC72: (0) as received, (A,B,C) after graphitization, (B1,C1) after activation. *:The cycle life (number of cycles n) was measured with rolled electrodes

The data in Table 1 illustrate that there is a correlation between the cycle life and the xylene density.

In Figure 1, the current-potential curves recorded with *pressed* electrodes containing graphitized carbons (B,C) and carbons which had been activated after graphitization (B1,C1) are shown. For comparison, a *rolled* electrode containing carbon black that was graphitized but not activated (A) is included. Negative values of current are those for the electrochemical reduction of oxygen at the air-fed gas-diffusion electrode, positive values of current are those for oxygen evolution occurring at more positive potentials. These current-potential curves clearly reveal the lower overpotentials exhibited by electrodes containing activated carbons. However, the rolled electrode containing carbon that was graphitized but not activated exhibited the lowest overpotential. It can further be seen that the overpotential does not only depend on the surface area. For the cycle life, however, activation is destructive, see Figure 2. Another interesting feature is seen in Figure 2, viz., the overpotentials of electrodes containing unactivated carbons decrease after a number of cycles. This means that cycling activates the elec-

trodes. We believe that this effect is due to an improvement of wetting of the porous electrode/electrolyte interface occurring during cycling. Activation by heating in air probably has a similar effect, since in this process hydrophilic surface groups are formed on the carbon, which enhance the wetting of the interface.
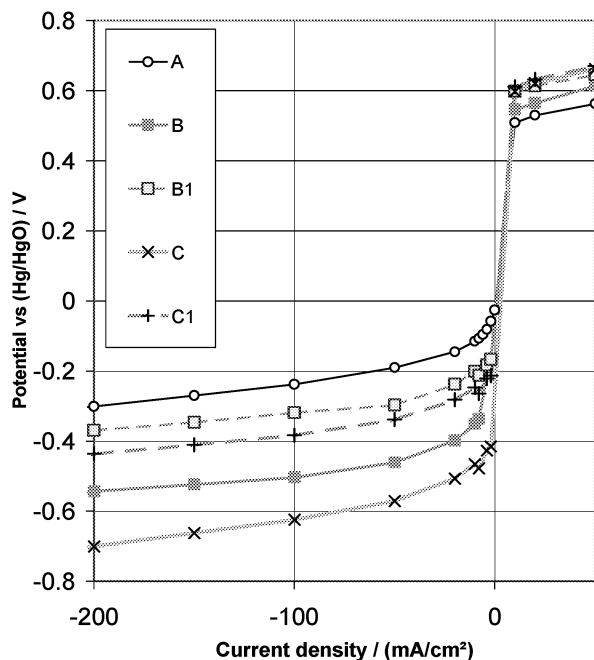
Fig. 1: Current-potential curves recorded at pressed air electrodes containing carbon blacks: (B,C) only graphitized, (B1,C1) graphitized and activated. (A) rolled electrode with graphitised carbon.

On the other hand, the cycle life of the pressed electrodes is much longer when the graphitized carbon has not been activated, see Figure 2.

One can also see from Figure 2 that graphitized carbons with a higher xylene density (C) have a better cycle life. This is reasonable, since the xylene density is a measure of the degree of graphitization, which is important for the chemical stability and corrosion resistance oft the carbon.

4 CONCLUSION

It was shown in the instance of Vulcan XC72 carbon that graphitizing a carbon black helps to increase the cycle life of bifunctional air electrodes made from it, but also leads to higher overpotentials at least during the first few cycles.
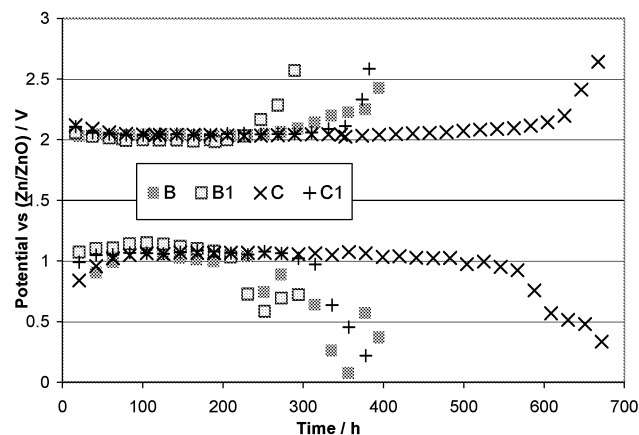
Fig. 2: Cycle life of pressed electrodes, as described in the experimental section.

Activating the graphitized carbon black at a higher temperature in air leads to a higher surface area and lower overpotential and to enhanced wetting of the electrode/electrolyte interface. However, this activation process shortens the lifetime of the bifunctional air electrodes.

Rolled electrodes exhibit a certain advantage in terms of overpotential compared to pressed electrodes .

The overpotentials of pressed electrodes containing unactivated carbon improves during the first few cycles. Thus, the best cycle life and the best cell efficiency over the lifetime can be achieved when unactivated or weakly activated carbon blacks with a high xylene density are used for making the active layer of bifunctional air electrodes.

5 ACKNOWLEDGEMENTS

6 REFERENCES

[1] S. Müller, K. A. Striebel, O. Haas, Electrochim. Acta **39**, 1661 (1994).

[2] S. Müller, F. Holzer, H. Arai, O. Haas, PSI Scientific Report 2000, **V**, 60 (2001).

[3] H. Arai, S. Müller, O. Haas, J. Electrochem. Soc. **147**, 3584-3591 (2000).

MODELING OF AN ELECTRICALLY RECHARGEABLE ALKALINE ZINC-AIR BATTERY

E. Deiss, F. Holzer, O. Haas

A numerical model has been developed to simulate the charging and discharge behaviour of an electrically rechargeable alkaline zinc-air battery. Further a galvanostatic experiment including three charge/discharge cycles has been performed. The cell voltages, the Zn electrode potentials versus a Zn reference, and the O_2 electrode potentials versus a Zn reference calculated with the model are in fairly good agreement with the corresponding experimental data. The model is expected to be useful for zinc-air battery design and for analysis of experimental data.

1 INTRODUCTION

Because of their high specific energy (>100 Wh/kg) and their inexpensive and environmentally benign materials, electrically rechargeable zinc-air batteries are promising power sources and energy storage devices [1]. For their best possible utilization, it will be necessary to optimise their design with respect to known difficulties such as OH^- ion depletion occurring during discharge and shape change (redistribution of the active solid materials Zn and ZnO) occurring as a result of cycling.

In this work we demonstrate as first a numerical model of an electrically rechargeable zinc-air battery allowing us to calculate from a galvanostatic experiment the response of cell voltage, Zn electrode potential (vs. Zn reference), O_2 electrode potential (vs. Zn reference), and the potential and concentration profiles of the participating chemical species.

2 EXPERIMENTAL

The experimental setup included a twin-cell sandwich arrangement with a (negative) Zn electrode in the center and a (positive) O_2 electrode on each side (Figure 1). The anode, a porous Zn electrode consisted mainly of Zn and ZnO, but contained traces of PbO, cellulose, and PTFE (Teflon). The PbO serves as inhibitor of corrosion reactions, while the cellulose fibers act as internal wicks to provide electrolyte channels which keep the electrode wet and porous. The two cathodes, bifunctional oxygen-diffusion electrodes, are two-layer electrodes where the active layer contains perovskite catalyst ($La_{0.6}Ca_{0.4}CoO_3$) supported by graphitized carbon and bonded with PTFE. The gas-diffusion layer consists of PTFE-bonded carbon black. In our experiments, pure O_2 rather than air was supplied to the cathodes during discharge.

The Zn electrode in the center had a total thickness of 0.14 cm, i.e., 0.07 cm on each side of the mirror plane of the cell arrangement. Three layers of 0.0025-cm (totally 0.0075 cm) Celgard 3401 separator (Hoechst
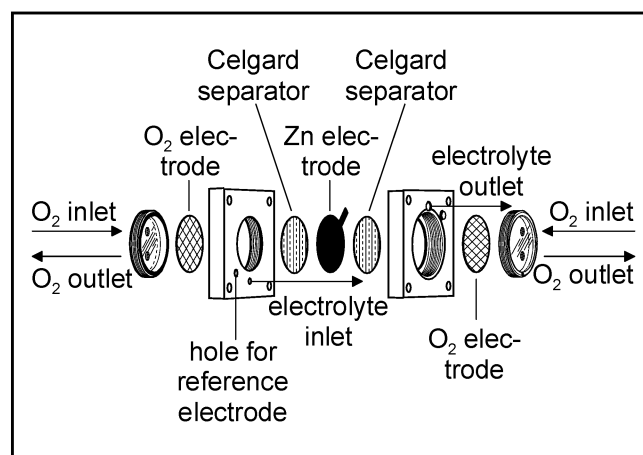
Fig. 1: Cell arrangement of the experimental zinc-air battery.

Celanese Corp. USA) were inserted between the Zn electrode and each of the O_2 electrodes to prevent shorts due to dendrite formation. The electrodes had the geometric shape of circles with a surface area of 25 cm^2, which gives a total active surface area of 50 cm^2 of the electrodes in the twin-cell arrangement employed. The electrolyte was a 15 % KOH solution presaturated with ZnO and contained 1.5 M in KF. A Zn wire was used as reference electrode to monitor the potential of the O_2 and Zn electrode individually during the experiments.

A galvanostatic experiment with three charge-discharge cycles has been performed with this cell arrangement. The values of cell voltage, the potential of the O_2 electrode vs. Zn reference, and potential of the Zn electrode vs. Zn reference measured in this three-cycle experiment are shown in Figure 2 (dotted lines).

3 MODEL DESCRIPTION

The model battery consists of a single cell with one Zn and one O_2 electrode, as shown in Figure 3. The (negative) Zn electrode consists of the solid materials Zn and ZnO, pressed together with PTFE and cellulo-
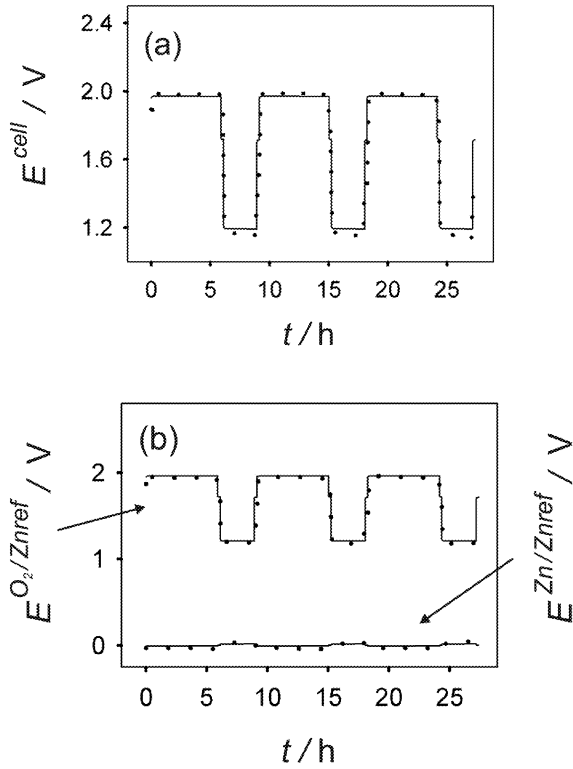
Fig. 2: Three-cycle experiment: calculated (full line) and experimental (dotted line) values vs. time t : (a) cell voltage $E^{cell}(t)$, (b) Zn electrode potential vs. Zn reference $E^{Zn/Znref}(t)$, and O_2 electrode potential vs. Zn reference $E^{O_2/Znref}(t)$.
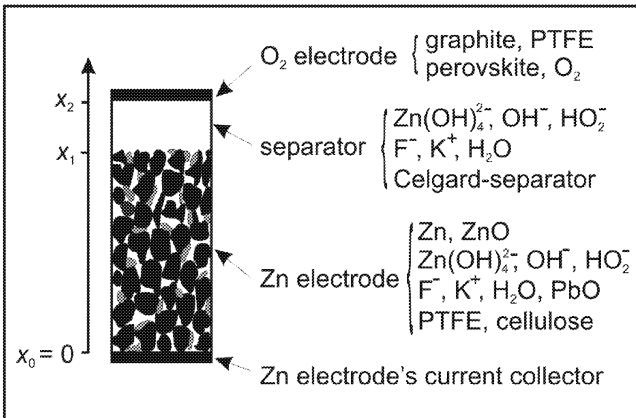
Fig. 3: Schematic drawing of the single-cell zinc-air battery used for the model.

se as binders. The separator between Zn and O_2 electrode consists of a porous polypropylene membrane. The electrolyte filling the pores of the Zn electrode and the separator is an alkaline solution with the five dissolved species $Zn(OH)_4^{2-}$, OH^-, HO_2^-, F^-, and K^+. The (positive) O_2 electrode consists of graphite with perovskite as catalyst and PTFE as binder. In contrast to the Zn electrode, the O_2 electrode will be treated as

a flat electrode. This single-cell model represents just one side of the specularly symmetric experimental cell (a sandwiched twin-cell arrangement with a Zn electrode in the center and an O_2 electrode on each side), and differs from the experimental cell arrangement only by the total current, which is one half of that in the experimental cell. The following effects described in detail in [2] are included in the zinc-air battery model:

a) diffusion and migration of the dissolved species $Zn(OH)_4^{2-}$, OH^-, HO_2^-, F^-, and K^+
b) reduction of $Zn(OH)_4^{2-}$ to Zn and reverse reaction
c) reduction of H_2O to H_2 in the Zn electrode
d) precipitation of ZnO from $Zn(OH)_4^{2-}$ and reverse reaction in the Zn electrode
e) reduction of O_2 to HO_2^- at the O_2 electrode
f) disproportionation of HO_2^- at the O_2 electrode
g) oxidation of OH^- to O_2 at the O_2 electrode
h) ohmic potential drop in the metallic Zn phase and potential drop in the electrolyte due to migration
i) time and position-dependent porosity in the Zn electrode, constant porosity in the separator

5   RESULTS

The model has been used to simulate the three-cycle experiment. In Figure 2 the calculated and experimental values of $E^{cell}(t)$, $E^{Zn/Znref}(t)$, and $E^{O_2/Znref}(t)$, are compared. The calculated values of $E^{cell}(t)$, $E^{Zn/Znref}(t)$, and $E^{O_2/Znref}(t)$ of the three-cycle experiment are in fairly good agreement with the experimental values. Therefore it can be used to predict experiments and to study in detail the dynamic behaviour of a zinc-air battery.

6   CONCLUSION

A galvanostatic experiment including three charge-discharge cycles has been performed, and a numerical model has been developed and was used to simulate the experiments. The model reproduces experimental data such as the cell voltage, the Zn electrode potential vs. Zn reference, and the O_2 electrode potential vs. Zn reference. Considering the agreement attained between model calculations and experiment, it is expected that the numerical model will be useful when optimizing zinc-air battery designs for specific applications.

7   REFERENCES

[1] J. Goldstein, I. Brown, B. Koretz, J. Power Sources **80**, 171 (1999).
[2] E. Deiss, F. Holzer, O. Haas, Electrochim. Acta **47**, 3995 (2002).

INTERFACIAL CAPACITANCE AND ELECTRONIC CONDUCTIVITY OF CARBON DOUBLE LAYER ELECTRODES

M. Hahn, M. Baertschi, J.-C. Sauter, R. Kötz

Double layer capacitance, C, and electronic conductivity, σ, of activated carbon electrodes in contact with an organic electrolyte solution show a similar dependence on the electrode potential, E, with a minimum near the potential of zero charge. We suggest a simple model, accounting quantitatively for these findings. According to this model the density of mobile electronic charge carriers is changed upon charging the double layer and controls both, the electronic conductivity as well as the capacitance of the space charge region, C_{SC}, on the solid side of the interface. C_{SC} is found to be considerably smaller than the (Helmholtz) capacitance of the solvent layer, C_H, and thus dominates the measured overall capacitance. The slight shift observed between the minima of C (E) and σ (E) can be accounted for by assuming an additional potential-dependence of C_H, being in reasonable agreement with the behavior reported in literature.

1 INTRODUCTION

Commercial double layer capacitors utilizing high surface area carbon electrode materials and aprotic electrolyte solutions have in common a pronounced minimum of the capacitance near the potential of zero charge, pzc. Up to now the origin of this important effect is not understood. In order to determine the possible contribution of the solid (carbon), we have studied the dependence of the electronic conductivity along the solid side of the double layer on the electrode potential.

The experimental situation resembles that of a (atomically) thin film electrode with the electrochemical double layer formed on its surface. The conductivity along the film, corresponding to the pore walls inside the activated carbon electrode, is then measured by applying a small voltage between the two opposing edges of the film. Unlike the capacitance, the electronic conductivity is a typical bulk property, and thus is only affected by the excess charge in the electrochemical double layer, if the screening length of the electric field inside the film (pore walls) is comparable to the film thickness. In fact, this condition is well fulfilled for activated carbon, where almost every carbon atom is part of the huge inner surface and hence the conductivity is expected to depend on the electrode potential.

2 EXPERIMENTAL

The electrode material used was a commercial PTFE-bound activated carbon with a BET-surface of around 1000 m^2/g. A solution of 1 mol/l Et_4NBF_4 in acetonitrile was employed as the electrolyte.

The experimental set-up is shown in Figure 1. The electrode sample (2 mm in diameter, 0.6 mm thick), clamped between two gold wires, is immersed into the electrolyte solution, and then is stepwise electrochemically charged against a counter electrode made from the same material. Since the counter electrode is much larger than the sample, its potential is effectively pinned upon charging. Thus the electrode potential, E, can be directly recorded with respect to the counter electrode, whose potential is considered to be the pzc.
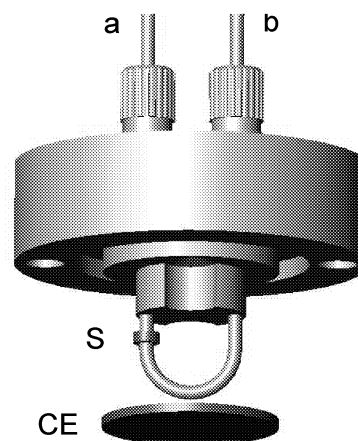
Fig. 1: Experimental set-up. The counter electrode (CE) is mounted at the bottom of the electrolyte container (not shown). The sample (S) is charged by applying a voltage, E, between the upper contact wire (a) and CE. The electronic conductance across the sample is measured between the two wires (a and b).

At each potential step both, the electronic conductance across the sample and the electrochemical impedance between the sample and the counter electrode are measured.

The electronic conductance, L = i/U, is determined by applying a small dc-current, i, across the sample and measuring the corresponding potential drop, U (some mV), between the two wires.

The capacitance, C, is calculated from the imaginary part, Z^{im}, of the electrochemical impedance at a frequency f = 10 mHz, according to C = $-1/(2\pi f Z^{im})$.

3 RESULTS

As shown in Figure 2, capacitance (referred to the BET-surface area) and electronic conductivity (normalized to its value at the pzc, σ_{pzc} > 500 S/m) show a similar dependence on the electrode potential with a minimum near the pzc. However, the capacitance minimum is slightly shifted towards more positive values.
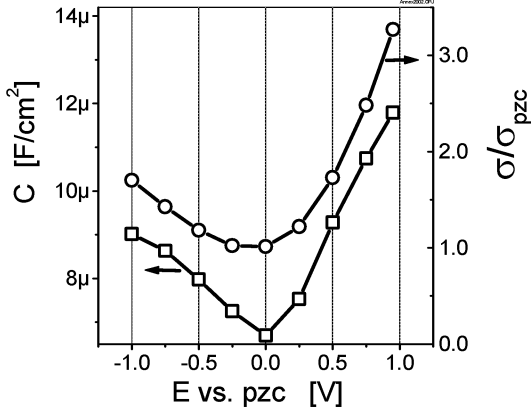
Fig. 2: Capacitance (squares) and normalized electronic conductivity (circles) vs. electrode potential.

4 THE MODEL

For a metalloid conductor with a finite density of electronic states at the Fermi level, N (ε_F), the conductivity may be described by [1]

$$\sigma = e\mu N(\varepsilon_F)kT ,$$ (1)

where μ is the electronic mobility. On the other hand, the capacitance of the space charge layer inside this conductor is given by [2]

$$C_{SC} = e\sqrt{\kappa N(\varepsilon_F)}$$ (2)

(κ: dielectric constant of the solid)

Assuming that μ is independent on the electrode potential, E, and relating C_{SC} (E) and σ (E) to their values at the pzc, $C_{SC,pzc}$ and σ_{pzc}, combination of equation (1) and (2) yields:

$$C_{SC} = C_{SC,pzc}\sqrt{\sigma/\sigma_{pzc}}$$ (3)

However, the total capacitance, C, is generally not identical with C_{SC}. In fact, C must be envisaged as a series connection of C_{sc} with the capacitance of the charge free solvent (Helmholtz) layer, C_H [3]:

$$\frac{1}{C} = \frac{1}{C_H} + \frac{1}{C_{SC}}$$ (4)

Finally, combination of equations (3) and (4) gives an expression for the potential dependence of the overall capacitance:

$$\frac{1}{C} = \frac{1}{C_H} + \frac{1}{C_{SC,pzc}\sqrt{\sigma/\sigma_{pzc}}}$$ (5)

At the pzc equation (5) simplifies to

$$\frac{1}{C_{pzc}} = \frac{1}{C_{H,pzc}} + \frac{1}{C_{SC,pzc}}$$ (6)

From the latter equation, and with a reasonable value for $C_{H,pzc}$ from literature [3], $C_{H,pzc}$ = 20 $\mu F/cm^2$, $C_{SC,pzc}$ can be estimated. Figure 3 shows C_H (E) and C_{SC} (E) calculated on this basis with the measured data from Figure 2. The calculated dependence C_H (E), with a minimum at the pzc, agrees reasonably with literature data for acetonitrile-like solvents [3].
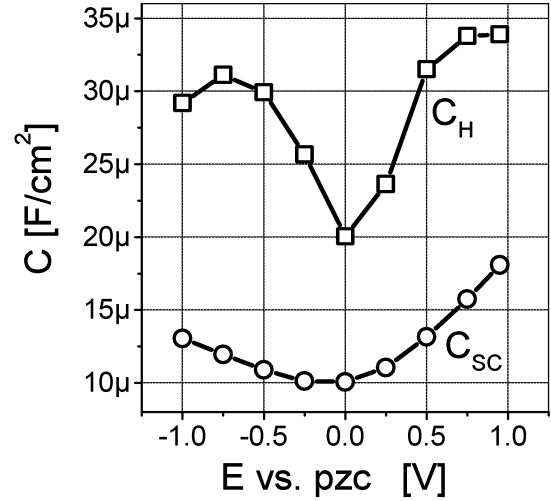
Fig. 3: Contributions of C_H (squares) and C_{SC} (circles) to the overall capacitance. Calculated from the experimental data in Figure 2 and $C_{H,pzc}$ = 20 $\mu F/cm^2$.

5 CONCLUSION

The suggested model quantitatively describes the experimentally observed correlation between interfacial capacitance and electronic conductivity of the porous solid. According to this model the density of mobile electronic charge carriers, being changed by charging the double layer, determines both, the electronic conductivity as well as the capacitance of the space charge region, C_{SC}, inside the solid. C_{SC} is found to be considerably smaller than the capacitance of the solvent layer, C_H, and thus dominates the measured double layer capacitance, C. However, the slight but significant shift observed between the minima of C (E) and σ (E) can only be accounted for by assuming an additional potential-dependence of C_H. The calculated dependence C_H (E), with a minimum at the pzc, is in reasonable accordance with literature data [3].

6 REFERENCES

[1] N.F. Mott, E.A. Davis, *Electronic Processes in Non-Crystalline Materials*, 2nd ed., Clarendon Press, Oxford (1979).

[2] H. Gerischer, J. Phys. Chem. **89**, 4249 (1985).

[3] B.E. Conway, *Electrochemical Supercapacitors: Scientific Fundamentals and Technological Applications*, Kluwer, New York (1999).

RAMAN SPECTROSCOPIC STUDY OF THE POLYMERISATION OF SOME SUBSTITUTED STYRENES

L. Steuernagel, D.E. Kaufmann (Technische Universität Clausthal), A. Wokaun,
G.G. Scherer, H.P. Brack

The susceptibility of the benzylic hydrogen of polystyrene (PS) towards radical abstraction is known to be a weak point in the chemical stability of membranes based on PS copolymers. The stability of such membranes can be improved by the use of substituted styrenes. Not only the stability of the copolymer formed is important, however, but also its ease and rate of preparation. In this investigation, the relative polymerisation rates of styrene and some derivatives have been studied by Raman spectroscopy.

1 INTRODUCTION

PSI is developing membranes for application as polymer electrolyte in electrochemical systems. In the radiation-grafting method, commodity fluoropolymer films are irradiated, then reacted with styrene and crosslinkers to graft polystyrene (PS) chains onto the fluoropolymer backbone, and finally sulfonated to introduce ionic conductivity through the presence of the sulfonated polystyrene chains (SPS) (Figure 1) [1].
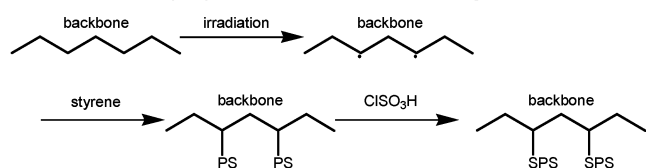
Fig. 1: Preparation scheme of PSI-membranes.

In spite of already demonstrating thousands of hours of stable continuous operation with fuel cells containing our membranes [1,2], our goal is to even further improve the lifetime and stability of our membranes in fuel cell applications, especially at elevated operating temperatures and under harsher operating conditions. Earlier work indicated that the weak part of our membrane system is the SPS component [2], which is susceptible to attack by radicals at the benzylic hydrogen position (drawn in bold in Figure 2) thereby initiating the membrane degradation process.
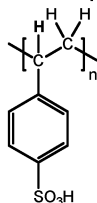
Fig. 2: Chemical structure of SPS-unit.

This inherent weakness of SPS and PS towards radical-induced degradation can be overcome by the use of substituted-styrene monomers. The benzylic hydrogens of SPS and PS (α-hydrogen of the styrene monomer in Figure 3) can be substituted by another element like fluorine to give a stronger bond that is less susceptible to scission. Alternatively a substituent can be introduced to the aromatic ring to modify the electronic structure and perhaps make the abstraction of the benzylic hydrogen less favourable.

Not only is the chemical stability of grafted substituted SPS chains in the membrane product critical, but it is also important that the appropriately substituted styrene monomer can be rapidly polymerised to yield the desired grafted polymer chains in the membrane production process (PS in Figure 1).
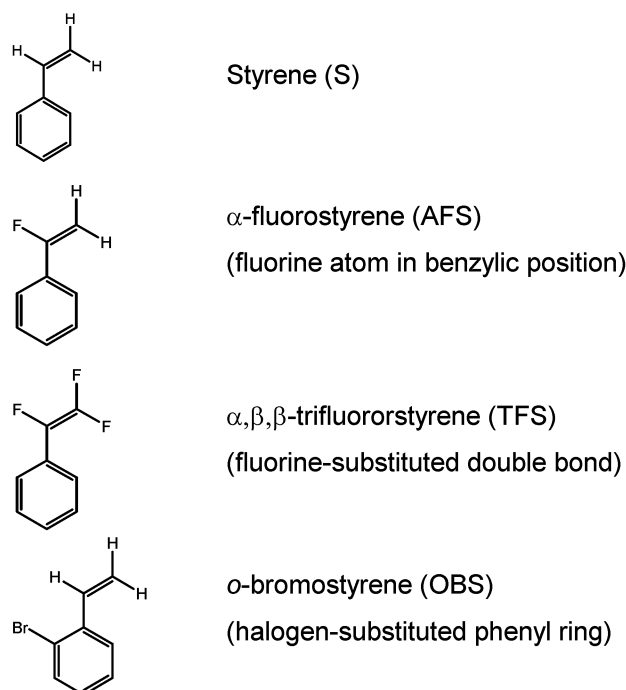
Fig. 3: Chemical structure of substituted styrenes.

Therefore this investigation was undertaken to investigate the polymerisation kinetics of some substituted styrenes. In one case, the benzylic position is substituted with fluorine (AFS); in another, the double bond is perfluorinated (TFS); and in the third case the ring has a halogen substituent (OBS) (Figure 3).

In the radical polymerisation of styrenic monomers, the active radical species ($PS_n^{\bullet}$) reacts with the double bond of the styrene monomer (S) to increase the chain length by one repeat unit in a propagation step:

$$PS_n^{\bullet} + S \xrightarrow{\ k_p\ } PS_{n+1}^{\bullet} \qquad (1)$$
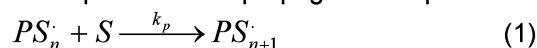
The rate constant for this reaction is defined as:

$$R_p = -\frac{d[S]}{dt} = k_p [PS^{\bullet}] * [S] \qquad (2)$$

As a result, the concentration of monomer, S, and thus double bonds decreases as polymerisation proceeds, whereas the concentration of phenyl groups, which do not directly react, remains constant. The rate

of decrease in the concentration of double bonds relative to the concentration of phenyl groups is thus equal to the overall rate of propagation for the polymerisation (R_p).

Because Raman spectroscopy is sensitive to both double bond and phenyl functional groups, it is a useful method for following the polymerisation kinetics of styrenic monomers [3]. For example, the Raman spectra of S and PS are shown in Figure 4. The spectrum of S shows two bands in this region, one at 1630 cm^{-1} for the double bond, and one at 1600 cm^{-1} for the phenyl ring. In the PS spectrum the band for the double bond has disappeared but the one for the phenyl ring remains. Thus by measuring the band area ratio (1630 cm^{-1}/1600 cm^{-1}) as a function of reaction time, d[S]/dt and the overall rates of propagation of each substituted styrene can be determined.

———— after 20 min — — — after 180 min - - - - - polystyrene
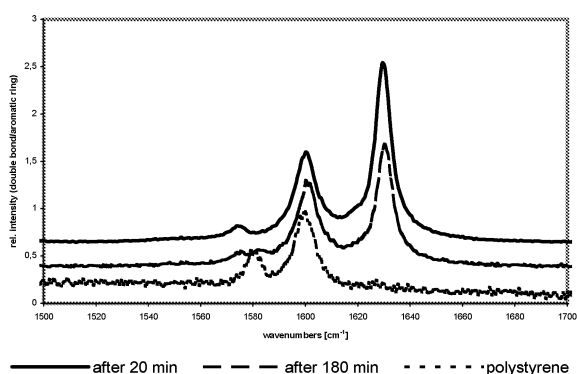
Fig. 4: Raman spectrum of S as a function of time.

2 EXPERIMENTAL

Each styrene derivative was reacted together with the radical initiator AIBN (2 mol % relative to monomer concentration) in a test tube sealed under N_2 and held at a constant temperature of 50, 60, or 70 °C. Raman spectra of the reactants were measured as a function of time, and the ratios of the areas of the bands at 1630 and 1600 cm^{-1} were calculated.

3 RESULTS AND DISCUSSION

Figure 5 shows representative data for one of the polymerisation temperatures investigated. The Raman band ratio (1630 cm^{-1}/1600 cm^{-1}) decreases with reaction time as monomer is converted to polymer and the double bond concentration decreases. The decrease in the ratio in most cases (Figure 5) appears to

◆ styrene ■ fluorostyrene ▲ o-bromostyrene ● trifluorostyrene
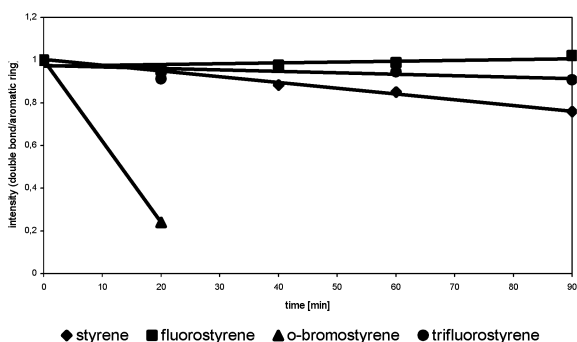
Fig. 5: Raman band ratios of derivates at 70 °C.

be quite linear during the initial stage of conversion occurring before the concentrations of $PS_n^{\bullet}$ and S change too greatly. The different monomers have quite different polymerisation rates. While S reacts fairly slowly, OBS reacts quite fast. TFS does not react as quickly as S, and AFS reacts the slowest of the four monomers. This order of relative reactivity, OBS>>S>TFS>>AFS, was valid over the entire temperature range investigated. Electronic, polar and steric influences of the halogen substituents, and perhaps to a lesser extent differences in monomer molar volume, are some of the factors responsible for the observed differences in monomer reactivity [4].
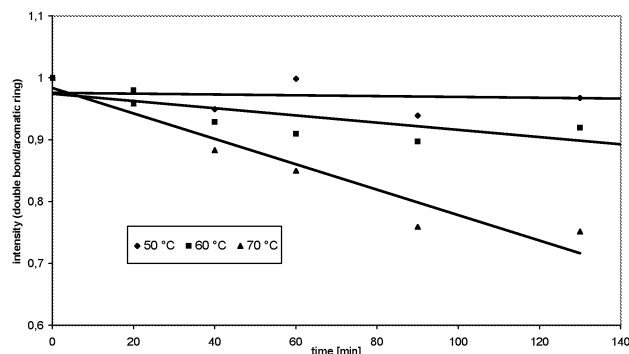
Fig. 6: Temperature dependence of styrene polymerisation.

Not only the time but also the temperature dependence of the rate of monomer disappearance can be readily studied using this Raman method (Figure 6). In general, the substituted styrenes in this investigation reacted more rapidly as the reaction temperature increased in this study. Raman investigations of the polymerisation of substituted styrenes at several different reaction temperatures are in progress, and they will allow us to determine the activation energies for the different monomer propagation reactions.

Of the various substituted-styrene monomers investigated in this study, OBS is the most reactive alternative monomer candidate to-date. In the next phase of this work it must be validated as to whether the ortho-halogen substituent indeed beneficially influences stability. The poor reactivity of our AFS and TFS monomers will be investigated also in more detail, and other candidate monomers will be evaluated.

4 REFERENCES

[1] J. Huslage, T. Rager, B. Schnyder, A. Tsukada, *Radiation-grafted membrane/electrode assemblies with improved interface*, Electrochim. Acta **48**, 247 (2002).

[2] H.P. Brack, F.N. Büchi, J. Huslage, G.G. Scherer, *Recent progress in the development of the radiation-grafted PSI membrane*, Electrochem. Soc. Proc. **98**-27, 52 (1998).

[3] K. Witke, W. Kimmer, *Ramanspektroskopische Verfolgung der Suspensionspolymerisation von Styrol*, Plaste und Kautschuk **23**-11, 799 (1976).

[4] G. Moad, D.H. Solomon, *The chemistry of free radical polymerization*, Pergamon, Oxford (1995).

INFLUENCE OF NITROGEN-CONTAINING ADDITIVES ON THE RADIATION-GRAFTING PROCESS

L. Steuernagel, S. Reich, D.E. Kaufmann (Technische Universität Clausthal), A. Wokaun,
G.G. Scherer, H.P. Brack

Triallylcyanurate (TAC) has been found in the past to have beneficial influences on both the process for the preparation of membranes by the radiation-grafting method and on the resulting membrane properties. In order to understand the effects of this compound on the grafting process, the influence of analogous organic additives on the polymerisation of styrene during both radiation grafting and homopolymerisation processes has been studied. The dominant effect of TAC and its basic analogs on the grafting process has been found to be a favourable influence on monomer partitioning between solvent and grafting film.

1   INTRODUCTION

For many years, PSI has developed proton-conducting membranes for fuel cell applications. The polarization properties and lifetimes of cells containing these membranes have been continually improved over time, and they are now stable over several thousands of hours of testing [1]. In our method, commodity fluoropolymer films like Teflon-FEP are radiation grafted via a radical mechanism with a mixture of low cost monomers, styrene and crosslinkers. The grafted film is then treated with chlorosulfonic acid to yield a proton-conducting membrane (Figure 1).

Fig. 1: Membrane production process.

One of the potential crosslinkers investigated in the past was triallylcyanurate (TAC), which yielded improved membrane mechanical properties and ionic conductivity [2]. Subsequent investigations found that TAC had a favourable promoting influence on the grafting reaction and the graft level obtained, but spectroscopic measurements failed to positively indicate that TAC was actually incorporated into the grafted films and membranes [3]. It was then speculated that TAC was not primarily acting as a crosslinking monomer (due to the poor reactivity of allylic groups in radical reactions), but that TAC had some other unidentified function as a grafting additive.

The present investigation was undertaken to understand this promoting effect of TAC on grafting reactions by investigating the influence of analogous compounds containing the two principle functionalities of TAC, namely the allylic group and the basic nitrogen-containing ring, on the grafting reaction.

2   EXPERIMENTAL

In the first part of this investigation, the influence of TAC and some analogous compounds on the grafting reaction was studied. Pre-irradiated Teflon-FEP films (10 kGy) were reacted with a mixture of styrene in either toluene or isopropanol (60:40 v/v%) and various concentrations of four additives (Figure 2) for 5 hours at 60 °C under nitrogen atmosphere. The grafting yield can be calculated from the following equation:

$$y_g = \frac{m_g - m_o}{m_o} * 100\%,$$

where
y_g: grafting yield,
m_g: mass of grafted film
m_o: mass of irradiated film.

triallylcyanurate (TAC)

tripropyloxycyanurate

(TAC without double bonds)

1,3-diallyloxybenzene

(allyl ether substituted ring)

pyridine

(N-containing basic ring)
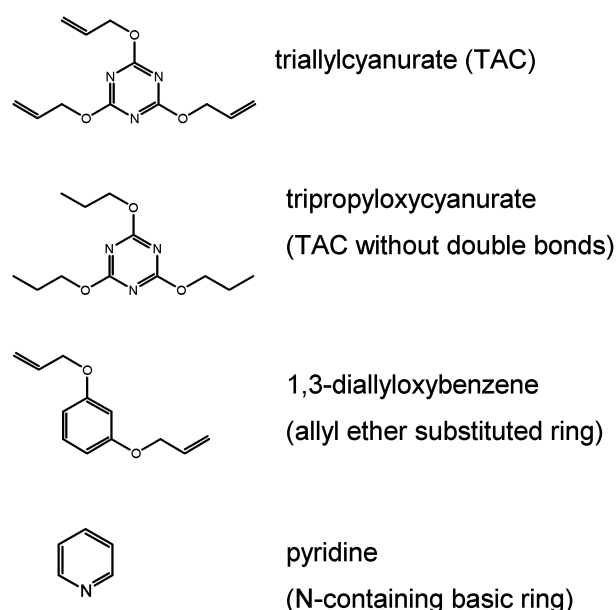
Fig. 2: Chemical structure of additives.

In the second part of this investigation, the effect of the presence of these additives on the radical polymerization of styrene in solution was investigated. The reactions were initiated using AIBN, and the polymerisations were carried out over 5 hours at 60 °C using either toluene or isopropanol as solvents.

In the third part of this investigation, the influence of these additives on the solubility of the monomer styrene in the solvent systems relative to the grafting film was evaluated by calculating the Hansen radius [4], which can be calculated by

$$R = \left(4(d_{D1}-d_{D2})^2 + (d_{P1}-d_{P2})^2 + (d_{H1}-d_{H2})^2\right)^{1/2}$$

where d_D: dispersive term
d_P: polar term
d_H: hydrogen bonding term

This value is an indicator for the solubility of a substance in a system. In general it can be said that as the values of the individual terms are more similar to each other for the solute and solvent, the magnitude of

the Hansen radius becomes smaller and the substance has a higher solubility in the solvent system.

3 RESULTS AND DISCUSSION

The grafting yield obtained in these various reactions relative to that for the reaction of styrene alone is shown in Figure 3. The relative grafting yield obtained when TAC is used as an additive increases steadily as the concentration of TAC increases. TAC does contain double bonds and could also be incorporated into the film during grafting and thus act to increase the graft level. No detectable TAC was found in the grafted films however. Tripropyloxycyanurate (TPOC) has a similar structure to TAC but does not have the potentially reactive allylic double bond group that TAC does. The relative grafting yield obtained when TPOC is used as additive increases much more quickly and to a greater extent than was found with TAC. Interestingly other nitrogen containing bases like pyridine (Figure 3) also yielded higher relative grafting levels than styrene alone. In contrast, the relative grafting yield obtained in the presence of 1,3-di-allyloxy-benzene (DAOB) was progressively lower as the concentration of DAOB increased. DAOB has a ring substituted with allyl ether groups like TAC, but the DAOB ring does not contain nitrogen and is not basic. Interestingly when these experiments were rerun in alcoholic solvent instead of toluene, no statistically significant difference was found between the grafting yields obtained in the presence or absence of the additives. From the first part of this investigation, it is clear that the bases promote the grafting reaction in toluene; whereas, allylic compounds inhibit the grafting reaction due to chain transfer reactions [3].
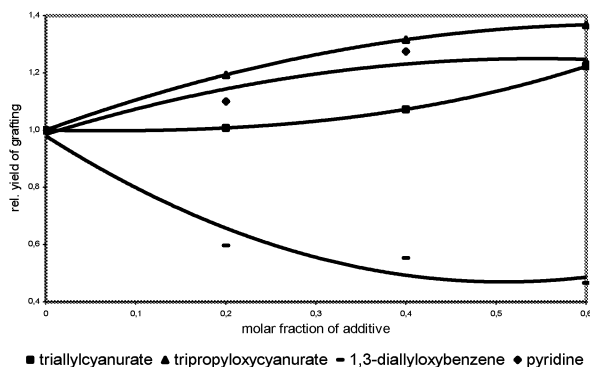
Fig. 3: Relative yields of grafting.

In the second part of this investigation, the influence of these additives on the polymerisation of styrene in solution was studied. Statistical analysis of the results found that the presence or absence of the additives had no significant influence on the yield of polymer product or its molecular weight. From these results it can be concluded that the promoting effects of the bases is limited to the radiation-grafting system.

In Figure 4 the value of the Hansen radius is shown for the solubility of styrene in either toluene or isopropanol as pyridine is added to the solvent system. As a comparison, the Hansen radius is shown for styrene in a grafted film matrix, FEP-g-PS. When the pyridine concentration increases, the Hansen radius increases in the toluene system, and the solubility of styrene

decreases relative to its solubility in the grafted film. Therefore it can be concluded that the base has a positive effect in terms of favouring the partitioning of styrene monomer into the grafted film where it is thus available for grafting. An increase in solubility rather than a decrease is observed when pyridine is added to iso-propyl alcohol. This analysis is only semiquantitative because we have considered the solvent and grafted film matrix as two separate and independent phases.
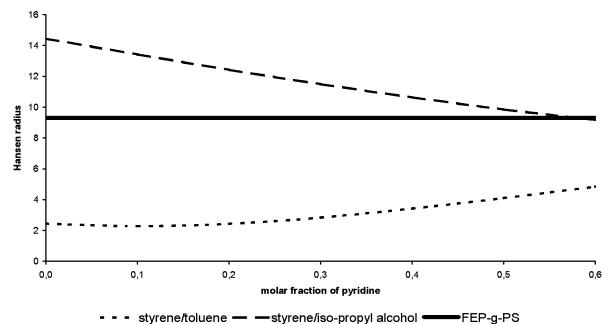
Fig. 4: Hansen radius for pyridine addition.

The results of this investigation indicate that the effect of TAC on the radiation-grafting process is primarily as a graft-promoting additive rather than as a crosslinker. The inhibiting chain transfer effect of the allyl groups is less important than the influence of the basic and polar ring in reducing the solubility of styrene monomer in non-polar solvents like toluene. This less favourable interaction with the grafting solvent system can act as a driving force in favouring the partitioning of monomer into the grafting film where its enhanced concentration acts to promote the grafting reaction and yield. The influence of these basic graft-promoting additives is somewhat similar to but of smaller magnitude than that of polar solvents like alcohols [5].

4 REFERENCES

[1] J. Huslage, T. Rager, B. Schnyder, A. Tsukada, *Radiation-grafted membrane/electrode assemblies with improved interface*, Electrochim. Acta **48**, 247 (2002).

[2] F.N. Büchi, B. Gupta, O. Haas, G. G. Scherer, *Performance of differently cross-linked, partially fluorinated proton exchange membranes in polymer electrolyte fuel cells*, J. Electrochem. Soc. **142**, 3044 (1995).

[3] H. P. Brack, G. G. Scherer, *Influence of crosslinkers on the water-swelling properties of radiation-grafted ion-exchange membranes*, ACS PMSE **79**, 457 (1998).

[4] Eric A. Grulke, in Polymer Handbook, 3rd ed., J. Brandrup and E. H. Immergut eds., Wiley, New York VII/519 (1989).

[5] T. Rager, D. Beckel, C. Noirtin, P. Muff, S. Schweri, O. Haas, J. Huslage, G.G. Scherer, *Radiation-grafted polymer films with improved mechanical properties*, PSI Scientific Report 2001, **V** 97-98 (2002).

INFLUENCE OF CROSS-LINKING ON THE PERFORMANCE AND STABILITY OF RADIATION GRAFTED MEMBRANES IN POLYMER ELECTROLYTE FUEL CELLS

T.J. Schmidt, K. Simbeck, M. Arcaro, T. Rager, G.G. Scherer

This contribution describes how cross-linking of radiation grafted and sulfonated FEP 25 membranes prepared at PSI influences the performance and stability of membrane electrode assemblies (MEA) based on these membranes. An optimum amount of cross-linking agent of 10 % was found to produce both the most stable and best performing membrane when used in polymer-electrolyte fuel cells (H_2/O_2 PEFC, 60°C to 80°C) with runtimes of more than 4000 hours without significant degradation.

1 INTRODUCTION

One of the main foci in polymer electrolyte fuel cell (PEFC) research at PSI is the development of a low-cost polymer electrolyte membrane with similar properties and performance than the state-of-the-art Nafion membranes. Recently, similar PEFC performance results as observed in Nafion 112 based cells could be obtained with PEFC consisting of MEAs with PSI's radiation-grafted and sulfonated FEP 25 membranes at 60 to 80°C over ca. 2500 h [1]. Generally, the addition of a cross-linker (*e.g.*, divinylbenzene) to the grafting solution is known to increase both the mechanical and chemical integrity of the membrane [2]. In this study, we systematically varied the concentration of divinylbenzene in the grafting solution between 0 % and 20 % and studied the behavior of the resulting membranes in MEAs in H_2-O_2 PEFCs.

2 EXPERIMENTAL

A Teflon FEP 100A film (*DuPont*) with 25 μm thickness was electron-beam irradiated with a dose of 3 to 5 kGy (*Studer AG, Switzerland*) and subsequently introduced into a stainless steel reactor with the grafting solution consisting of a mixture of styrene (S, *Fluka purum*) and divinylbenzene (DVB, *Fluka techn.*) in isopropanol/water (*Fluka purum* with deionized water) solvent. The DVB content in the monomer mixture was set to 0%, 2%, 5% 10%, and 20%. The degree of grafting of the samples was between 16 % and 19 %. Subsequently, the film was completely sulfonated with 2 vol-% chlorosulfonic acid in CH_2Cl_2 at room temperature [3]. For brevity, we refer to these membranes as PSI membranes in the following.

The swollen membrane and ELAT-electrodes from E-Tek (Natick, USA) with a Pt-loading of 0.6 mg cm^{-2} (20 % Pt/Vulcan XC72) and an additional impregnation (0.6-0.7 mg cm^{-2} dry mass) with solubilized Nafion® were hotpressed at 120°C [2]. MEAs were tested in graphite fuel cells with an active area of 30 cm^2 in a temperature range between 60 and 80°C using H_2 (humidified at the cell temperature) and dry O_2. The cells were operated at 1 bar$_a$ with a gas stoichiometry of λ=1.5.

In situ characterization of the radiation grafted and sulfonated FEP 25 membranes was carried out using electrochemical impedance spectroscopy (EIS, *Zahner IM6*) and an auxiliary current pulse method.

3 RESULTS

The initial behavior of the MEAs with differently cross-linked membranes was studied in PEFCs operated at 60°C. Figure 1 shows the cell voltage as a function of the DVB concentration in the grafting solution at varying current densities. Over the complete current density range, it turned out that the best performance could be obtained with a MEA consisting of a membrane with a S:DVB ratio of 10 %.
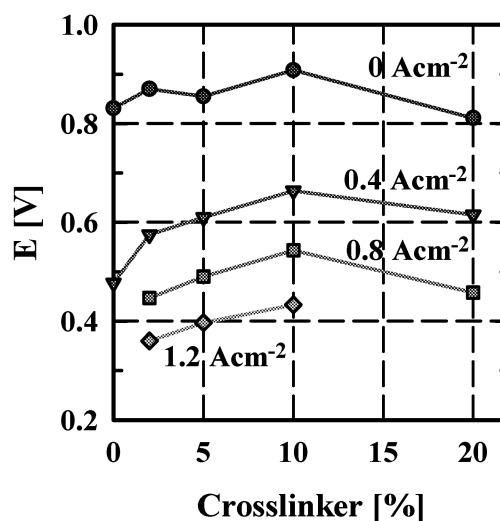
Fig. 1: Performance of H_2-O_2 PEFCs with PSI membranes with varying amounts of DVB at several current densities at 60°C.

For both lower and higher cross-linked membranes the performances of the cells were considerably less. In order to get more insight into the differences of the overall cell performance, electrochemical impedance spectroscopy, EIS, was performed. The resulting impedance spectra were carefully analyzed using modelling of the equivalent circuit representing a single fuel cell. Figure 2 illustrates the values of the electrolyte (membrane) resistance, R_{el}, and the charge transfer resistance, R_{CT}, as a function of DVB concentration in the grafting solution. Note that under our experimental conditions, R_{CT} is representative of the charge transfer on the cathode only. Interestingly, with the exception of the non-cross-linked membrane, the electrolyte resistance is increasing with increasing DVB content. Assuming that the DVB molecules in the final membrane are not sulfonated and the proton conductivity is

reduced *vs.* the non-cross-linked membrane, this finding is not surprising. On the first view, however, this observation contradicts the findings from Figure 1. However, Figure 2b gives a plausible explanation, since R_{CT} is significantly decreasing with increasing DVB content and appears to overcompensate the increasing membrane resistance. That is, in a general view, the sum of both R_{el} and R_{CT} is determining the cell performance and is lowest for the membrane with 10 % DVB. However, the puzzling question why the charge transfer resistance, which is carrying only electrochemical (kinetic) information, is dependent on the nature of the membrane can not be unambiguously answered. Our preliminary interpretation of that result is that membrane fragments, *i.e.*, initial degradation products, are transported to the electrodes and devastatingly influencing the kinetics of the electrochemical reactions.
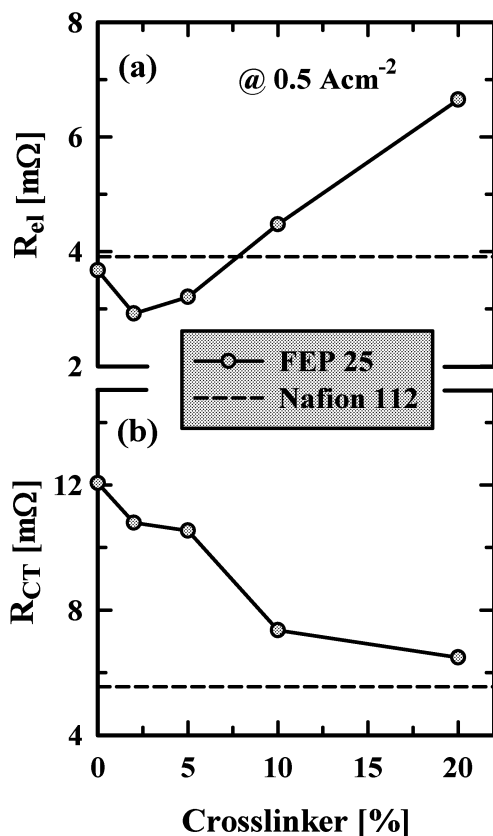
Fig. 2: Data of (a) electrolyte and (b) charge transfer resistance as a function of DVB concentration in the membrane extracted from impedance spectra (100 mHz to 20 kHz) at 0.5 Acm^{-2} and 60°C. The value for Nafion 112 is plotted as a reference.

To prove this hypothesis, all cells were operated at 60°C at 0.5 Acm^{-2} for ca. 200 hours in order to get an impression on the stability under operating conditions. It turned out that the MEAs with the 10 % and 20 % cross-linked FEP 25 membranes were the most stable without performance loss, whereas the lower cross-linked membranes showed significant degradation which was reflected by decreasing cell voltage concomitant with increasing membrane and charge trans-

fer resistance (data not shown). This finding at least does not contradict the aforementioned interpretation. Finally, we decided to run a long-time test with the best performing membrane (10 % DVB), see Figure 3. The cell was operated at 80°C at 0.5 Acm^{-2}. As obvious from Figure 3a, the cell voltage was very stable over the testing period of ca. 4600 hours. Additionally, the membrane resistance was followed continuously during the test (Figure 3b). Although a small tendency of slightly increasing membrane resistance determined in-situ by the auxiliary current pulse method (plotted as the specific area resistance) with increasing runtime can be observed, it can be considered as very stable. That is, no significant membrane degradation seems to occur. Additional results from EIS recorded every ca. 500 hours during the test clearly demonstrated the same result with respect to R_{el}, but with a slight increase of R_{CT} (ca. 10 % in the first 3000 hours). Increasing charge transfer resistances over several thousand hours operation is a typical result and can be interpreted by the surface area loss of the cathode [4] due to particle growth.
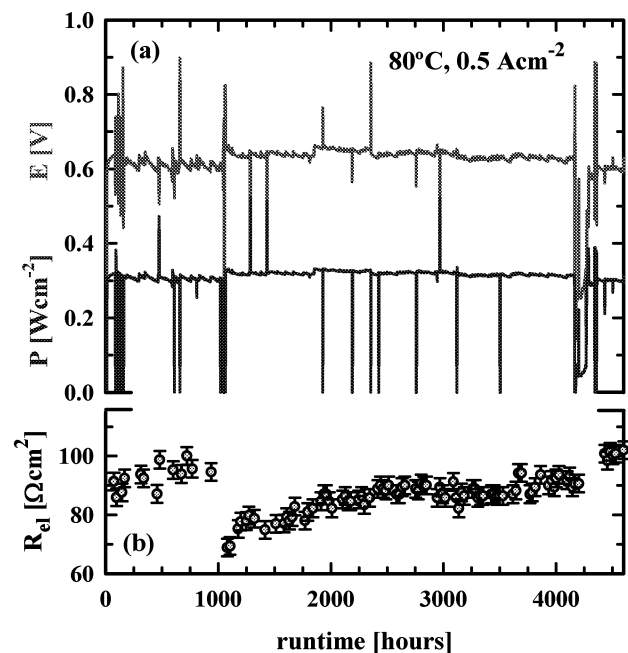
Fig. 3: (a) Long-time performance of a PEFC single cell with a FEP 25 membrane (10 % DVB) at 80°C and 0.5 Acm^{-2}. (b) Electrolyte resistance recorded during the long-time test.

4 REFERENCES

[1] T.J Schmidt, T. Rager, G.G. Scherer, PSI Scientific Report 2001, **V**, 95 (2002).

[2] B. Gupta, G.G. Scherer, J.G. Highfield, Angew. Makromol. Chem. **256,** 81 (1998).

[3] J. Huslage, T. Rager, B. Schnyder, A. Tsukada, Electrochim. Acta. **48,** 247 (2002).

[4] M.S. Wilson, F.H. Garzon, K.E. Sickafus, S. Gottesfeld, J. Electrochem. Soc. **140,** 2872 (1993).

CO-SPUTTERED Pt/C-LAYERS CHARACTERIZED BY CYCLIC VOLTAMMETERY, SMALL ANGLE X-RAY SCATTERING AND X-RAY PHOTOELECTRON SPECTROSCOPY

F. Hajbolouri, G.G. Scherer, T. Vad (FZ Jülich), M. Horisberger, B. Schnyder, A. Wokaun

PtC layers, 500 nm thick, have been co-sputtered by DC magnetron sputtering technique on smooth Glassy Carbon substrates. They were characterized by different techniques such as Cyclic Voltammetry (CV), X-ray Photoelectron Spectroscopy (XPS) and Small Angle X-ray Scattering (SAXS). The CV-measurements showed that the PtC layers are electrochemically active. A surface roughness of 14 cm^2 active area/cm^2 geometric area was calculated from the H-desorption peaks. The specific active surface area was estimated from the CV- and SAXS-results to 35 m^2/g, which is relatively large compared to the commercial Pt electrodes, with a value of 20 m^2/g.

1 INTRODUCTION

Commercial electrode catalysts are generally prepared by chemical wet impregnation methods. The challenge is to find alternative techniques to prepare reproducible catalysts with low loading and a narrow particle size distribution. In this work, we explore the potential of the sputtering technique for preparation of fuel cell electrodes. Sputtering is a flexible and simple method, which allows coating of large areas with uniform composition and high reproducibility. As a first attempt, we have co-sputtered thin layers of platinum and carbon (PtC) as well as pure carbon (C) on Glassy Carbon (GC) substrates and characterized them by mean of CV, SAXS and XPS.

2 EXPERIMENTAL

Sample preparation. Thin layers of C and PtC, 500 nm, were deposited on GC-substrates, 1 cm^2, in a DC magnetron apparatus built in-house, called TIPSI. *Sample characterization.* The cyclic voltammetry measurements were carried out in a electrochemical glass cell with three electrode arrangement purged with argon using 0.5 M H$_2$SO$_4$ as electrolyte. The XPS-analysis was performed in an ESCALAB 220i XL Photoelectron Spectrometer at PSI using monochromated AlKα (1486.6 eV) radiation. To determine the chemical composition as a function of depth, the sample surface was sputtered by an Ar-ion beam. The SAXS-measurements were performed at HASYLAB on PtC films co-sputtered on Al-foil.

3 RESULTS

Cyclic Voltammetry. Figure 1 shows the electrochemical behaviour of the C- and PtC-layers, measured by CV in a half cell containing 0.5 M H$_2$SO$_4$ as electrolyte. The H$_2$-adsorption and –desorption peaks in the voltammogram of the PtC layer confirm the electrochemical activity and the presence of the Pt particles in the layer. The C-layer contributed only to a small double layer capacity. The sputtering process proved to create a homogeneous film within a region of 4 x 4 cm, which was explored by comparing the voltammograms from four neighbouring samples.
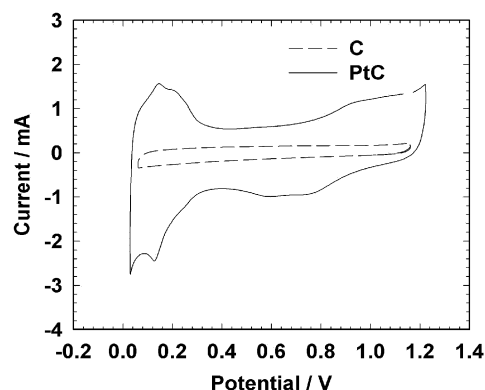
Fig. 1: Cyclic voltammograms of the sputtered C respective co-sputtered PtC in Ar-saturated 0.5 M H$_2$SO$_4$ at 25 °C.

The roughness of the samples was estimated to 14 cm^2 active area/cm^2 geometric area from the H-desorption peaks. Considering the low Pt loading, ~40 µg/cm^2 found by SAXS and ~70 µg/cm^2 estimated from the sputtering rate, this active area is relatively high compared to the commercial electrodes.

X-ray Photoelectron Spectroscopy. A Pt-loading of 3 at% on the surface and 9 at% in the bulk was found by XPS in the co-sputtered PtC-sample.

Small Angle X-ray Scattering. The size and the distribution of the Pt particles were measured by SAXS. We found two scattering centres in the co-sputtered PtC layers. The average particle size for the small and the big particles was approximatively 1.25 nm respective 4.8 nm.

4 CONCLUSION

It is possible to prepare electrochemically active PtC films, which have a specific active surface area comparable to the commercial Pt electrodes, by co-sputtering. The various sputter parameters have to be optimised.

5 ACKNOWLEDGEMENT

DEVELOPMENT OF CATALYSTS FOR THE OXYGEN REDUCTION REACTION

N. Lempola, B. Steiger, T.J. Schmidt, G.G. Scherer, A. Wokaun

The performance of direct methanol fuel cells (DMFC) is strongly hampered by the poor kinetics of both the methanol oxidation reaction (MOR) and the oxygen reduction reaction (ORR). In addition to the kinetic issues, the DMFC cathodes are also depolarised by methanol that is permeating through state-of-the-art polymer electrolytes. The aim of this work is to study the kinetics of perovskites and pyrochlores as electrocatalysts for both MOR and ORR in acid solution using the thin film rotating ring-disk electrode technique.

1 INTRODUCTION

Traditional strategies for the development of direct methanol fuel cells (DMFC) concentrate on the development of efficient catalysts for methanol oxidation reaction (MOR) and the oxygen reduction reaction (ORR) while separating them with solid electrolyte semipermeable membranes that prevent methanol to diffuse to the cathode side where it causes depolarisation. This cell design would require very low methanol permeable membranes. An alternative would be to use an oxygen reduction electrode, which is not depolarised by methanol. Our studies concentrate on perovskites and pyrochlores. The study on the oxide catalysts aims at gaining a general view on the electrocatalytic behaviour towards the ORR and the MOR in order to select the best materials for more detailed and defined studies.

2 EXPERIMENTAL

Oxides were prepared using drop-pyrolysis and solid-state reaction techniques. Samples were characterized by powder X-ray diffraction. Kinetics of oxygen reduction of ruthenium containing perovskites and pyrochlores were studied using the rotating-ring disk electrode technique [1]. For comparison a commercially available catalyst of 20 wt-% platinum supported on Vulcan XC72 was used. Electrodes were prepared using a glassy carbon electrode onto which an aliquot of catalyst suspension was pipetted. The catalyst was attached to the electrode with an ultra-thin Nafion film. Oxides were either unsupported or supported with Vulcan XC72. Measurements were conducted in a three-compartment electrochemical cell using an interchangeable ring-disk electrode setup with a bi-potentiostat and rotation control. Measurements were conducted at room temperature.

3 RESULTS

Sr_3NiPtO_6 could be prepared as a single-phase oxide. $SrPt_{0.5}Ru_{0.5}O_3$ and $Bi_2Pt_{0.5}Ru_{1.5}O_{7.3}$ could not be prepared as single-phase oxides, there was always some metallic platinum present. The amount of pure platinum in ruthenium containing samples could not be estimated and so its impact on the results is not unambiguously clear. Pyrochlores and perovskites that contained ruthenium but no platinum ($Bi_{1.25}Na_{0.75}Ru_2O_7$, $Bi_{1.6}Ag_{0.4}Ru_2O_7$, and $SrRuO_3$) did

not show activity for ORR in acidic solution. Sr_3NiPtO_6, showed activity for ORR. Diffusion limited currents were not reached for the ORR implying mixed kinetic diffusion-controlled ORR at potentials over the entire potential range. All ORR active catalysts showed some activity for the methanol oxidation.
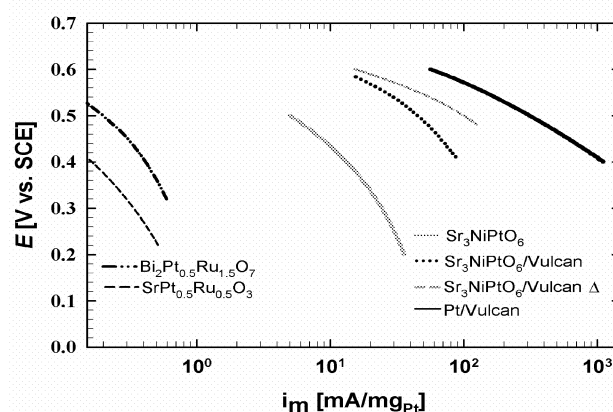
Fig. 1: Mass-specific Tafel plots for Pt/Vulcan (14 $\mu g_{Pt}/cm^2$), $Bi_2Pt_{0.5}Ru_{0.5}O_7$ (300$\mu g_{Pt}/cm^2$), $SrPt_{0.5}Ru_{0.5}O_3$ (300$\mu g_{Pt}/cm^2$) and Sr_3NiPtO_6 (50 $\mu g_{Pt}/cm^2$) unsupported and Vulcan supported (with heat treatment (Δ) and without), 1600 rpm, RT.

Figure 1 shows the mass-specific Tafel-plots for Pt/Vulcan and for Sr_3NiPtO_6 in three different pretreatments. The best activity was achieved by mixing catalyst and Vulcan XC72 followed by heat treatment at 600 °C for one hour. The difference between heat treated and not treated catalyst is not significant. A possible cause for the enhanced activity could be a better contact of the catalyst and the support through heat treatment. A direct quantitative comparison of catalysts is not possible because the mean particle sizes and the catalyst loadings differ from each other. According to the Tafel-plots among the oxide catalysts Sr_3NiPtO_6 shows the best activity for the pure ORR. The ruthenium containing catalysts show considerably lower catalytic activity for ORR compared to the Pt/Vulcan or Sr_3NiPtO_6.

4 REFERENCES

[1] T.J. Schmidt, H.A. Gasteiger, G. Staeb, P.M. Urban, D.M. Kolb, R.J. Behm, J. Electrochem. Soc. **145**, 2354 (1998).

STRUCTURAL MODIFICATIONS OF MODEL Cu/ZnO CATALYSTS DURING METHANOL REFORMING

F. Raimondi, J. Wambach, A. Wokaun

The structural changes of Cu/ZnO/Si model catalysts during methanol reforming have been investigated by X-ray photoelectron spectroscopy (XPS), Ar-ion XPS depth profiling and atomic force microscopy (AFM). ZnO migration onto the surface of the Cu clusters is observed during methanol reforming in the absence of water. The formation of Cu(II) when water is present in the reactant mixture is associated with an increase of the dispersion of the Cu phase. Both surface modifications are observed for industrial Cu/ZnO-based catalysts under the same reaction conditions, leading to a pronounced decrease of the catalytic activity.

1 INTRODUCTION

One of the most promising processes for the on-board production of hydrogen-rich gas mixtures in fuel cell-powered vehicles is methanol autothermal reforming:

$$4\ CH_3OH + 3\ H_2O + \tfrac{1}{2}\ O_2 \Rightarrow 4\ CO_2 + 11\ H_2$$
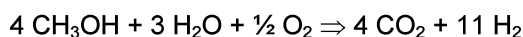
This process is effectively catalysed by Cu/ZnO-based materials at temperatures between 200 and 300°C. The chemical and structural properties of the catalyst surface during methanol reforming are strongly affected by the specific reaction conditions (e.g. temperature and composition of the reactant mixture) [1]. The characterisation of a Cu/ZnO/Si model catalyst by XPS, Ar-ion XPS depth profiling and AFM after exposure to various methanol reforming conditions was undertaken in order to study the dependence of the catalyst structure on the methanol reforming conditions.

2 EXPERIMENTAL

The model catalysts were prepared in ultra-high vacuum (UHV) by evaporation of Cu onto 100 nm thick ZnO films deposited on Si(100) by DC magnetron sputtering [2]. Prior to the spectroscopic characterisation experiments, the model catalysts were exposed to various methanol reforming conditions at 280°C and 1.5 bar for 16 hours in the high-pressure reactor integrated in the UHV system.

3 RESULTS

The oxidation state of Cu on the model catalyst surface is a function of the composition of the methanol reforming feed. In the absence of water and with an O_2/CH_3OH molar ratio ≥ 0.33 Cu(I) is predominant, whereas at lower O_2/CH_3OH molar ratios Cu remains in the metallic state. When Cu is in the metallic state migration of ZnO onto the surface of the Cu islands occurs, as shown by the Ar-ion depth profile in Figure 1. The increase of the Cu $2p_{3/2}$/Zn $2p_{3/2}$ atomic ratio observed in Figure 1 at etching times lower than 1000 s indicates that a layer of ZnO covering the Cu surface forms during methanol reforming and is removed by the Ar-ion etching treatment.

In the presence of water in the feed Cu(II) is formed after methanol reforming with an O_2/CH_3OH molar ratio ≥ 0.42. The AFM images shown in Figure 2 indicate that formation of Cu(II) is associated with higher dispersion of the Cu phase. As a matter of fact, more abundant and smaller Cu clusters are observed on the Cu(II)-containing surface (Figure 2b) than for the

Cu(II)-free sample (Figure 2a). ZnO migration onto the surface of the Cu clusters and redispersion of the Cu phase in the presence of Cu(II) are observed under the same reaction conditions for industrial Cu/ZnO-based catalysts as well, leading to a pronounced decrease of the catalytic activity.
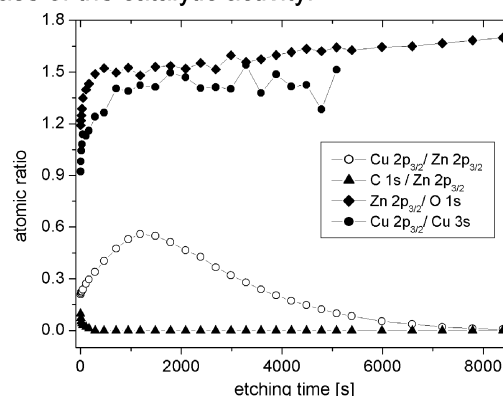
Fig. 1: Ar-ion XPS depth profile of a Cu/ZnO/Si model catalyst after methanol reforming with an O_2/CH_3OH molar ratio of 0.11 (no water in the feed).
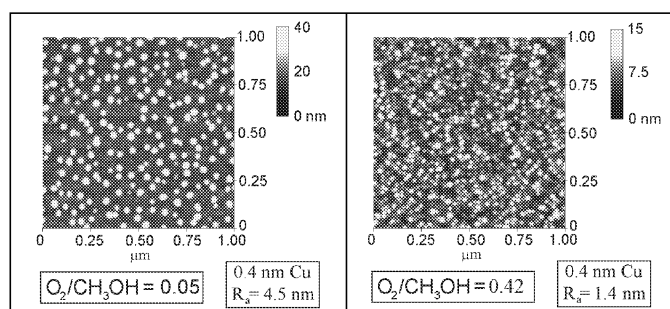
Fig. 2: AFM images of Cu/ZnO/Si model catalysts after methanol reforming with two different O_2/CH_3OH molar ratios (water present in the feed). R_a indicates the average surface roughness calculated from each AFM image.

4 ACKNOWLEDGEMENTS

5 REFERENCES

[1] F. Raimondi, K. Geissler, J. Wambach, A. Wokaun, Appl. Surf. Sci. **189**, 59 (2002)

[2] F. Raimondi, B. Schnyder, R. Kötz, R. Schelldorfer, T. Jung, J. Wambach, A. Wokaun, Surf. Sci., in press.

ENHANCEMENT OF CO-TOLERANCE IN POLYMER ELECTROLYTE FUEL CELLS BY INCREASED CELL TEMPERATURE

F. Hajbolouri, B. Andreaus, G. Scherer, A. Wokaun

AC-impedance spectroscopy has been employed to investigate the temperature dependence of CO-poisoning in a 30 cm² fuel cell for commercial Pt E-tek electrodes. An inductive behavior was shown to be characteristic for the CO-poisoning on Pt at higher current densities, above 200 mA/cm², and for CO-contents higher than 50 ppm. At lower current densities where the CO-oxidation is slight or negligible no inductive behavior was observed. The increase of cell temperature from 90 °C to 100 °C decreased the charge transfer resistivity by a factor of 4. A simple model was established for a quantitative analysis of CO-poisoning.

1   INTRODUCTION

Carbon monoxide, CO, is a severe catalyst poison for the Pt anode electrode and leads to significant performance degradation by blocking most of the catalyst sites for the hydrogen oxidation reaction (HOR) in polymer electrolyte fuel cells. In principal, all solutions to avoid the CO-poisoning on a Pt catalyst are aimed to either decrease the catalyst surface coverage by CO or promoting the catalytic oxidation rate of the adsorbed CO-species (CO_{ads}). Higher temperatures promote the electro-oxidation rate of H_2 and CO, and also reduce the CO-coverage on the Pt surface, since adsorption is an exothermic reaction.

This study is devoted to the investigation of the influence of the cell temperature and CO-content on CO-poisoning for commercial Pt and PtRu E-tek electrodes by means of AC-impedance spectroscopy. A simple model has been established in order to estimate the parameter values of the CO-poisoning from the impedance spectra [1].

2   EXPERIMENTAL

All measurements were performed in a 30 cm² test cell with meander flow field graphite plates. Commercially available Pt/C or PtRu/C (50:50 atom%) gas diffusion electrodes from E-Tek, (0.6 $mg_{noble\ metal}/cm^2$) were used as anode and Pt (0.6 mg_{Pt}/cm^2) as cathode. Nafion 115 membranes served as electrolyte. Both inlet gases, fuel and oxidant, were humidified at a dew point of 95 °C and pressurized at 3 bar_a. The cell temperature ranged between 80-100 °C. With our cell setup, operating temperatures above 100 °C lead to a drying out of the electrolyte membrane, even at dew points of 95 °C of the gases, causing a performance loss of the fuel cell. Impedance measurements were performed using an IM6 electrochemical workstation and an EL300 high current load. The spectra were recorded in galvanostatic mode and a frequency range from 50 mHz to 10 kHz.

3   RESULTS

Influence of the cell temperature

Figure 1 shows a comparison of the polarization curves for the fuel cell using a Pt, respectively a PtRu electrode, as anode in the temperature range 80-100 °C. The polarization curves for Pt and PtRu over-

lap with each other when H_2 is used as fuel. For the H_2/100 ppm CO fuel, at 100 °C, the Pt electrode shows a superior performance compared to the PtRu electrode, while this ranking is reversed at temperatures below 100 °C. A significant enhancement of the CO-tolerance was obtained for the Pt anode electrode when the cell temperature was increased from 90 °C to 100 °C. For this reason, AC-impedance measurements were carried out in a complete fuel cell to study the temperature influence at 90 °C and 100 °C on the behaviour of the Pt-anode electrode.
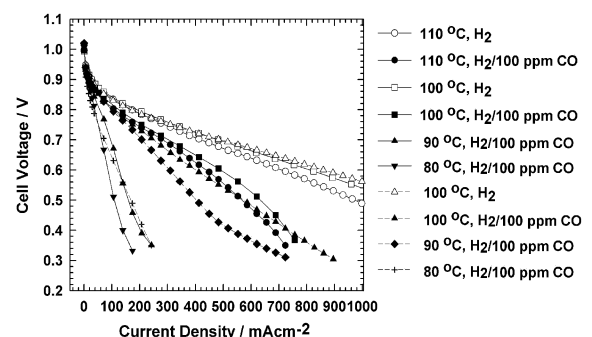
Fig. 1: Influence of the cell temperature on the fuel cell performance, using H_2 respective H_2/100 ppm CO as fuel. P_{O2} = P_{H2} = 3 bar_a, T_{hum}=95 °C. Comparison between Pt (solid lines) and PtRu (dotted lines) anodes.
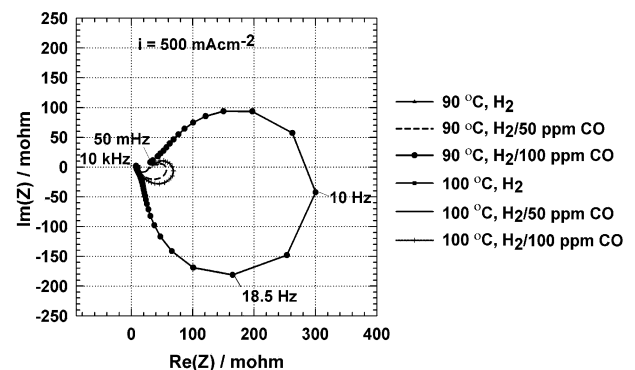
Fig. 2: Nyquist plots of the fuel cell impedance for pure H_2, H_2/50 ppm CO respective 100 ppm at 90 °C and 100 °C. The Nyquist plot of the pure H_2 spectrum is vanishingly small. E-Tek Pt-anode.

Figure 2 illustrates the influence of temperature and CO-content on the impedance response of the cell. Below 100 Hz an inductive behaviour was found to be

characteristic for CO-poisoning at a cell current density of 500 mA/cm^2. The boundary, where the inductive behavior disappeared in the impedance spectrum showed to be <50 ppm CO and >100 °C for our experimental set up. The limit for the cell current density was found to be 200 mA/cm^2, which means that below this current density no inductive loop was observed. Above 200 mA/cm^2 the anode over-potential reaches values suitable for oxidation of CO_{ad} on Pt.

Modeling of the impedance response due to CO-poisoning

In order to understand the impedance spectra and to extract the relevant system parameters, e.g., the charge transfer resistance for HOR and the CO-surface coverage, a simple kinetic model for the impedance response of a PEFC with H_2/CO as a fuel was set up. It is based on the kinetic equations for the reactions involved:

$$2H_{ad} \xrightarrow{\ k_r^H\ } 2H^+ + 2e^- \qquad (1)$$

$$CO + Pt \xleftrightarrow{\ K_{CO}\ } Pt - CO_{ad} \qquad (2)$$

$$CO_{ad} + OH_{ad} \xrightarrow{\ k_r^{CO}\ } CO_2 + H^+ + e^- \qquad (3)$$
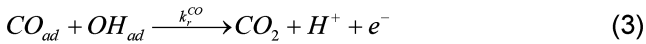
$K_{CO} = k_{ad}^{CO}/k_{des}^{CO}$ represents the equilibrium constant of the CO-adsorption. We assume that the CO-adsorption, described by the CO-coverage θ_{CO}, is governed by a Langmuir-isotherm. In view of the very low exchange current density for the CO-electrooxidation, the observable current can be set equal to the faradaic current from the hydrogen oxidation reaction.

$$j = j_H = 2Fc_H k_r^H \left(1 - \theta_{CO}\right)^2 \sinh\left(\frac{\eta_{anode}}{b_H}\right) \qquad (4)$$

To allow for an analytical solution of the impedance response, we did not include any mass transport phenomena for hydrogen as well as for CO. The resulting impedance function $Z(\omega)$, including the faradaic impedance in parallel to the double layer charging, can be expressed as follows:

$$Z(\omega) = i\omega C_{dl} + \left\{\frac{1}{R_{ct}} + \frac{1}{R_0 + i\omega L}\right\}^{-1} \qquad (5)$$

C_{dl} represents the double layer capacity, R_{ct} the charge transfer resistance of the HOR defined by $R_{ct} = \delta\eta_{anode}/\delta j$. R_0 and L represent parameters, which depend on the rate constants of equations (1) - (3). The faradaic impedance part of $Z(\omega)$ may be represented by the well known equivalent circuit of a resistivity R_0 in series with the inductivity L, branched in parallel to R_{ct}.

The model is able to qualitatively reproduce the impedance pattern of a CO-poisoned fuel cell as shown in Figure 2, but fitting of the experimental spectra to the model is difficult due to temporal instabilities of the

recorded spectra, additional unidentified impedance features, and the abundance of relatively ill-defined model parameters like the adsorption/desorption rate constants and the current-overpotential characteristics for the CO-electrooxidation.
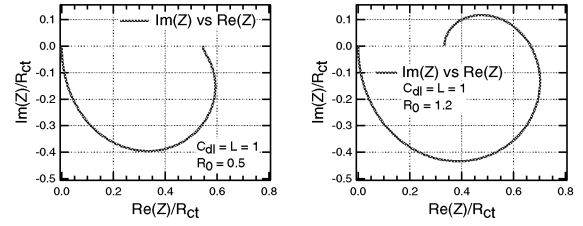
Fig. 3: Model spectrum at low (left graph) and at high (right graph) anode overpotential. The CO-surface coverage of the right figure will be lower, provided that the same model parameters are used.

As observed with the experimental spectra, the model may include, in the Nyquist representation, a transition from a pure capacitive semi-circle to a spectrum with an inductive arc at the low frequency end as shown in Figure 3.

4 CONCLUSION

An inductive loop at low frequencies showed to be characteristic for CO-poisoning on Pt electrodes of E-Tek type at current densities above 200 mA/cm^2, cell temperatures below 100 °C and CO-contents above 50 ppm. Therefore, it can be concluded that the inductive behaviour originates from a synergic effect between a certain CO-coverage and the reaction mechanisms belonging to the electro-oxidation of CO. The phenomena observed for the commercial E-Tek Pt/C and PtRu/C electrodes inclusive their temperature-performance dependence might be specific for the features of these particular electrodes, but the fact that the CO-tolerance increases by increasing the cell temperature is well-explored and should be the challenge for the future research. A simple kinetic model of the impedance response of an H_2/CO-O_2 fuel cell allows for the estimation of important cell parameters like the charge transfer resistance of the HOR and the CO-surface coverage without the need of fitting the experimental data to the model.

5 ACKNOWLEDGEMENTS

6 REFERENCES

[1] F. Hajbolouri, B. Andreaus, G.G. Scherer and A. Wokaun, *Temperature dependence of CO-poisoning in a polymer electrolyte fuel cell,* Extended Abstracts, 2002 Fuel Cell Seminar, Palm Springs, USA, November 18-21 (2002).

ON THE PROBLEM OF REFERENCE ELECTRODES IN POLYMER ELECTROLYTE FUEL CELLS

H. Kuhn, B. Andreaus, G.G. Scherer, A. Wokaun

A reference electrode incorporated in the fuel cell would give a better insight into the processes at the anode and cathode interfaces. However, due to the small membrane dimensions, efforts have to be under-taken in order not to disturb the current distribution or to induce a change in the membrane water balance. A reference electrode arrangement besides the anode was investigated. First AC-impedance spectroscopy measurements between the anode and the cathode with respect to the reference electrode are presented.

1   INTRODUCTION

The availability of *in situ* diagnostic tools to reveal the rate limiting processes of H_2/air polymer electrolyte fuel cells (PEFC) is of utmost importance for the further development of this technology. A powerful method to perform such measurements is the electrochemical impedance spectroscopy, EIS. It allows for the determination of the charge transfer kinetics as well as a quantitative analysis of the double layer capacity and the ionic resistance of the electrolyte membrane. Usually, the EIS measurements are carried out on the whole cell and the anode contributions of the H_2 oxidation reaction (HOR) to the total cell impedance are neglected, the measured impedance being attributed completely to the cathode and the O_2 reduction reaction (ORR) and the electrolyte. However, it was shown that the anode might contribute substantially to the cell potential loss, especially at high current densities [1,2]. The most common way to separate anode and cathode contributions to the cell potential losses is to use a reference electrode (RE). For PEFCs, several problems occur with the incorporation of a reference electrode at a defined and stable potential due to the thin solid electrolyte.

In the following, we investigate a possible reference electrode arrangement, discuss its limitations and present first results of EIS-measurement.

2   REFERENCE ELECTRODE ARRANGEMENT

In one possible arrangement, the reference electrode (RE) is placed sidewise of an electrode, as shown in Figure 1. This arrangement has already been tried for PEFCs as well as for other fuel cell types [3].
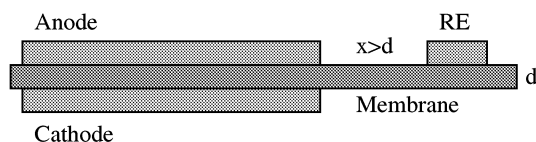
Fig. 1: Reference electrode arrangement of the electrodes employed in the experiments.

If the electrodes are congruent and the reference electrode is placed more than one membrane thickness away of the electrode edge, the RE is probing the potential in the middle of the electrolyte membrane. However, such a perfectly congruent electrode assembly is difficult to achieve and a realistic view is

that the electrodes edges are displaced. Figure 2 shows a distribution of the potential Φ between the electrodes in a fuel cell where the electrode edges are displaced by one half of the membrane thickness d (for Nafion112 the membrane thickness is nearly d = 60 μm, a value which is below practical fuel cell assembly precision). The electrode potentials are arbitrarily chosen to have values of -1 and 1. The potential measured by the RE deviates significantly from the potential value in the middle of the membrane. In fact, it may vary undeterminably between the potential of the anode or the cathode [3].
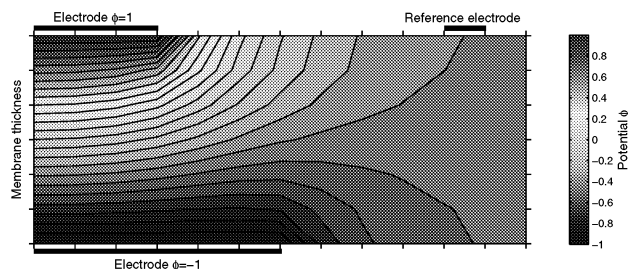
Fig. 2: Potential distribution in the interspace of displaced electrodes.

To overcome the problem of the undefined electrolyte potential drop due to the electrode misalignment, we have thought of another type of RE. Here, a very thin glass capillary should be brought in contact with the electrolyte membrane to form a Luggin-type RE. However, several problems hindered the successful incorporation of this type of RE: In order not to disturb the local current distribution around the RE sensing point, the capillary diameter should not exceed the dimensions of some 10 μm. Moreover, the membrane acidity and water balance should not be disturbed by the electrolyte of the capillary. Further work on this kind of reference electrodes is in progress.

3   EXPERIMENTAL

A graphite cell with a rectangular active area of 29 cm^2 and with a reference electrode located beside the anode was used. To apply the reference electrode as a NHE, it is supplied with hydrogen from the meander-type flow-field. E-TEK electrodes with a catalyst loading of 0,6 mg/cm^2 Pt/C, impregnated with 0,6 mg/cm^2 Nafion solution, were employed for both anode and cathode. Nafion 115 from DuPont served as electrolyte. The cell was operated at a cell tem-

perature of 60°C. The hydrogen was humidified at a dew point of 65°C. The EIS measurements were carried out using a Zahner IM6 workstation (Kronach, Germany) in addition with a current sink EL300. The measurements were performed in galvanostatic mode with an AC current amplitude of 0.2 A.

4 RESULTS

Figures 3-5 show the first results for the EIS measurements done with the proposed RE arrangement.

Figure 3 exhibits the measured spectra between the cathode and the reference electrode. This kind of spectrum is well known and is akin to measurements between anode and cathode. The charge transfer resistance R_{ct} for the ORR and the ohmic resistance between the cathode and the RE can be extracted out of this plot.
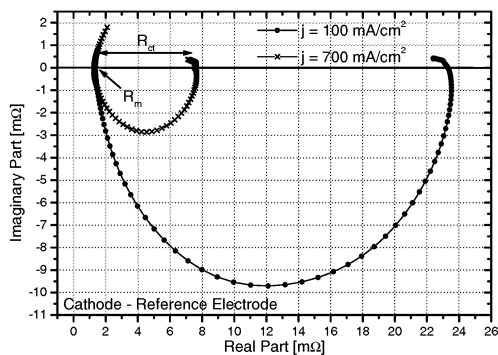
Fig. 3: Impedance measurement between cathode and RE at current densities of 100 and 700 mA/cm^2.

The spectrum interpretation becomes less evident for the measurements between the anode and the RE. As depicted in Figure 4, several semi-circles occur in the spectra, including an inductive loop in the mid-frequency range. Up to now, it is not clear for us whether this is an artifact from the experimental setup or whether it can be attributed to the hydrogen oxidation reaction (HOR). As it is described below, limited interpretation is still possible even when the spectra are not understood at this time. These findings suggest that the measured spectra may represent the HOR in a meaningful way.
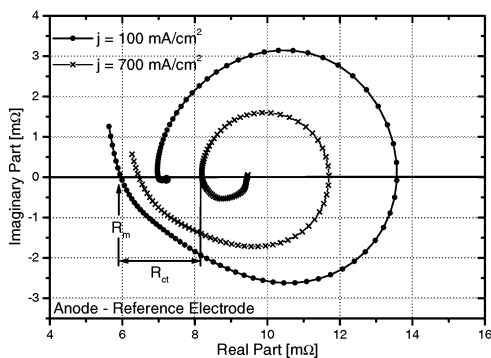

Fig. 4: Impedance Measurement between anode and RE at current densities of 100 and 700 mA/cm^2.

Figure 5 shows the comparison between the EIS measurements for the anode as well as the cathode against the RE to the results of EIS measurement between anode and cathode at several current densities. Evaluated are the membrane resistance R_m and the charge transfer resistance R_{ct}. R_m can be expressed as the sum of the ohmic resistances of the single measurements and, as it may be seen from Figure 5, it fits well to the value of R_m of the anode-cathode measurement.
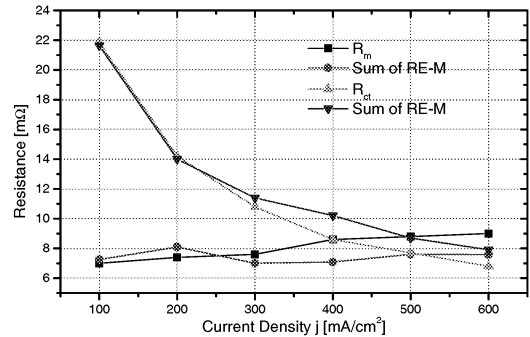
Fig. 5: Evaluated data of measurements at different current densities compared to an anode-cathode EIS.

The values of the charge transfer resistance, R_{ct}, may be brought in accordance if the R_{ct}-value of the anode-RE measurement is determined as the difference between the high frequency and the low frequency real axis intersection, as displayed in Figure 4. From this observation, one might speculate whether the hydrogen adsorption step, expressed by the inductive loop in the impedance spectra, might become limiting for the HOR.

5 OUTLOOK

In order to determine the system parameters of both electrodes, anode and cathode, it is necessary to introduce a reference electrode into the fuel cell. Preliminary impedance measurements results with a reference electrode arranged sideways of the anode showed that the cathode impedance shows the characteristic pattern for a charge transfer resistance, whereas the anode spectra are not yet fully understood. A further investigation with regard to capillary reference electrodes might lead to more accurate results and is therefore still needed.

The overall problem are the small dimensions of the membrane and hence the influence of a reference electrode on the local current distribution at the sensing point of the reference electrode.

6 REFERENCES

[1] B. Andreaus, A.J. McEvoy, G.G. Scherer, Electrochim. Acta **47**, 2223 (2002).

[2] B. Andreaus, G.G. Scherer, Solid State Ionics, to be published.

[3] B. Andreaus, Ph. D. Thesis, no 2598, EPF Lausanne, Switzerland (2002).

INTERPRETATION OF THE CURRENT-VOLTAGE CHARACTERISTICS OF POLYMER ELECTROLYTE FUEL CELLS BY IMPEDANCE SPECTROSCOPY

B. Andreaus, A.J. McEvoy (EPF Lausanne), G. Scherer

We applied electrochemical impedance spectroscopy (EIS) to elucidate the origins of the voltage losses of a H_2/O_2 polymer electrolyte fuel cell (PEFC) as a function of current density. The results indicate that the commercial electrodes utilized in these experiments suffer from a substantial loss in active catalyst surface already at relatively low current densities. The drying out of the electrolyte in the membrane adjacent to the anode as well as in the anode active layer results in an additional voltage loss at high current densities. Therefore, the purely structural aspects of a robust triple phase boundary sustaining harsh conditions under load is at least equally important as the proper choice of catalyst for a high performance PEFC-electrode.

1 INTRODUCTION

The current-voltage (IE) characteristic represents a simple and efficient method to estimate and to compare a specific fuel cell membrane-electrode assembly. This method determines the voltage and therefore also the power density as well as the efficiency as a function of the cell current density j. With increasing current density, the voltage drops exponentially from the "practical" equilibrium potential (or OCP) at around 1 V (small current density region) until the voltage decays proportionally beyond approximately $j = 100$-200 mA/cm^2. This intermediate current density regime is followed by an additional voltage drop at high current densities.

However, the underlying mechanisms, which limit the cell potential for different current densities, cannot be assessed by this method, because the contributions of the different fundamental processes overlap and are difficult to separate. Therefore, to gain further insight in the origins of the voltage limitations at different current densities, we have applied electrochemical impedance spectroscopy, EIS.

2 EXPERIMENTAL

All experiments were carried out in 28.3 cm^2 active area stainless steel cells without a flow field to keep the current distribution as homogeneous as possible. The cell was operated with H_2/O_2 with an excess of 50% in stoichiometric gas flow, at ambient pressure, and at 75°C. We used electrodes from E-Tek Corp., USA, with a platinum loading of 0.6 mg/cm^2 Pt/C and Nafion 115 membranes of 125 μm_{dry} thickness. The EIS spectra were recorded by means of an IM6 electrochemical workstation from Zahner in galvanostatic mode, but with a potential perturbation of 5 mV.

3 RESULTS

Limiting step at low current density

The exponential decay of the voltage curve at low current densities is due to the activation of the oxygen reduction reaction (ORR), a fact, which is well known in literature [1]. The impedance measurements corroborate this assumption, as only a charge transfer limitation is observed in the impedance plots. The contribution of the reversible hydrogen oxidation reaction (HOR) to this charge transfer resistance can be neglected.

Limiting step at intermediate current density

The linear slope of the voltage function has often been attributed to the ohmic resistance of the fuel cell. This resistance would mainly be due to the electrolyte membrane resistance for proton conduction [2]. In contrast to this assumption, the impedance results reveal that two different processes contribute to the voltage loss in this regime, and that the linearity is rather accidental.
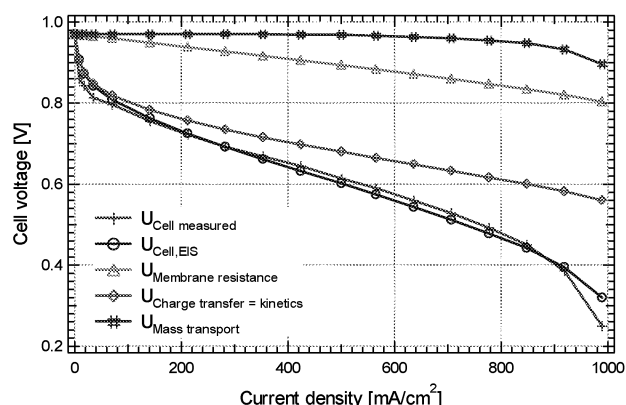
Fig. 1: Contributions of the different fundamental processes to the voltage drop of a PEFC as a function of the current density. Also shown is the good agreement between the measured current voltage plot and the one extracted from the EIS data.

In Figure 1, the contributions of the different fundamental processes to the voltage drop, as extracted from EIS measurements, are plotted as a function of the current density. In the linear range of the voltage function, the slope of the voltage drop due to the membrane resistance is only half of the total slope of the IE-curve. Therefore, the contribution of the membrane resistance to cell voltage drop is only around 50% to the total voltage loss. The other part stems from the continuing rise of the charge transfer resistance, which does not level off even at high current densities.

At a first glance, this behavior seems rather surprising because the Butler-Volmer kinetics predict an exponential decay of the charge transfer resistance, R_{ct}. Thus the contribution of the charge transfer process to the cell potential loss at these over-potentials should become negligible. The difference between the observed R_{ct} and the R_{ct} predicted from the Butler-Volmer theory is depicted in Figure 2.
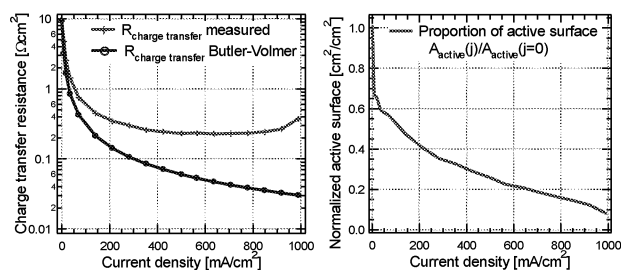
Fig. 2: a) Comparison of the measured R_{ct} with its values given by the Butler-Volmer equation as a function of current density. **b)** Proportion of active surface when compared to the active surface at open circuit $A_{active}(j=0)$, the latter value being extracted from *in situ* CV measurements.

We have interpreted this discrepancy in R_{ct} by the loss of active surface area with increasing current density. As R_{ct} is inversely proportional to the active surface area A_{active}, a loss of A_{active} has a significant influence on the value of R_{ct}. Having determined $A_{active}(j = 0)$ by *in situ* cyclic voltammetry measurements, we have estimated the active surface loss from the R_{ct} measurements. The losses are substantial: As shown in Figure 2b, the active surface at $j = 500$ mA/cm^2 is only roughly 25% of its open circuit value $A_{active}(j = 0)$. Moreover, only 30-35% of the catalyst surface area is active at open circuit conditions for this type of catalyst [3]. Therefore, at a current density of 500 mA/cm^2, only approx. 8-9% of the whole catalyst surface area remains active.

It is difficult to spot the exact origins of the loss regions. In view of the significant loss in A_{active} at already low current densities, we believe that mainly the small pores inside of a Pt/C-PTFE-Nafion agglomerate in the cathode are blocked by flooding of product water [4]. With increasing current densities, a contribution from the anode may arise from the drying of the electrolytic channels in the anode active layer.As a conclusion, the porosity and the wetting properties of the active layer structure are vital for a sufficient catalyst utilization.

Limiting step at intermediate current density

We have already shown [5-7] that for a H_2/O_2 fuel cell, the additional voltage loss at high current densities originates from the drying out of the electrolyte at the anode. Due to the electro-osmotic drag, water is transported off the anode to the cathode.

The drying out of the electrolyte has two effects: First, the low water content in the membrane leads to a high local membrane resistivity and therefore to an increased total membrane resistance. Second, the lack of water molecules in the electrolytic channels of the anode active layer inhibits the hydration of the protons formed by the HOR. Therefore, many catalytic sites become inactive and the charge transfer resistance for the HOR rises due to the decrease in active surface.

In the impedance spectra, these phenomena appear as an increased high frequency resistance (corresponding to a increased membrane resistance) and as a rise in the charge transfer resistance, due to the increased anode charge transfer resistance. In the low frequency range, an additional mass transport resistance arises due to both effects, the low water content in the membrane as well as in the electrolytic channels of the anode active layer.

4 CONCLUSION

In this report, we have shown that electrochemical impedance spectroscopy allows for the determination of the limiting processes in a PEFC at different current densities. We have demonstrated that for the commercial electrodes used in these experiments, the loss in active surface is substantial with increasing current densities. Therefore, with an optimized active layer structure, significant enhancements of the cell performance are possible without increasing the noble metal catalyst content.

5 ACKNOWLEDGEMENTS

6 REFERENCES

[1] Fuel Cell Handbook, 5th ed., *EG&G Services, US Dept. of Energy*, (2000).

[2] J. Kim, S. M. Lee, S. Srinivasan and C. E. Chamberlin, *J. Electrochem. Soc.* **140**, 2670 (1995).

[3] M. Staub, Ph.D Thesis, No. 11285, ETH Zürich (1996).

[4] M. Uchida, Y. Aoyama, N. Eda and A. Ohta, *J. Electrochem. Soc.* **142**, 4143 (1995).

[5] F. N. Büchi and G. G. Scherer, *J. Electrochem. Soc.* **148**, A183 (2001).

[6] B. Andreaus, A. J. McEvoy and G. G. Scherer, *Electrochim. Acta* **47**, 2223 (2002).

[7] B. Andreaus and G. G. Scherer, *Solid State Ionics*, submitted.

IN SITU INVESTIGATION OF THE TWO-PHASE FLOW PATTERNS IN FLOW FIELDS OF DIRECT METHANOL FUEL CELLS AND LOCALLY RESOLVED CURRENT MEASUREMENTS

A.B. Geiger, D. Kramer, P. Vontobel, E. Lehmann, A. Wokaun, G.G. Scherer

The two-phase flow patterns occuring on the anode and cathode side of a DMFC have been studied. In addition, this method has been combined with the measurement of locally resolved currents. The combination of both methods yields unique information on the two phase flow patterns and was applied to study the effects of carbon dioxide clusters in the anodic flow field of DMFC's on its current distribution. Future developments and opportunities of the simultaneous use of these two methods but also its current limitations are discussed.

1 INTRODUCTION

From the oxidation of methanol, the anodic reaction product of a direct methanol fuel cell (DMFC) is CO_2, which is evolved as a gas in the cell leading to a two-phase flow at the anode. Large amounts of CO_2 may accumulate in the channels of the flow field and hinder the supply of reactants to the electrochemically active area. Therefore, the efficient release of the gaseous CO_2 from the catalyst layer to the channels and from the cell has to be ensured to maintain effective reaction conditions [1, 2]. On the cathode side, the two-phase flow develops from liquid water as reaction product and air as oxidant. Water droplets may accumulate within a channel of the flow field and flood it partly, thus blocking the channel from the supply with air. Unfortunately, the impact of the two-phase flow on the performance of DMFC's cannot be easily assessed with standard electrochemical methods, *e.g.*, current-voltage curves. Therefore, a thorough investigation of this rather complex system asks for additional "real-time" and *in situ* methods to give a better understanding of the mass transport related phenomena involved in operating DMFC's.

As we describe below, neutron radiography (NR) is well suited to visualize the two-phase flow of a gas and a liquid *in situ* and in 'real time'. In our experiments the two-phase flow at the anode and cathode side of DMFC's has been studied. However, from the NR images we only get an information about the state of the flow field (gas / liquid) but we do not know its effect on the cell performance. Thus, we have combined this method with the measurement of locally resolved currents to explore the effects of carbon dioxide clusters on the current distribution (CD) in the anodic flow fields of DMFC's. Unique results and the promising use of the combination of these methods for the DMFC research are shown.

2 EXPERIMENTAL

Similar to the principle of X-rays, the probe under investigation is penetrated by neutrons, attenuated by the elements with high neutron attenuation and finally, the transmitted neutrons are collected by a detector (CCD-camera system). The result is a two-dimensional image of the object with dark areas indicating regions of highest neutron attenuation. The light areas show regions of lowest neutron attenuation. In con-

trast to X-rays however, neutrons are very sensitive to some light elements (*e.g.*, hydrogen) and allow to detect even thin layers of these elements. A detailed discussion of the opportunities but also the limitations of NR for the PEFC research can be found in reference [3].

The CD across the active area was measured with a "quasi-segmented" approach of the flow-field plate as described in reference [4]. Closed-loop Hall effect current sensors were used for mapping the CD across the electrode area and the method is described in reference [5]. The DMFC under investigation was designed for an active area of 100 cm^2.

3 RESULTS AND DISCUSSION

An effective gas removal from the flow field could be a critical issue for DMFC's, especially, if the flow rate of the aqueous methanol solution is varied. The latter is, for instance, of importance if a stoichiometric supply of the aqueous methanol solution is introduced to lower the methanol crossover. The DMFC was operated with the supply of the aqueous methanol solution from the bottom at a cell temperature of 45°C, and a constant airflow of 2 l_N min^{-1}. NR images were taken along polarization curves that were measured for various anodic flow rates (6, 12, 24, and 36 ml min^{-1}). Subsequently these images were quantitatively analysed, with results given in Figure 1.
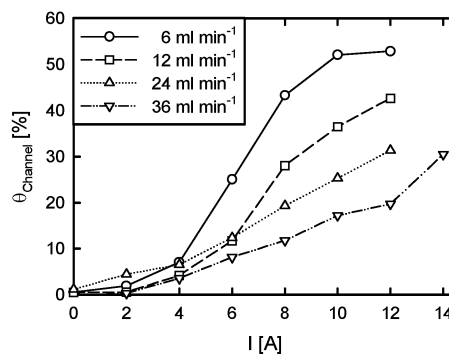

Fig. 1: The effect of the anodic flow rate on the void fraction of gas in the flow channels. The data are derived from the analysis of NR images.

In general, we conclude that the anodic flow rate has a large impact on the CO_2 content present in the flow field on the anode side (see Figure 1). This could, for

instance, be of relevance if a DMFC system is operated with a stoichiometric supply of the methanol-water mixture. In that case, the dynamics of the DMFC on large load demands may be rather slow because a considerably parts of the anodic compartment may be gas-filled, which may impose mass-transport limitations on the load response of a DMFC. On the other side, the beneficial effect of gas when in contact with the membrane has also to be considered. The methanol permeation across the membrane will be significantly lower if the membrane is in contact with the gas phase [6] because of the phenomenon of a lower uptake of the membrane from a gas phase.

Nevertheless, the impact of gas-filled channels on the DMFC performance cannot be studied with the information of the state of the flow field alone. Therefore, NR images of the cell were taken simultaneously with the measurement of the current distribution of the cell. As illustrated in Figure 2, the DMFC was operated in co-flow mode with horizontal flow channels. The inlet of the aqueous methanol solution (0.5 M) and of air was at the upper left side and the outlet was located on the diagonally opposite side.
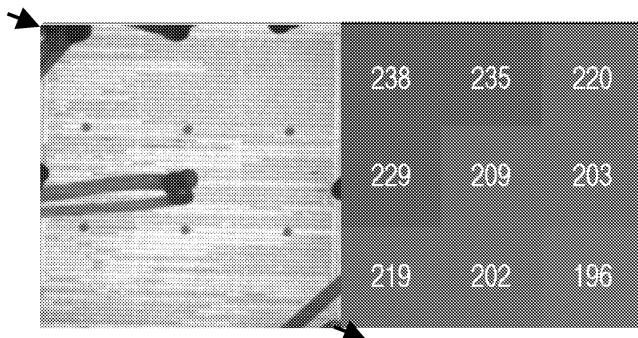

Fig. 2: Gas / liquid distribution within the flow field (right side) and the corresponding CD across the active area at an average current density of 220 mA cm^{-2}. The cell conditions were as follows $T_{Cell} = 70°C$, $c_{MeOH} = 0.5$ M, $Q_{MeOH} = 12$ ml min^{-1}, $Q_{air} = 2$ l$_N$ min^{-1}, and p = 3 bar$_{abs}$.

The segmental analysis of the NR images revealed that, in principle, the gas content increases vertically from the inlet to the outlet as depicted in the NR image of Figure 2 (left side). In contrast, the current production decreases from the top to the bottom as illustrated on the right side of Figure 2. The segments at the top have the highest current density, the segments in the middle row perform about average, while all segments at the bottom perform below average (average current density was 220 mA cm^{-2}).

Nevertheless, it is not possible from Figure 2 to correlate the CD to the degree of gas content in the segments. The area at the entrance (upper left side of the flow field), for instance, carries a high gas loading, which is comparable to those at the bottom. Nevertheless, this segment performs better than any other part of the flow field. However, one has to keep in

mind, that the liquid distribution within the diffusion layer is unknown and may compensate for any effects of CO_2 clusters at the low current densities studied. Therefore, the impact of carbon dioxide clusters in the anodic flow field on the CD cannot be answered yet.

4 SUMMARY

The consequences of the anodic flow rate on the gas-liquid distribution in DMFC's were studied. In addition, the impact of carbon dioxide clusters in the anodic flow field of a DMFC on its CD was investigated. At present, a correlation between product rich areas in the anodic flow field and low current production in these areas could not be observed within the current density range. However, the gas liquid distribution within the diffusion layer is unknown and may account for the insensibility of the CD on the presence of anodic CO_2 clusters. Nevertheless, the general trend of the CD, as yet, could be related to the oxygen distribution on the cathode side.

5 ACKNOWLEDGEMENTS

6 REFERENCES

[1] P. Argyropoulos, K. Scott, and W.M. Taama, *Carbon dioxide evolution patterns in direct methanol fuel cells*, Electrochim. Acta **44**, 3575-3584 (1999).

[2] P. Argyropoulos, K. Scott, and W.M. Taama, *Gas evolution and power performance in direct methanol fuel cells*, J. Appl. Electrochem. **29**, 661-669 (1999).

[3] A.B. Geiger, A. Tsukada, E. Lehmann, P. Vontobel, A. Wokaun, and G.G. Scherer, *In Situ Investigation of Two-Phase Flow Patterns in Flow Fields of PEFC's by Neutron Radiography*, Fuel Cells, in print.

[4] F.N. Büchi, A.B. Geiger, and R.P.C. Neto, *Current Distribution Measurements in PE Fuel Cell of Technical Relevance*, PSI Annual Report / Annex V, ISSN 1423-7342, Paul Scherrer Institut, Villigen (2001).

[5] A.B. Geiger, R. Eckl, G.G. Scherer, and A. Wokaun, *A Novel Method to Measuring Locally Resolved Currents in Polymer Electrolyte Fuel Cells*, to be published

[6] R. Savinell, E. Yeager, D. Tryk, U. Landau, J. Wainright, D. Weng, K. Lux, M. Litt, and C. Rogers, *A Polymer Electrolyte for Operation at Temperatures up to 200°C*, J. Electrochem. Soc. **141**, L46-L48 (1994).

1 + 1 DIMENSIONAL MODEL OF A PE FUEL CELL OF TECHNICAL SIZE

S. Freunberger, A. Tsukada, G. Fafilek (Vienna University of Technology), F.N. Büchi

The performance of polymer electrolyte fuel cells strongly depends on the cell water management. Based on a literature approach for the cell water distribution, a full cell model realized in a 1 + 1 dimensional approach was developed to get a deeper insight into the behaviour of the cell. The model can describe the co- and counter-flow regimes in a cell. A combination of these regimes was used, to describe the water management of the given technical cell flow field. The calculations allowed to identify the contributions of the different mechanisms of performance losses with respect to operating conditions, flow field and electrochemical components.

1 MOTIVATION

Normally a fuel cell is characterized by a current voltage curve and the majority of previous modelling approaches had the goal to reproduce or predict this characteristic.

A simple current voltage curve however, although describing the true performance of the cell is, due to its shapeless form, insensitive in distinguishing the different loss mechanisms in the cell. Therefore using a current voltage curve is problematic for model validation. This is even more evident in cells of technical size, because there lateral effects and in homogeneities are more pronounced than in laboratory cells. However these phenomena are poorly reflected in an i/E curve. In order to optimise technical cells, models are needed which focus on the effects of inhomogeneity in the cell.

Based on a literature approach for the cell water distribution [1], a full cell model realized in a 1+1 dimensional approach was developed to get a deeper insight into the behaviour of the cell. The model can describe the co- and counter-flow regimes and a combination of these regimes was used to describe the water management of the given technical cell flow field (see Figure 1).

2 MODEL APPROACH

In principle each gradient of physical properties leads to corresponding balancing flows. The mathematical description of these phenomena leads to differential equations, which are solvable only numerically. Compared to usually used techniques like the Finite Element Method (FEM) the complexity of the calculation can be lowered substantially by considering only the predominant exchange processes in the cell. These are on the one hand the transport of water, protons and reactant gases perpendicular to the membrane surface. On the other hand the exchange processes parallel to the membrane are dominated by the mass flow in the flow field channels.

This concept leads to an "1+1 dimensional" model approach. The whole task can be divided into two initial problems (i) flow along the anode and cathode channel; (ii) perpendicular fluxes through the layers of the cell. The equations for the flow in the channels describe an ideal plug flow assuming immediate mixing over the entire channel cross-section and no diffusive mixing in flow direction. The flow regime (co- or counter-flow respectively) must be considered for

the integration. The theory of thermodynamics of irreversible processes allows for deriving the equations for the fluxes through the porous electrodes and the membrane, taking into account the kinetic coupling of the fluxes. In case of the water transport through the membrane this leads to interaction of electro-osmotic and diffusive flux.

For an assumed initial distribution of the current density this calculation leads to the distribution of the gas partial pressures in the channels and at the electrode/membrane interfaces and to the local degree of swelling of the membrane. This allows to estimate the local composition of the overvoltages. In a real cell the high conductivity of the electrodes and flow field plates avoids an inhomogeneous voltage distribution in the cell-plane and consequently the current density is adjusted in order that the sum of all overvoltages is equal in each point of the cell. The obtained distribution of the current density is used as a better assumption for the calculation of the local partial pressures. An iterative calculation is performed until convergence is achieved.

The given flow field consists of co– and counter–flow regimes interlinked through small cross-flow sections in the manner as shown in Figure 1.
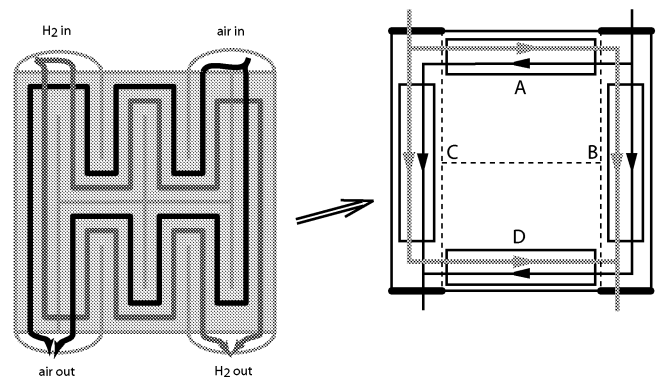
Fig. 1: Abstraction of the real flow field (left) by two co-flow sections (B, C) and two counter-flow sections (A, D) with the given gas connections (right).

3 EXPERIMENTAL

For the measurement of the local current density the semi-segmented plate principle was used. The cathode flow field of the 200 cm² cell contains nine electrically insulated sub areas of 10 cm², where the local current can be measured individually. This principle is described in detail in [2].

Nafion® 112 and standard E-Tek electrodes (1 mg Pt/cm² MEA) were used as electrochemical components.

4 RESULTS

A comparison of calculated values of the local current density for the variation of the air stoichiometry with corresponding measurements are shown in Figure 2. The cell was operated at 70 °C with fully humidified gases, gas pressures of 2 bar$_a$ and a hydrogen stoichiometry of 2.
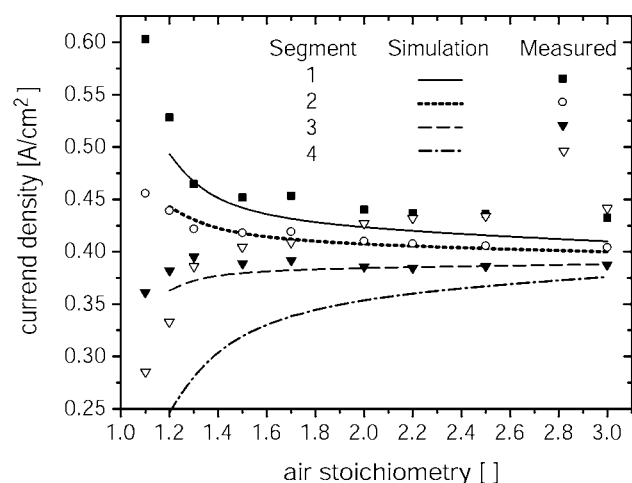
Fig. 2: Calculated vs. measured current density for the segments 1-4 (see figure 3 (a)) as a function of air stoichiometry. Average current density 400 mA/cm².

The calculation can provide additional information on the distribution of the overvoltages as shown in Figure 3 for current density, ohmic and concentration overvoltages.

In Figure 2 where both gases are saturated the calculated inhomogeneities results only from varying concentration overvoltage. For decreasing stoichiometry the segments at the end of the air path produce less current due to oxygen depletion, and consequently the segments early in the path have to produce more current. Differences between simulation and experiment result from difficulties in the measurement and some uncertainty of parameters in the calculation.

Figure 3 shows the calculated current density for the real cell geometry and the underlying mechanisms of performance losses for a cell operated on dry hydrogen (Dew point T$_d$ = 25 °C) and humidified air (T$_d$ = 65 °C). The increased membrane resistance is the dominating reason for the substantially lowered power at the entry of the dry hydrogen due to its dehumidifying impact.

The results show that this kind of model calculation can deliver complementary information to experiments or in an improved form as a substitute for experimentally expensive measurements and offers additional information in high spatial resolution.
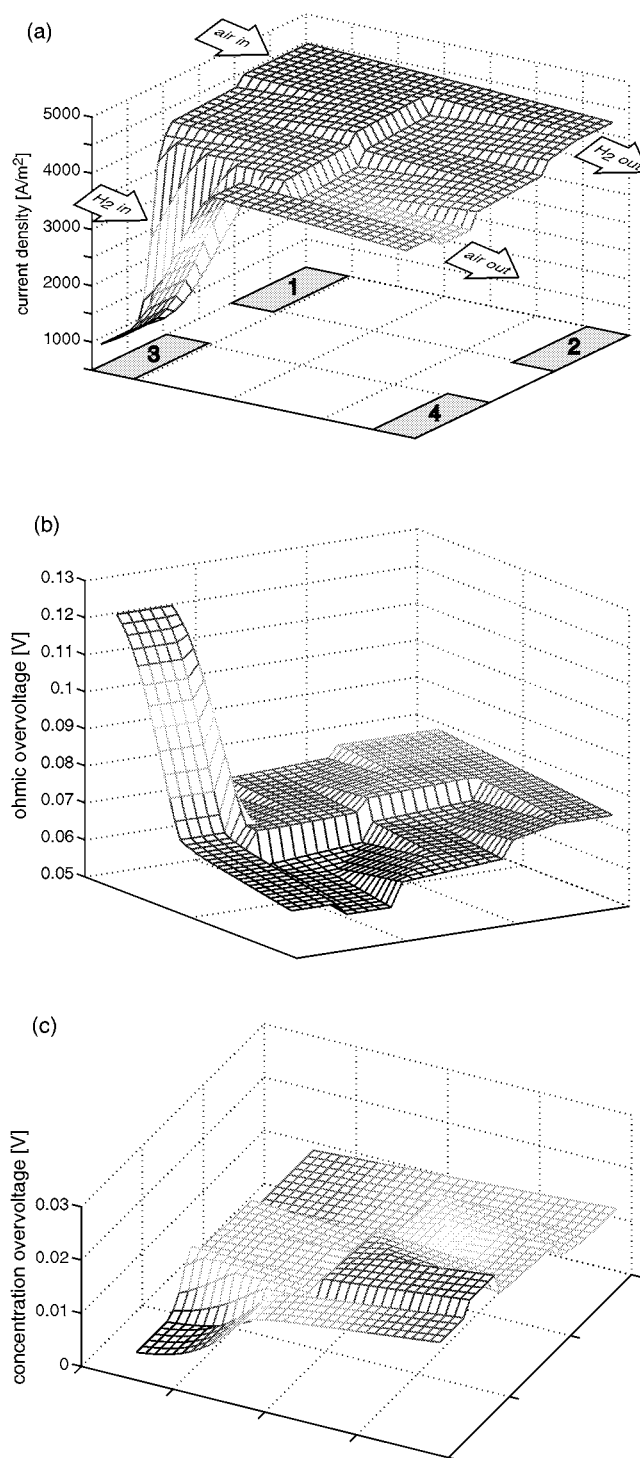
Fig. 3: Model calculations (a) current density, (b) ohmic overvoltage and (c) concentration overvoltage displayed for the real cell geometry for a cell operated on dry hydrogen (Dew point T$_d$ = 25 °C) and humidified air (T$_d$ = 65 °C). Numbered segments in (a) show locations of experimental current measurements.

5 REFERENCES

[1] G.J.M. Janssen, J. Electrochem. Soc. **148**, A1313 (2001).

[2] F.N. Büchi, A.B. Geiger, R.P.C. Neto, PSI Scientific Report 2001, **V**, 91 (2002).

STACK AND SYSTEM CONCEPTS FOR PE FUEL CELL SYSTEMS IN THE kW-RANGE

M. Santis, D. Schmid (ETH Zürich), M. Ruge (ETHZ), F.N. Büchi

New concepts, jointly developed by PSI and ETHZ, are being implemented in a 1 kW polymer electrolyte fuel cell system fuelled with hydrogen and air. The process air humidification is incorporated into the stack, so that no external humidification device is needed. This makes the system simpler and cheaper. A new concept for the unification of 2-part bipolar plates using flexible graphite foils was developed and for the current collector a composite of a small copper metal plate sandwiched between graphite foils is used.

1 INTRODUCTION

"PowerPac" is a joint project of PSI and ETHZ for developing a product family of portable/mobile power generation systems based on hydrogen/air polymer electrolyte fuel cells. In a first phase, a 1 kW system is being realized. The further development of 0,5 kW and 2 kW systems will be done in a later phase.

The analysis of the complete fuel cell system shows that process air humidification and hydrogen recirculation are the biggest obstacles for a high performing portable system in the kW-range. For the "PowerPac"-project a new architecture of the cell has been designed, constructed and tested which includes an internal, fully scalable humidification concept. Humidification of the process air is achieved by transferring the humidity of the exit air to the fresh air within the cell. In order to reduce the burden for hydrogen recirculation the hydrogen flow field has been designed according to a new concept.

On the level of the fuel cell stack, the biggest advances seem possible by optimisation of the unification of 2-part bipolar plates and simplification and weight reduction of the current collectors.

2 NEW CONCEPTS

Humidification of the process air is one of the most critical operating parameters in PE fuel cells. In order to optimise the fuel cell system, through function integration, the elimination of the separate process air humidification sub-system is of outmost interest.

In the "PowerPac" cell the humidification of the incoming process air is achieved by transfer of product water from the exhaust air, through part of the membrane, to the dry intake air (see Figure 1) [1]. Tests have shown that cells using the concept of internal humidification and operated with dry air have almost the same performance as when operated with external humidification (see Results).

The integration of the humidification into the stack, i.e. into each individual bipolar plate makes the process independent from the number of cells and operating mode and thus makes the concept fully scalable, independent of stack size and system performance.
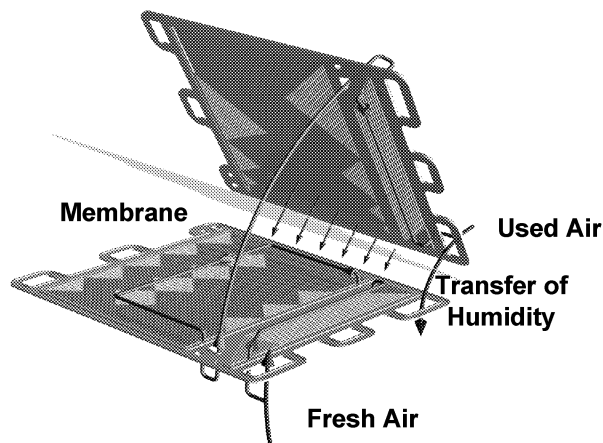
Fig. 1: Concept of internal process air humidification by transfer of humidity from the used air to the fresh air within each cell.

A low hydrogen stoichiometry reduces the burden on the system for hydrogen recirculation. A stepwise reduction of the number of hydrogen flow channels along the active area allows for an almost constant gas speed in the channels, even if the volume flow of the gas decreases because of consumption along the channels due to current generation. The constant gas speed guarantees for optimum water removal from the channels and as a result, a hydrogen stoichiometry as low as 1.1 is enough for stable operation and only a small amount (10%) of the hydrogen must be recycled.

The gluing process normally used for joining the sub-plates of internally cooled bipolar plates has disadvantages such as heat cycle requirements and leak testing [2]. Therefore a new concept for joining the sub-plates has been developed. An intermediate layer of graphite foil is placed between the two sub-plates. Ribs on the sub-plates easily and reliably guarantee tightness for all media [3]. This new concept provides an important step towards a simpler, easier and cheaper way for constructing and assembling fuel cell stacks.

In previous stack concepts, current collectors made from gold-coated copper metal plates have been used. Reducing the contact resistance and corrosion protec-tion made a gold-coating of the copper plate necessary.
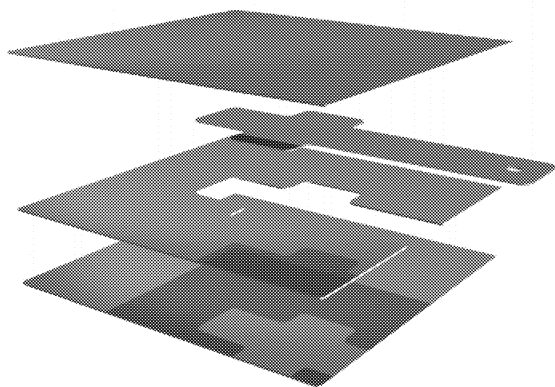
Fig. 2: Composite arrangement for the current collector at the ends of the stack.

In the previous architecture, the copper plate was heavy because it covered the entire cross section of the stack. The new concept for the current collector uses a compound of graphite foil and a reduced size copper plate. The small copper plate is pressed between two graphite foils with high in-plane conductivity and thus homogeneous current collection and corrosion protected is achieved (Figure 2). The gain in weight is about 50%.

3 RESULTS

The new concepts for the internal humidification and low hydrogen stoichiometry were verified in a 4-cell stack equipped with conventional electrochemical components (Nafion® 112 membranes, ELAT electrodes with Pt-loading of 0.5 mg/cm²). A comparison of the performance achieved with dry and well-humidified process air is shown in Figure 3.
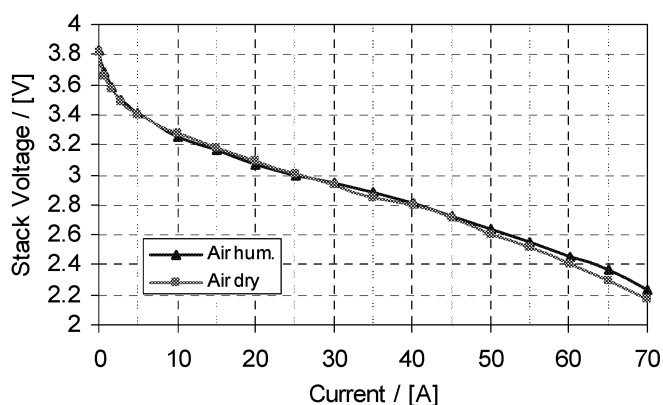

Fig. 3: Comparison of performance of self-humidifying cell concept with and without humidification of the process air. Cell temperature = 70°C, gas pressures =1.5 bar, stoichiometry hydrogen = 1.1, air = 1.5.

At a stack temperature of 70°C, the loss of performance when operating with dry air is of only a few percent: at 0.6 V/cell the current produced with external humidified air is 63 A, while with dry air 60 A i.e. a loss of 5 %.

The design of the hydrogen flow field allows for operating the stack with a hydrogen stoichiometry as low as 1.1 reducing the amount of hydrogen to be recycled to only 10 %.

The dependence of the performance on the operating temperature is shown in Figure 4.
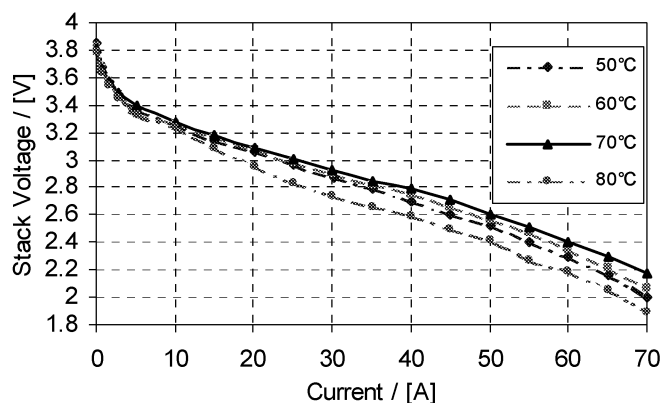
Fig. 4: Current/voltage characteristics of a 4-cell stack at different operating temperatures (as indicated). Gas pressures = 1.5 bar, stoichiometry hydrogen = 1.1, air = 1.5.

The internal humidification of the process air, i.e. the performance of the fuel cell, depends on the operating temperature. When the temperature of the stack exceeds 70°C, then the process air is not humidified well enough. As a consequence the ohmic-resistance of the membrane increases and the stack performance decreases.

4 ACKNOWLEDGEMENT

5 REFERENCES

[1] D. Schmid, M. Ruge, F.N. Büchi, Swiss Patent Application Nr. 1031/02, June 17, 2002.

[2] M. Ruge, F.N. Büchi, Proceedings of the Electrochem. Soc. **PV 2001-23**, 165 (2001).

[3] D. Schmid, M. Ruge, Swiss Patent Application Nr. 1131/02, June 30, 2002.

SUPERCAPACITOR PERFORMANCE DURING SIMULATED AND MEASURED DRIVING CYCLES FOR THE HY.POWER® FUEL CELL CAR

M. Baertschi, R. Kötz, P. Dietrich

Performance tests in terms of simulated and measured driving cycles have been carried out on a down-scaled Supercapacitor module and with the HY.POWER® Fuel Cell/ Supercapacitor electric vehicle. The measurements showed a highly dynamic performance of the Supercapacitor and a good scalability between the two modules.

1   INTRODUCTION

Hybrid electric vehicles are claimed to be the most promising candidates for the future of sustainable mobility. In this content, also the subsystems of such a drive train, e.g. Fuel Cells (FC) and Supercapacitors (SC) became a very popular subject of investigation [1]. In an interdisciplinary project called BRESA, a FC/SC powered hybrid electric vehicle (HY.POWER®) was developed at PSI together with academic and industrial project partners [2].

In order to improve our understanding of the SC as a single component, it was necessary to perform several preceding tests on an intermediate scale. Due to the linearity of SC modules with respect to the number of parallel or serially connected single cells [3], it was supposed that these data can be extrapolated to the final SC module.

2   EXPERIMENTAL

At first, a small SC module, consisting of 10 SCs (1600 F, 2.5 V), two cells in parallel and five pairs in series, leading to a terminal voltage of 12.5 V, was used to measure simulated driving cycles. The raw data for these driving cycles were calculated from measurement data received from a battery powered passenger car driving over a pass in the Swiss Alps. From the total power demand, the share of the supercapacitor was calculated at a given power management for the projected hybrid drive train of the HY.POWER® (FC / SC).

Once the HY.POWER® was accomplished, further measurements were performed on a dynamometer at the EMPA in Dübendorf. During these measurements real driving cycles were carried out, and the power share of the SC was recorded. The SC module of the HY.POWER® consisted of 282 single cells (1600 F, 2.5 V), two in parallel and 141 in series, leading to a terminal voltage of 360 V.

2.1   Simulated driving cycles

To perform the measurements of the 12.5 V module, a 10 kW test bed, consisting of a power supply (Topcon, 100 VDC / 320 A), an electronic load (Höcherl & Hackl, 120 V / 500 A) and a data acquisition system (Agilent data acquisition/switch unit) with a time resolution of 0.5 s were used. From the calculated power profile, a current input profile for the test bed was calculated (the current being the same for both modules).

With the measured current and the terminal voltage of the SC module, the power behaviour during the driving cycle was calculated.

2.2   Measured driving cycles

On the dynamometer the New European Driving Cycle (NEDC) was carried out, and the power flows between the FC, the SC and the inverter were recorded against time and vehicle speed.

3   RESULTS

3.1   Simulated driving cycles

The calculated power profile, shown in Figure 1, reflects the road topography: In the first section the vehicle is driven with relatively constant speed and thus the SC is rarely used for load sharing. However, in the second section (> 1900 s) the SC is extensively used for breaking and subsequent acceleration along the steep and winding uphill road.
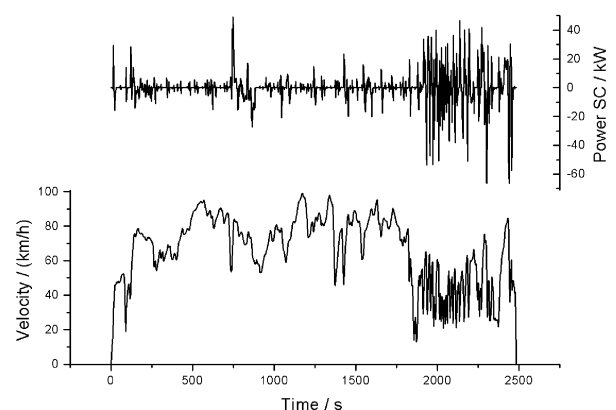
Fig. 1: Calculated power profile for the SC module and the corresponding measured vehicle speed during the drive over a pass in the Swiss Alps.

The capability of the SC module to follow the power demand during the high duty part of this driving cycle is shown in Figure 2. The differences between the actual power (solid line) and its set point (dotted line) are smaller 5%. These differences arise mainly from delayed response of the electronic load in the test bed, and cannot be interpreted as a failure of the SC module. In the particular hybrid drive train and on this particular route, the SC module satisfies the system requirements and covers the power peaks.
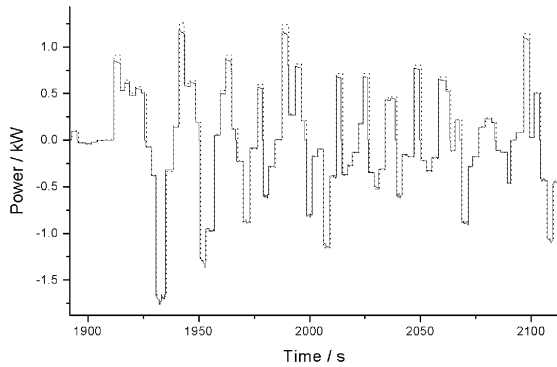
Fig. 2: High duty part of the driving cycle, exhibiting the difference between the set points (doted line) and the actual power (solid line) of the SC module.

3.2 Measured driving cycles

The speed profile of the NEDC, achieved with the HY.POWER® car is shown in Figure 3. It starts with a highway section, where the vehicle is accelerated up to 100 km/h, and is followed by four identical urban sections with frequent braking and subsequent acceleration and ends with another highway section.
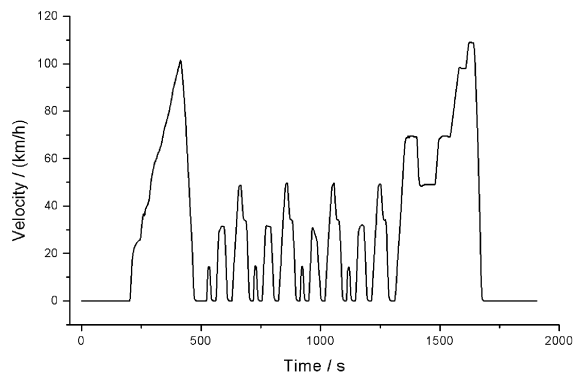
Fig. 3: New European Driving Cycle (NEDC), consisting of two highway sections (begin and end) and four subsequent identical urban sections (middle part).

The measured power to and from the inverter (which is connected to the electric motor), the shares of the FC and the SC during the last urban section and the beginning of the final highway section is plotted in Figure 4. Clearly, the SC perfectly satisfies the power demands of the vehicle, which the FC alone would not be able to compensate. Therefore a highly dynamic driving mode is possible, while the FC can be operated in a more continuous mode, thus increasing the overall fuel efficiency.
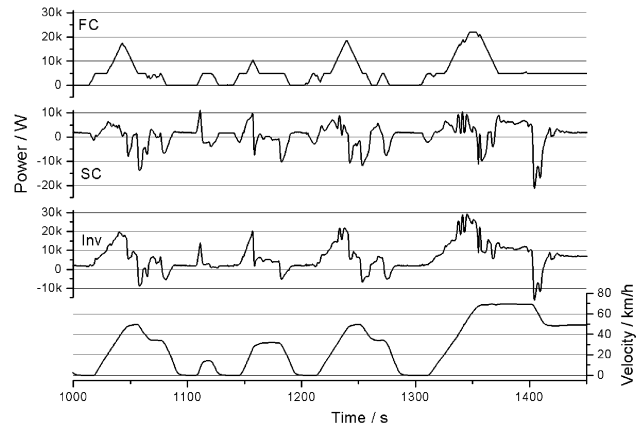
Fig. 4: Power flow at the FC, SC and the Inverter during the last urban section and the beginning of the final highway section of the NEDC, positive values indicate acceleration, negative values recuperation of braking energy into the SC.

These measurements confirmed the results of the preceding experiments with the smaller 12.5 V module on the 10 kW test bed. It is proved that a SC is a highly dynamic device, being able to take or to deliver power peaks in the magnitude of several tenths of kilowatts. Thus, the SC combined with a slow adapting power source provides a highly dynamic hybrid system, with superior driving performance compared to a pure fuel cell electric vehicle.

4   ACKNOWLEDGEMENTS

5   REFERENCES

[1]   R. Kötz, S. Müller, M. Bärtschi, B. Schnyder, P. Dietrich, F. N. Büchi, A. Tsukada, G. G. Scherer, P. Rodatz, O. Garcia, P. Barrade, V. Hermann, R. Gallay: *Super-capacitors for peak-power demand in fuel-cell-driven cars,* Advanced Batteries and Supercapacitors, G. Nazri, R. Kötz, B. Scrosati, P. A. Moro, E. S. Takeuchi, Edts., ECS Proc. Vol. PV 2001-21, p. 545, The Electrochemical Society, Inc., Pennington, NJ (2002).

[2]   F. Büchi, A. Tsukada, P. Rodatz, O. Garcia, M. Ruge, R. Kötz, M. Bärtschi, P. Dietrich, Fuel Cells 2002, Lucerne, (2002).

[3]   R. Kötz, M. Bärtschi, F. Büchi, R. Gallay, Ph. Dietrich, *the 12th international seminar on double layer capacitors and simsilar energy storage devices,* Deerfield Beach, Florida, (2002).

TESTING FUEL CELL AND SUPERCAP TECHNOLOGY IN THE HY.POWER® HYBRID ELECTRIC VEHICLE

*P. Dietrich, F.N. Büchi, P. Rodatz (ETH Zürich), A. Tsukada, O. Garcia (ETHZ),
M. Wollenberg (Volkswagen AG), M. Bärtschi*

A fuel cell system based on six stacks combined with an electrical energy storage device including 282 double-layer-capacitor cells have been integrated in an electric hybrid power train. This power train is integrated in the HY.POWER® vehicle, which has been tested as technology platform on test benches and on public roads for more than 1000 test kilometres.

1   INTRODUCTION

The results achieved in the fields of fuel cell (FC) stack development and fuel cell system architecture as well as in the fields of double-layer-capacitor (SC) electrodes lead to the idea to verify the performance in a test vehicle. We are convinced that the integration of new technologies in a passenger car gives access to a larger group of persons to the performance of these new technologies. The judgement based on a test drive is much more impressive than to make up one's mind based on measurement data taken at a test-bench. To prove the advantages of the FC and the SC as short time energy storage device, a sophisticated system structure had to be designed. The project has been realized as a collaboration between Paul Scherrer Institut, Swiss Federal Institute of Technology Zurich, Volkswagen AG, FEV Motorentechnik GmbH and montena components SA.

2   SYSTEM DESIGN

The design of the structure of the hybrid power train is driven by optimal fuel consumption within city driving and the possibility to demonstrate the drivability of the vehicle. Further a certain flexibility to vary the component size to reduce costs should be possible. The chosen architecture is shown in Figure 1. The maximum power output of the fuel cell system is defined by the desired continuous top speed of the vehicle. In the HY.POWER® vehicle this demand led to a peak power of the FC system of 40 kW. The size of the electrical storage device is defined according the ability to store the braking energy of the vehicle and to assure a defined acceleration performance of the car. Therefore the energy content had to be 300 –400 Wh and a peak power of 60 kW output of the SC was necessary.
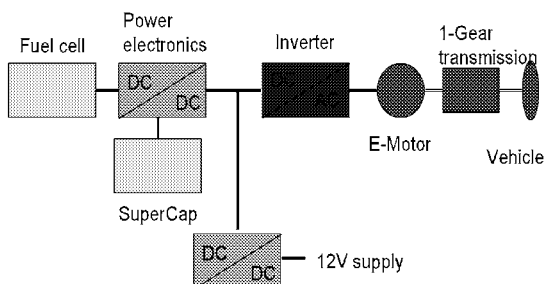
Fig. 1: Structure of the hybrid power train with a FC system, a SC energy storage, a DCDC-converter and an electric motor with a gearbox.

The architecture of the fuel cell system is shown in more details in [1-3] and [5]. The double-layer capacitor unit is described more detailed in [1] and [4]. To combine the fuel cell system and the storage device with the electric machine of the vehicle a DCDC-converter had to be realized, which is optimised for best efficiency (Figure 2).
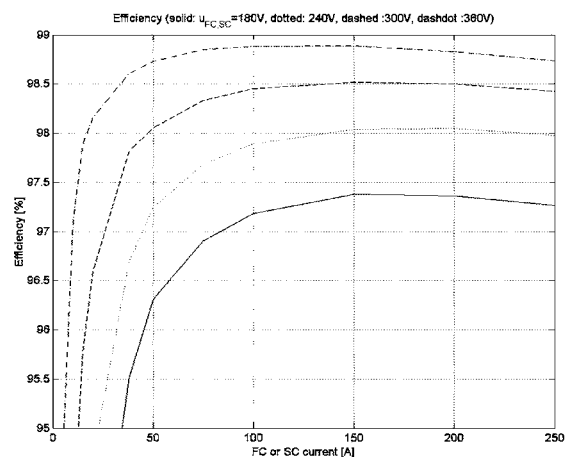
Fig. 2: Efficiency of the DCDC-converter at different input voltages of the FC and the SC.

The architecture of the power train has been tested on the level of a 6 kW FC system together with a 10 kW SC module and a full size DCDC-converter. An electronic load has replaced the electric machine. Based on the experience gained with this pilot power train system, the full size power train was realized. The pilot system allowed also to design the control-system including hardware and software of the principal parts for the full size system.

The full size system has been built combining sub-system by subsystem on a dynamic test bench. The integration of the power train in the vehicle is shown in Figure 3. The FC system is located in the trunk, the SC modules are split, one unit is located below the rear seats and the other unit is placed in the motor compartment. The DCDC-converter and the electric machine are placed in the motor compartment too. Several systems of the vehicle had to be adapted to the electric operation:

- 12-V board net supply (DCDC-converter from 400V)
- Electro-hydraulic steering.
- Electric vacuum pump for brake assist.
- Cooling circuit for the electric machine.
- Electric heating including controls.
- Hydrogen detection system.
- Wiring of the signals and of the power cables.
- Adaptation of the vehicle management device.
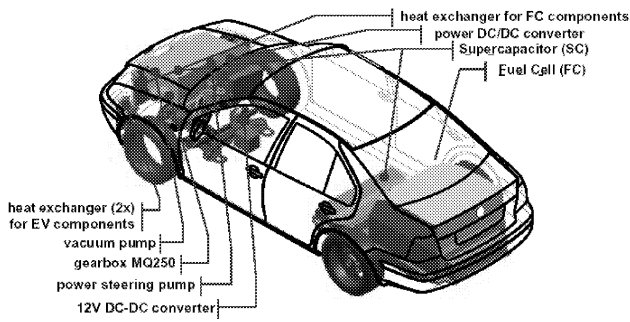
Fig. 3: Arrangement of the components in the test vehicle Volkswagen BORA HY.POWER®·
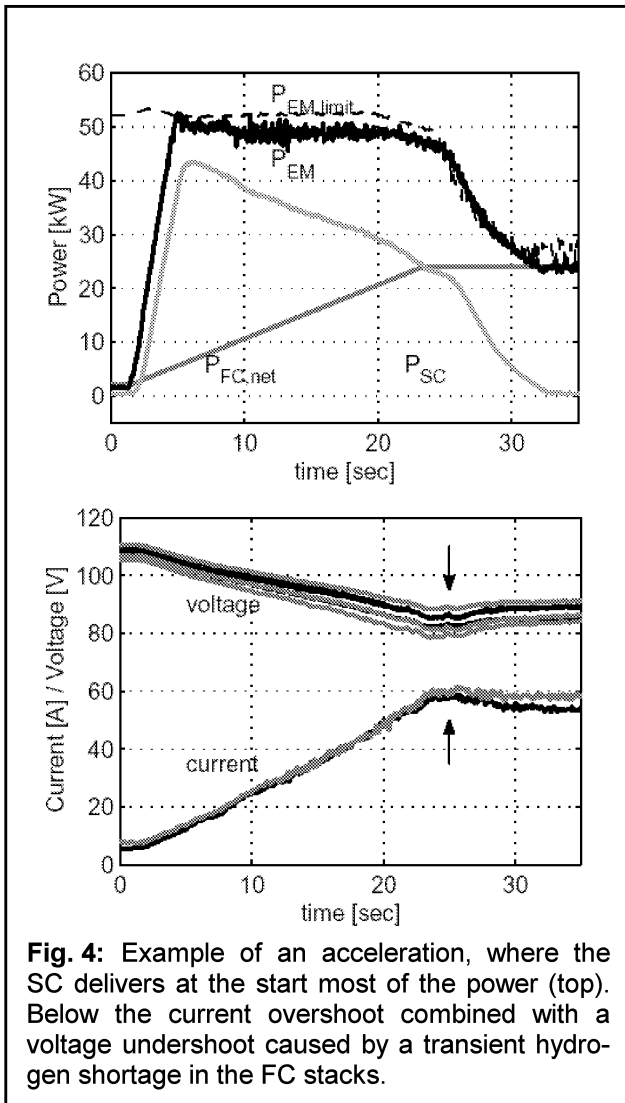
Fig. 4: Example of an acceleration, where the SC delivers at the start most of the power (top). Below the current overshoot combined with a voltage undershoot caused by a transient hydrogen shortage in the FC stacks.

The power train system was integrated into the vehicle in January 2002 and test runs also began in January 2002. More than 1000 km of test-driving has been accomplished in the year 2002.

3 RESULTS

The HY.POWER® has been extensively tested on the road. The test drive across the Simplon Pass on January 16th, 2002 demonstrated the maturity of the po-

wer train under severe road conditions. The system was working even at a height of 2000 m a.S.L. In Figure 4 an example of the combination of the power of the SC and the FC is shown. To accelerate from rest, the SC is depleted to deliver in a first phase the main part of the power. In this experiment the dynamics of the FC is limited to 1 kW/s. Normally the FC system is operated at a rate of 2.5 kW/s. The fluctuation of the performance of the individual stacks in the fuel cell system during road test drives is shown in Figure 5. The dynamic operation shows a wide range of operating points for the individual FC-stacks.
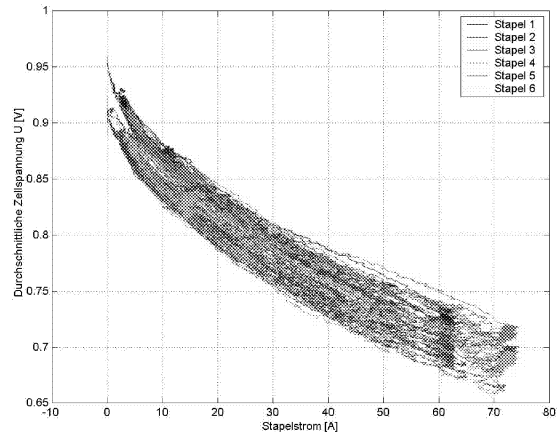
Fig. 5: Voltage-current curves of the six stacks operated in the HY.POWER®·

Fuel consumption measurements in the New European Driving Cycle (NEDC) have shown, that the use of the recuperation of braking energy can reduce the fuel consumption by 14.9%.

4 ACKNOWLEDGEMENTS

5 REFERENCES

[1] P. Dietrich et al., Hy.Power – *A Technology Platform Combining a Fuel Cell System and a Supercapacitor Short Time Energy Storage Device,* Proceedings SATG Conference, Wil, ISBN 3-906483-03-7, September 13 (2002).

[2] F.N. Büchi et al., PSI Scientific Report 2002, **V**, 102-103 (2003).

[3] F.N. Büchi et al., PSI Scientific Report 2001, **V**, 93 (2002).

[4] R. Kötz et al., *Supercapacitors for peak power demand in fuel-cell driven cars,* Advanced Batteries and Super Capacitors, ECS Proceedings Volume PV 2001-21, The Electrochemical Society, Inc., Pennington, NJ (2002).

[5] A. Tsukada and P. Rodatz, PSI Scientific Report 2001, **V**, 88 (2002).

FUEL CELL SYSTEM FOR THE HY.POWER® HYBRID ELECTRIC VEHICLE

F.N. Büchi, P. Rodatz (ETH Zürich), A. Tsukada, P. Dietrich

A fuel cell system based on an array of 6 stacks was designed, constructed and finally tested on a dynamic testbench and in the HY.POWER® hybrid electric vehicle. The architecture of the fuel cell system includes a pulsed hydrogen recycling loop and air cooling and humidification through water injection in the compressor. The system delivered 36 kW gross and 30 kW net power.

1   INTRODUCTION

The power train for the HY.POWER® electric vehicle was realized in a hybrid electric configuration with a hydrogen fuelled, polymer electrolyte fuel cell system as converter unit and prime mover and a super-capacitor system as electric storage unit [1]. This combination, on the one hand, allows for sizing the fuel cell system considerably smaller than required by the peak power during acceleration. On the other hand the requirements with respect to the dynamics of the fuel cell are moderate because the supercapacitor system has the inherent ability for levelling power requirements at a high rate.

2   SYSTEM DESIGN

In the hybrid system architecture, the requirements for the fuel cell system are given by the desired continuous top speed of the vehicle. In the HY.POWER vehicle this demand led of a peak power of the fuel cell system of 40 kW and a dynamic behaviour of 5 kW/s.

The architecture of the fuel cell system is shown in Figure 1. For the fuel cell itself a layout with an array of 6 stacks was chosen. The development of these 125-cell stacks with a rated power of 8 kW$_e$ and their

combination to a stack array of 6 stacks has been described previously [2]. The stacks were arranged electrically as two strings of 3 units in series with the two strings connected in parallel. This led to the desired voltage span between 250 V at full load and 360 V at open circuit to match the 400 V of the d.c. circuit in the car as closely as possible.

Basically the fuel cell system, complementing the stacks, consists of 3 media loops, (i) process air supply, (ii) hydrogen fuel supply and recycling, and (iii) cooling. The 3 media were fed in parallel, through a manifolding plate, into the 6 stacks of the array, shown only schematically in Figure 1.

Process air was filtered and preheated before being compressed to 2 bar(abs) by means of a double screw type compressor. For cooling and humidification of the compressed air FEV Motorentechnik (Aachen, Germany) had developed a high pressure (20 bar) water injection system directly into the compressor [3]. The resulting air dew point in the order of 50 °C was high enough for a stable operation of the stacks at temperatures in the range of 65 – 70 °C. For efficiency reasons, the compressor was fed electrically directly form the fuel cell electric outlet. Therefore a separate 12 V blower was used for starting the system.
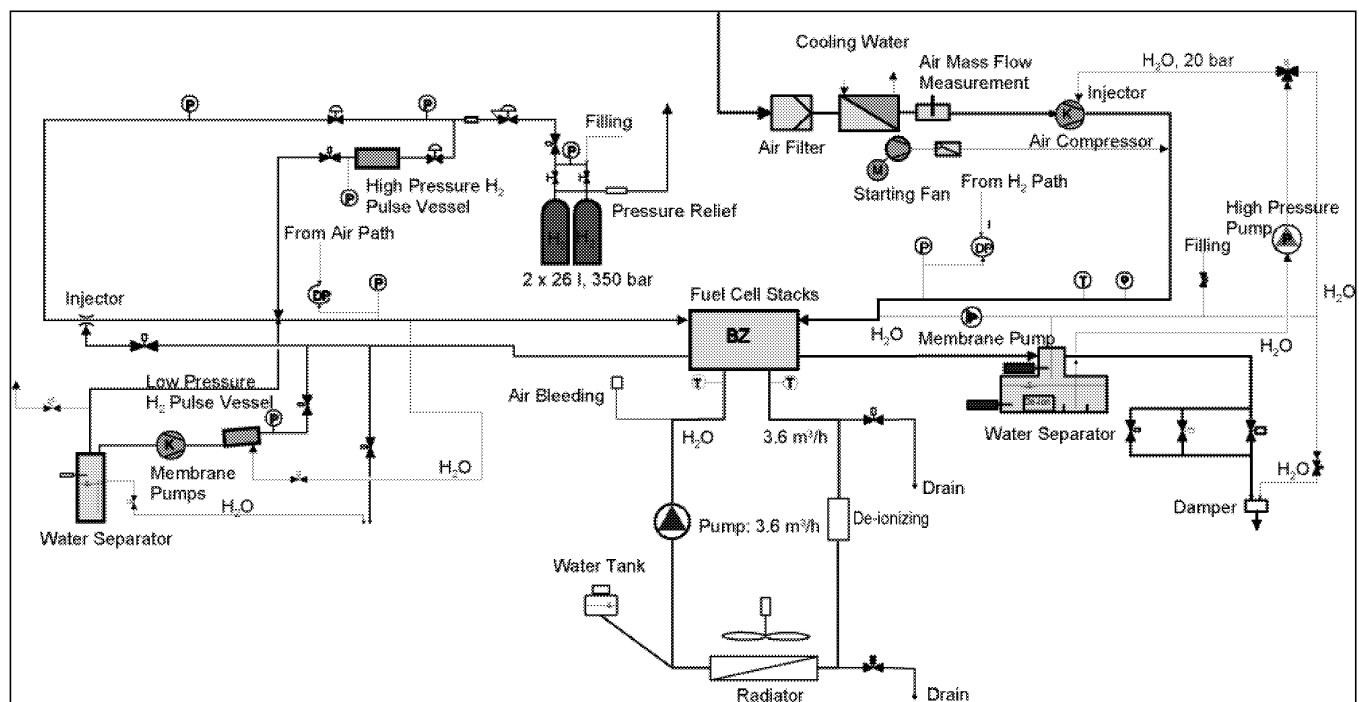
Fig. 1: Schematic layout of the fuel cell system. Left side hydrogen loop with pulsed recirculation; right side air path with water injection into double screw type compressor; bottom cooling loop.
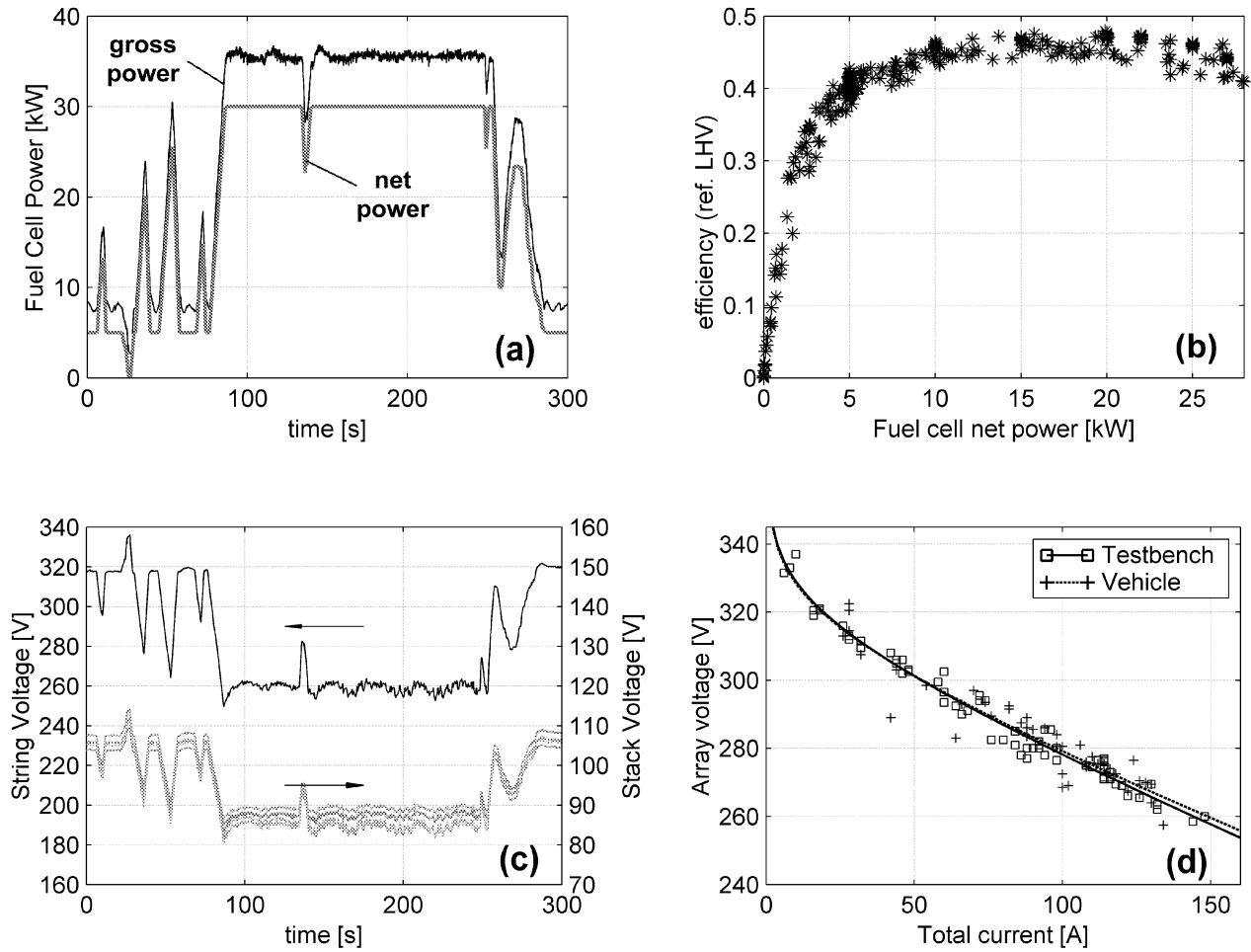
Fig. 2: (a) Power, (b) voltages, (c) efficiency and (d) i/E characteristics of the fuel cell system for a simulated drive on the lowest 5 km of the Simplon pass. In the i/E characteristic (c) values from the test rig and the road are compared.

Hydrogen was stored in two 26l tanks at up to 350 bar and fed in a pressure controlled mode into the stacks. For a stable operation an excess of hydrogen is fed to the stacks. For an efficient use of the fuel, hydrogen was recirculated. To avoid a high parasitic load the hydrogen recirculation was realized in a combination of an injector and a pulsed mode using high and low pressure pulses [4].

3 RESULTS

The fuel cell system was extensively tested on a dynamic test rig. Figure 2 shows results from a simulated test drive on the lowest 5 km of the Simplon pass. The fuel cell system was operated with a dynamic of 2.5 kW/s, which is sufficient when the power requirements of the drive train is levelled by the supercapacitor. Due to a certain fluid dynamic inhomogeniety and condensing of water in the manifolding plate of the stack array, the stacks were performing with slight differences (voltage of top stacks better than of bottom stacks, see Figure 2b) Therefore the maximum gross power of the fuel cell was limited to 36 kW and net power to 30 kW (see Figure 2a). The efficiency of the fuel cell system (calculated on the basis of LHV of converted hydrogen) exceeds 40% in

over the range of 5 – 30 kW net power output (Figure 2c).

The fuel cell system characteristics on the test rig were identical to the performance of the system in the HY.POWER® vehicle. This is shown in Figure 2d as comparison of the i/E characteristic of gross power of the stack array in both environments.

4 ACKNOWLEDGEMENT

5 REFERENCES

[1] P. Dietrich et al., PSI Scientific Report 2002, V, 100-101 (2003).

[2] F.N. Büchi et al., PSI Scientific Report 2001, V, 93 (2002).

[3] P. Dietrich et al., Proc. SATG Konferenz, Wil, ISBN 3-906483-03-7, September 13 (2002).

[4] A. Tsukada and P. Rodatz, PSI Scientific Report 2001, V, 88 (2002).

SURFACE CHARACTERISATION OF WC-Co AFTER ELECTRO-DISCHARGE MACHINING

C. Stössel-Sittig, B. Schnyder, R. Kötz

Wire electro-discharge machining (W-EDM) of tungsten carbide with Co-binder (WC-Co) may lead to corrosion and discolouration at the surface. To avoid corrosion it is important to get a better understanding of the processes involved. In a first step the surfaces of WC-Co produced with W-EDM are investigated by X-ray photoelectron spectroscopy (XPS) / Auger electron spectroscopy (AES) and scanning electron microscopy (SEM). These investigations show that the surface is covered by a layer containing Zn and Cu oxides and sometimes also W and Co. The composition of this layer is influenced by the EDM process parameters and / or the machine (e.g. water quality). Further on it is shown that with decreasing surface roughness, the surface morphology changes not only in terms of roughness but also in the general pattern.

1   INTRODUCTION

Wire Electro-Discharge Machining (W-EDM) is a very promising approach towards micro- and nanomachining. In order to improve the accuracy of the work piece and the surface finish a better control of the machining parameters and especially of the thermally affected zone is required. But possible corrosion attack and discolouration of the work piece (Figure 1) during W-EDM in water makes all further efforts towards micro- and nanomachining useless. The corrosion problem can be reduced or avoided by performing the erosion in oil, nevertheless erosion in water has several advantages (higher erosion rate, easier to control, no risk of burning), which justify efforts to study the W-EDM process in water. Therefore, in May 2002 a project was started by a manufacturer of EDM machines, AGIE SA, together with the academic partners ETHZ, University of Berne and PSI, to study the corrosion aspects of the W-EDM process. Since the corrosion effects of eroded work pieces were often observed on tungsten carbides, first experiments were performed on tungsten carbide with Co-binder (WC-Co). One first step was to investigate the surface of WC-Co after W-EDM to get a better knowledge of the initial state.
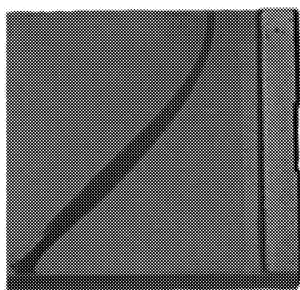
Fig. 1: Discolouration induced during the W-EDM process on the surface of a WC-Co sample.

2   EXPERIMENTS

To investigate the effect of the W-EDM process onto the WC-Co sample surface, AGIE SA produced several sets of samples. On the one hand the samples were produced on different EDM machines at different dates, on the other hand they were produced with different surface roughnesses. Table 1 gives an overview of the different investigated samples. All samples were eroded with a brass wire coated with zinc. The sample size was about 15 x 15 mm^2.

The investigations were performed by X-ray photoelectron spectroscopy (XPS) and Auger electron spectroscopy (AES) to determine the surface composition and by scanning electron microscopy (SEM) to image the surface morphology.

Set	EDM machine	Production date	R_a (μm)	No. of samples
1a	A	June 2002	0.2	2
1b	A	July 2002	0.2	2
2	B	Sep. 2002	0.2	7
3	C	Oct. 2002	0.1	3
4	C	Oct. 2002	<0.1	1

Table 1: Overview of the different investigated sample sets, which were produced on different EDM machines at different dates, with different surface roughness (R_a), as well as the number of the analysed samples of each set.

3   RESULTS

On the first sample set (1a and 1b) 15 to 16 spots per sample were analysed by XPS. The analysed spots had a distance of about 3 mm from each other to investigate the overall elemental distribution on the surface. However, no general trend of the overall elemental distribution was found. Consequently, the other sets (2 – 4) were analysed on 2 to 4 spots per sample only. The results of the XPS analyses are shown in Figure 2.

The XPS analyses show that the surface, which was produced in the W-EDM process, is covered with Zn and Cu. Zn and Cu probably either originate from the brass wire and its Zn coating and / or from the water used during the W-EDM process. In the case of set 4 the covering with Zn and Cu of the surface produced with W-EDM is too thick to detect W and Co with XPS. On the sets 1 and 3, only a small amount of W was detected by XPS in addition to Zn and Cu. It is not clear, if the W originates from the WC-Co base mate-

rial or from the water used during the W-EDM. On set 2 the covering with Zn and Cu seems to be quite thin or discontinuous so that W and even Co were detected by XPS. Also in this case it is not clear if the W and Co signals originate from the base material or if they are integrated into the layer of Zn and Cu. Angle resolved XPS analyses as well as XPS depth profiling are planned to get a better knowledge of the elemental distribution in the first layers. On all surfaces Zn and Cu were detected in oxidised form.
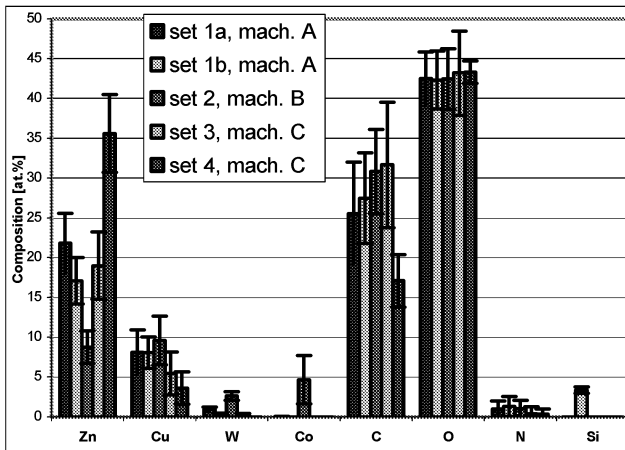
Fig. 2: XPS analyses of the different sample sets show differences in the sample surface, which was produced by W-EDM (mean value +- standard deviation; see also table 1 and text).

The difference between set 1 and set 2 could be explained with the use of different EDM machines. The machines are similar according to AGIE SA, but the quality of the water used during the W-EDM process, which is in contact with the sample surface during the process, is probably not the same and still under investigation. Although the sets 1 and 3 are produced with different roughness they look quite similar in the XPS analyses.
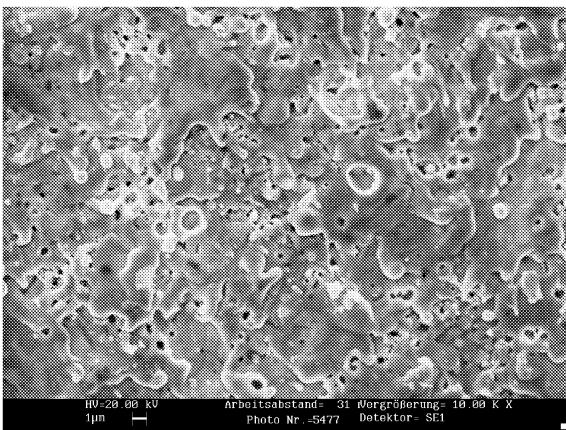
Fig. 3: SEM image of a sample of set 1a.

In the C 1s signal no carbidic C was detected with XPS. C, N, Si and partly O are contaminations either from the water or from the storage of the samples in air, where e.g. C is a typical contamination.

Investigations with the SEM show that the surface morphology of the sets 1 and 2 are similar and give an impression of a melted zone that was formed during

the W-EDM process (Figure 3). Also set 3, which was produced with a finer roughness, still give the impression of this melted zone (Figure 4), while the morphology of the sample with the smallest roughness looks very different (Figure 5).
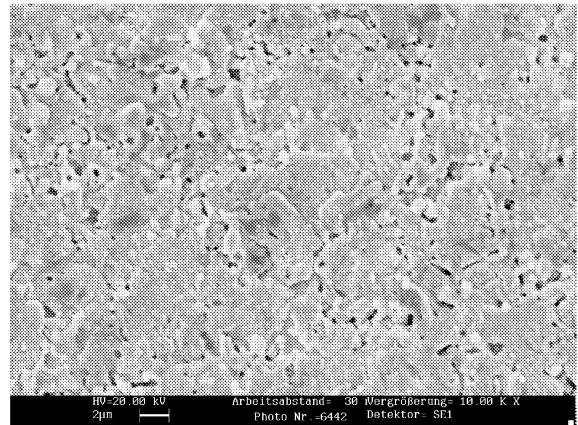
Fig. 4: SEM image of a sample of set 3.
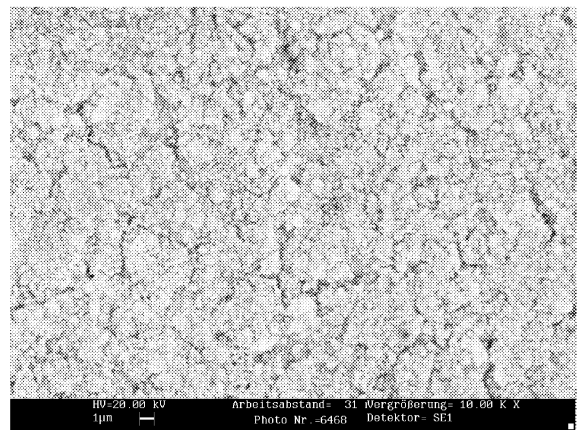
Fig. 5: SEM image of a sample of set 4.

4   CONCLUSION

The surface of a sample produced by W-EDM depends on the process parameters used. Therefore, it is important to know these parameters as well as the machine or at least the water quality of the machine, which was used for the production of the samples.

The initial surface completely changed in terms of composition during the W-EDM process since Zn and Cu either from the wire or from the water are covering the surface at least partly. Therefore, also Zn and Cu have to be included in further investigations of the corrosion behaviour of the eroded WC-Co samples.

SEM images show that the surface morphology changes not only in terms of roughness, but also in the general pattern with decreasing R_a. While the samples of the sets 1 - 3 still show a melted zone at the surface, the sample surface of set 4 (with the smallest R_a value) appears completely different.

5   ACKNOWLEDGEMENTS

UV-IRRADIATION INDUCED MODIFICATION OF PDMS FILMS INVESTIGATED BY XPS AND SPECTROSCOPIC ELLIPSOMETRY

B. Schnyder, R. Kötz, T. Lippert, A. Wokaun, V.-M. Graubner (TU München), O. Nuyken (TU München)

UV-irradiation (172 nm) induced changes of poly(dimethyl-siloxane) (PDMS) surfaces were investigated with X-ray photoelectron spectroscopy (XPS) and spectroscopic ellipsometry (SE). Both methods indicate the modification of the PDMS to a silica-like surface (SiO_2). These conclusions could be drawn from the elemental composition determined by XPS and the binding energy shifts in the XPS spectra of the Si 2p and O 1s levels. Similarly the refractive index n determined with ellipsometry reaches a value close to the one of SiO_2. Additionally, ellipsometry allows to monitor the decrease of the original film thickness with increasing UV-irradiation time.

1   INTRODUCTION

For many polymer applications the surface needs to be modified in order to improve its properties like wettability or adhesion. Consequently the modification of technically relevant polymers like poly(dimethylsiloxane) (PDMS) is a growing research field. The surface modification of PDMS by ultraviolet radiation in the presence of atmospheric oxygen [1] or by plasmas generated by partial corona discharge [2] was reported previously. The described processes suffer from restricted atmospheric conditions and rather long reaction times. Ambient conditions with shorter reaction times are more desirable. Photochemical modification of the PDMS surface by irradiation with lasers and eximer-lamps in the vacuum UV region is a promising alternative. The induced surface modification can result in the conversion of the polymer surface from hydrophobic to hydrophilic without ablation of the polymer. One possible application of modified PDMS films could be computer-to-plate driography, where anhydrous ink is used and no development steps are necessary.

2   EXPERIMENTAL

For the XPS measurements films of crosslinked PDMS were prepared by bar coating on poly-(ethylene terephthalate) plates (PET-plates) with a 12 wt% solution of vinyl-functionalized poly-(dimethylsiloxane), poly-(methylhydrosiloxane) as a cross linker and a Kartstedt platinum catalyst in isooctane. After evaporation of the solvent the films were cured for 5 minutes at 100°C, resulting in an average film thickness of about 8 μm. For ellipsometry measurements films of crosslinked PDMS were prepared by spin-coating (1500 and 2500 rpm) with the same solution (1 - 6.5 wt%) on silicon wafers. After the spin-coating process the films were cured for 5 min at 100°C. In order to obtain different thicknesses(50 – 250 nm) the rotation speed and/or the solution concentration was varied.

Exposure to short incoherent UV light was performed with a water-cooled UV excimer lamp (cf. Figure 1), mounted in a Plexiglas box. The discharge was initiated in an annular gap between two coaxial quartz tubes containing xenon at 750 mbar emitting at a wavelength of 172 nm. The PDMS films were irradiated with intensity of approximately 20 mW/cm² in a

distance of about 5 mm from the outer tube surface of the xenon excimer lamp.
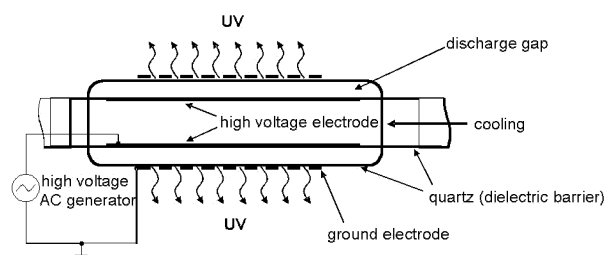
Fig. 1: Sketch of water-cooled Xe_2^* excimer lamp (λ = 172 nm).

XPS spectra were recorded with an ESCALAB 220i XL instrument (Thermo VG Scientific). In order to reduce the degradation of the PDMS films, the magnesium X-ray source ($h\nu$ = 1253.6 eV) was operated at a power of 100 W.

Spectroscopic Ellipsometry was performed using a spectroscopic ellipsometer (MOSS model ES 4G, SOPRA, France) at an angle of incidence of 70° and a xenon arc lamp (75 W) as light source.

3   RESULTS

XPS measurements indicate large changes in the chemical composition of the irradiated PDMS even after a short irradiation time of a few minutes. The XPS C 1s signal decreases drastically with increasing UV-irradiation time. After 3 minutes the carbon content decreased from 47 at%, which is close to the theoretical value of 50 at%, to 17 at%, to reach a final value of 4 at% after 40 minutes of exposure. Additionally, the atomic concentration ratio of O/Si starting at about 1 reaches values close to two, which would correspond to a composition close to SiO_2.

This fact is also confirmed by the shifts of the peak positions of the Si 2p and the O 1s levels, illustrated in Figure 2 for the Si 2p level. The Si 2p binding energy for untreated PDMS is 102.0 eV and shifts to 103.5 eV after 40 minutes of UV-light exposure. This peak position corresponds well with a measurement of SiO_2 quartz powder (cf. again Figure 2) and literature values of 103.3 - 103.7 eV [3] for SiO_2. For the O 1s level the measured value corresponds again quite well to published data for SiO_2[3].
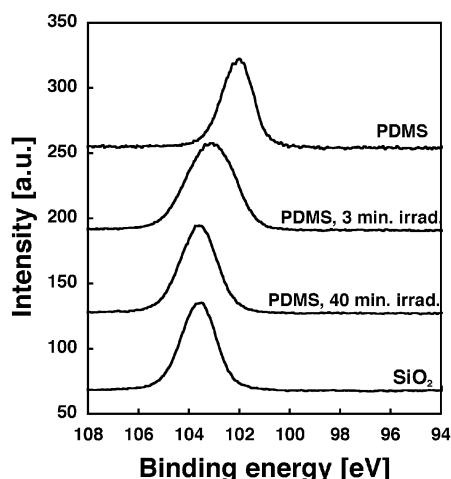
Fig. 2: Comparison of the XPS spectra of Si 2p level for a reference sample of SiO_2, as received PDMS films, and two irradiated PDMS films.

For these transparent untreated and irradiated PDMS films (k=0) spectroscopic ellipsometry allows to determine the film thickness and the refractive index n simultaneously.
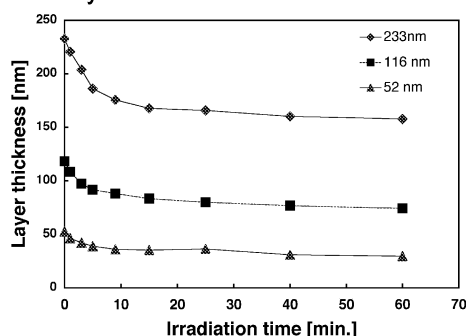
Fig. 3: Film thickness determined with ellipsometry of three different PDMS films on silicon substrates vs. irradiation time.

Figure 3 shows the thickness of three different PDMS films as function of the UV-irradiation time. Plotting the relative thickness of these three films as function of the irradiation time, the three curves fall more or less on each other (not shown here). The corresponding values for n at a photon energy of 2.0 eV are 1.405 for untreated PDMS, which increases to 1.445 after 60 minutes of exposure (cf. Figure 4). This value is close to the literature value for SiO_2 of 1.457 [4].

The surface and bulk modifications of PDMS films could originate from photons, heat, ozone/active oxygen species formed by the VUV light [5], or various combinations. The fact that the relative thickness changes induced by the irradiation are the same for all films can only be explained by a mechanism which takes place in the whole volume and not only at the surface. Active oxygen species would react mainly at the surface of the polymer and can thus be excluded. Ozone could probably diffuse into the polymer and influence the modification of the PDMS in the bulk material. Photons and heat can modify the material to the whole extent. The thermal load of the sample is reduced by the water-cooling of the excimer lamp and

should therefore play only a minor role. Finally, the photons would be the important parameter for the mechanism of surface modification of PDMS.

In further experiments we will investigate the mechanism in more detail.
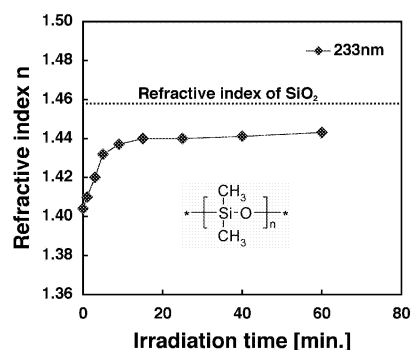
Fig. 4: Change of the refractive index n of a 233 nm thick PDMS films on silicon substrates vs. irradiation time. Inset: Molecular structure of Poly (dimethylsiloxane) (PDMS).

4 CONCLUSION

The UV-irradiation results in a decrease of the carbon content of the PDMS surface with irradiation time. Additionally the binding energies of the Si 2p and O 1s and the atomic concentration ratio O/Si indicate the formation of a SiO_2-like surface. SE revealed a decrease of the PDMS films thickness due to the UV-irradiation. Similar to the electronic properties, the optical properties of irradiated PDMS become also silica-like. However, ellipsometry is probing the whole sample thickness and not only the surface regime like XPS.

5 ACKNOWLEDGEMENTS

6 REFERENCES

[1] M. Brinkmann, V.Z.-H. Chan, E.L. Thomas, V.Y. Lee, R.D. Miller, N. Hadjichristidis, and A. Avgeropoulos, Chem. Mater. **13**, 967 (2001).

[2] H. Kim and M.W. Urban, Langmuir **15**, 3499 (1999).

[3] J. F. Moulder, W. F. Stickle, P. E. Sobol, and K. D. Bomben, in Handbook of X-ray Photoelectron Spectroscopy, J. Chastain (Ed.), Perkin-Elmer Corp., Eden Praire, MN, 1992.

[4] Handbook of Optical Constants of Solids, Vol. 1 and 2, Ed. E. D. Palik, Academic Press, Inc., 1985 and (1991).

[5] B. Eliasson, and U. Kogelschatz, OZONE, Sci. Eng. **13**, 356 (1991).

LASER MICROMACHINING: NEW CONCEPTS FOR FABRICATION OF OPTICAL ELEMENTS IN QUARTZ

G. Kopitkovas, T. Lippert, C. David, J. Gobrecht, A. Wokaun

Micro-optical elements in quartz with continuous profiles were fabricated by laser induced backside wet etching. This method allows microstructuring of quartz with a XeCl or KrF excimer laser at laser fluences well below the damage threshold of quartz at these wavelengths. Fresnel lenses were created by applying diffractive grey tone phase masks, which were prepared by e-beam lithography.

1   INTRODUCTION

Micro-optical elements with continuous structure profiles (e.g. beam homogenisers for high power lasers) are usually made by photolithography, and subsequent transfer of the resist profile into the quartz surface by reactive ion etching [1]. This technique requires an excellent control of the exposure dose, the resist characteristics, and the proportional etching process. A simpler method for the fabrication of micro Fresnel lenses in polymers has been reported by David et al. [2]. However, quartz glass is transparent to the common laser wavelength and can only be structured by VUV lasers (157 nm), or ultrafast (fs) lasers.

We are presenting an alternative method for a one step process of micro-optical elements in quartz by combining laser induced backside wet etching (LIBWE) [3] and a simple projection method [2].

2   EXPERIMENTAL

The experimental set-up for the fabrication of micro-optical elements in quartz is shown in Figure 1. A KrF (248 nm, 30 ns) or XeCl (308 nm, 30 ns) are applied as irradiation sources. Diffractive grey tone phase masks, fabricated by e-beam lithography are used to modulate the laser intensity which is projected onto the quartz sample by a lens. The wet etching solution is pyrene in acetone at a concentration of 0.4 M/l.
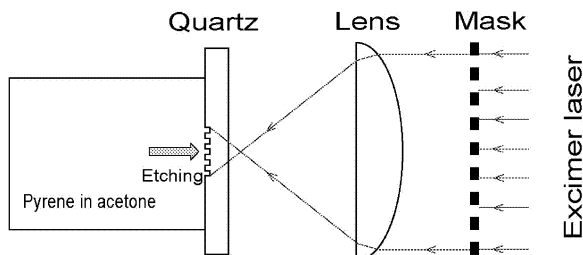
Fig. 1: Experimental setup.

3   RESULTS AND DISCUSSION

The etching of quartz by LIBWE reveals a behaviour similar to ablation of polymers, where a threshold fluence of ablation exists. The threshold for quartz by LIBWE was determined experimentally by measuring the etch rates at various laser fluences (shown in Figure 2). The threshold fluences for irradiation at 308 nm is 0.5 J·cm^{-2} and for 248 nm irradiation is 0.3 J·cm^{-2}. The obtained threshold fluences are well below the

damage threshold of quartz, which is in the range of 10 – 20 J·cm^{-2} at the applied laser wavelengths.

A Fresnel lens fabricated in quartz with a XeCl excimer laser at a fluence of 1 J·cm^{-2} is shown in Figure 3. This Fresnel lens is the result for the fabrication of complex patterns with continuous profiles in transparent optical materials with LIBWE.
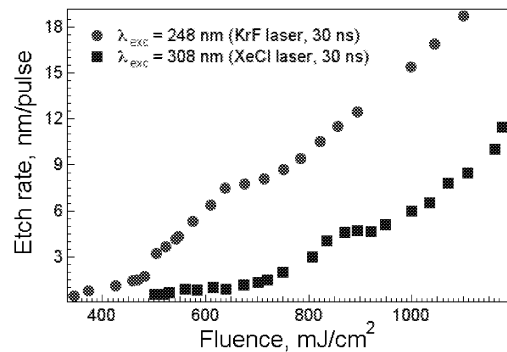
Fig. 2: Etch rate versus laser fluence.
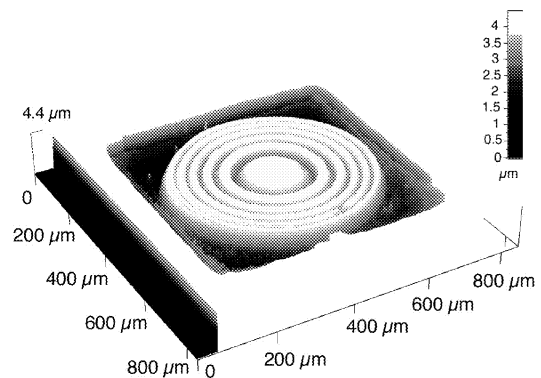
Fig. 3: 3D profilometer scan of a Fresnel lens etched in quartz by LIBWE using a XeCl laser

4   REFERENCES

[1]   See for example: Micro-optics, Ed.: H.P. Herzig, Taylor&Francis, London (1998).

[2]   C. David, T. Lippert, J. Wei, A. Wokaun, Microelectron. Eng. **57-58**, 453-460 (2001).

[3]   J. Wang, H. Niino, A. Yabe, Appl. Phys. A **68**, 111-113 (1999).

TIME-RESOLVED ANALYSIS OF THE PLASMA CREATED BY ABLATION OF La$_{0.6}$Ca$_{0.4}$CoO$_3$ TARGETS

M.J. Montenegro, T. Lippert, S. Müller, P.R. Willmott, A. Wokaun

The ablation plasma of La$_{0.6}$Ca$_{0.4}$CoO$_3$ (LCCO) produced by KrF excimer laser (248 nm) irradiation, with and without a synchronized N$_2$O gas pulse, is analyzed by spatially and temporally resolved optical emission spectroscopy. The spectra reveal higher intensities for all peaks when the gas pulse is applied. The maximum intensities of the plasma with the gas pulse are observed later in time and further away from the target.

1 INTRODUCTION

During the interaction of a high power density laser with a target, highly excited species are formed in the plasma plume. The chemical state of the plasma exhibits a very dynamic behavior, especially when a reactive gas pulse is applied. The plasma velocity, energy, and composition affect the morphological and structural properties of the produced films [1,2]. The properties of the plasma have been measured as a function of time, distance, and gas pressure for various atomic species.

2 EXPERIMENTAL

Pulsed Reactive Crossed-Beam Laser Ablation combined with emission spectroscopy of La$_{0.6}$Ca$_{0.4}$CoO$_3$ has been carried out using a KrF excimer laser under the same conditions as for film deposition. The time delay between the gas pulse and the laser pulse was 400 μs, where the maximum interaction between the ablation plasma and the gas pulse is achieved. The plasma formed during the ablation process is analyzed in the range of 300-800 nm. The spectra were collected at different distances from the target and different gate delays in vacuum, 8x10^{-4} mbar O$_2$ background pressure, and the same background pressure with the additional N$_2$O gas pulse. The plasma emission is imaged from the plume via a fiber optic to a spectrometer with an I-CCD camera.

3 RESULTS AND DISCUSSION

Figure 1 shows the time where the maximum emission intensity is observed, for La II, Ca I and Co I, as a function of the distance from the target with oxygen (upper row) and with the additional gas pulse (lower row). In this annotation "I" means neutral species, while "II" is a singly ionized species. A higher maximum intensity is observed at later times for the gas pulse. The time of the maximum intensity at a certain distance remains the same for positions within the first 2 mm, both in oxygen background and for the gas pulse. For positions > 2mm, the maximum intensity, obtained with the gas pulse, occurs at later times. The lifetime of the excited states of the analyzed species are in the range of several ns to $\cong$ 200 ns, while the maximum emission in the presence of the gas pulse is observed after delays of several hundred of nanosec-

onds to a few microseconds. This significant difference indicates that the emission is related to species that have been created significantly after the ablation by collisional excitation with the gas pulse.
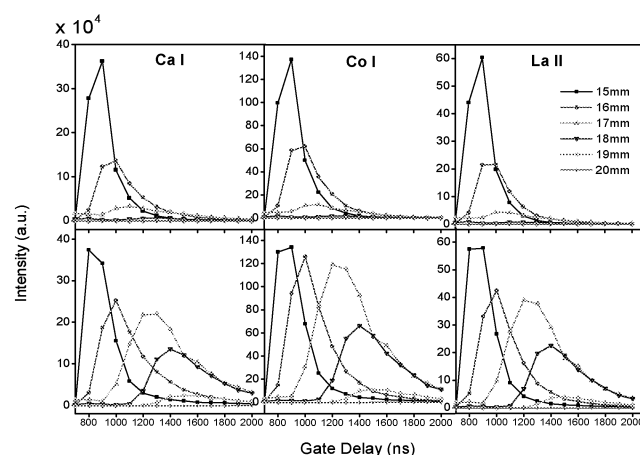
Fig. 1: Time vs. maximum emission intensity of La II, Ca I and Co I at different distances from the target. **Top:** with oxygen background. **Bottom:** with additional gas pulse.

4 CONCLUSION

Higher intensities for the emission lines of all elements are observed in the presence of gas pulse. The time and space resolved measurements reveal that the maximum intensity occurs at later times and can be observed further away from the target. According to these results, the main role of the gas pulse is to increase the collisions between the gas molecules and the plasma particles in a large volume. A more detailed analysis of these gas phase chemical reactions is in program.

5 REFERENCES

[1] R.A. Gunasekaran, J.D. Pedarnig and M. Dinescu, Appl. Phys. A **69**, 621 (1999).

[2] A.M. Haghiri-Gosnet, J. Wolfman, B. Mercey, Ch. Simon, P. Lecoeur, M. Korzenski, M. Hervieu, R. Desfeux and G. Baldinozzi, J. Appl. Phys. **88**, 4257 (1994).

LASER ABLATION INDUCED SHOCKWAVE STUDIED BY TIME RESOLVED SHADOWGRAPHY

M. Hauer, T. Lippert, A. Wokaun

Pulsed lasers emitting at 193 nm and 1064 nm were used to ablate an energetic polymer. The shockwave and ejected particles that were created during the laser ablation process, are visualized by time-resolved shadowgraphy. The measurements reveal that the speed of the shockwave increases with laser fluence and decreases with the irradiation wavelength.

1 INTRODUCTION

One possible application of the laser ablation process is its use in laser plasma thrusters (LPT's). In these devices the ejected material provides the thrust that is used to stabilize the trajectory of satellites in space. It has been shown that an energetic polymer produces a ratio between thrust and laser energy that is higher than for other polymers [1]. An additional absorber has normally to be added to the polymer, to allow the application of IR laser diodes (small and very efficient laser sources). The expansion velocities of shockwaves created in air may be used as an indication for the energy which is released during ablation [2] and therefore for the performance of these materials in LPT's. Different irradiation wavelengths were applied to compare the influence of the absorption site (the polymer chain or the absorbent) on the propagation speed of the shockwave.

2 EXPERIMENTAL

A solution of the energetic polymer in ethylacetate with carbon (to induce absorption in IR) and hexamethylene diisiocyanate (as cross linker) was solvent cast onto a glass substrate. The material was ablated by a pulsed pump laser (i.e. 193 nm or 1064 nm). A probe laser is used to generate fluorescence (ns) of a laser dye in a quartz cuvette at specific delays after the pump laser. This fluorescence is used to create time resolved images of the ablation products and shockwaves.

3 RESULTS

Figure 1 shows the shadowgraphy image of the energetic polymer taken 1610 ns after a 1064 nm pump pulse.
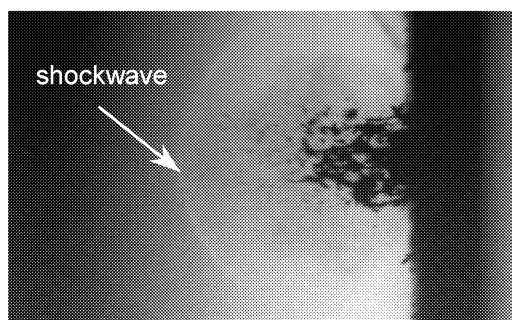
Fig. 1: Shadowgraphy image taken 1610 ns after the pump pulse (1064 nm).

The ejection of particles is clearly visible in addition to the hemispheric shockwave, which can be seen as a bright ring. At shorter irradiation wavelengths, no particles are visible in the ablation plume (not shown here), suggesting a decomposition of the polymer into small gaseous fragments.

Figure 2 shows the propagation of the shockwave for irradiation with different wavelengths. The shockwave after 193 nm irradiation with 1.56 mJ/pulse is as fast as the shockwave released after 1064 nm irradiation with 11.22 mJ/pulse. This indicates that at shorter wavelengths, more gaseous products are released (confirmed by the absence of the large fragments), which results in higher pressures of the products that support the shockwave. The required energy for shockwaves of the same velocities is much lower for UV irradiation wavelengths.
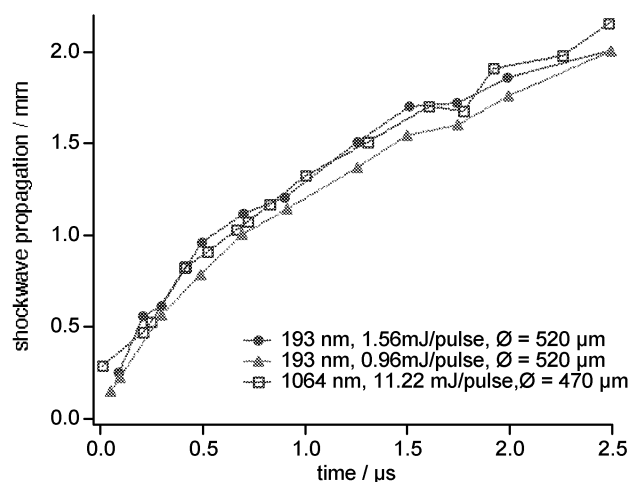
Fig. 2: Propagation of the shockwave at different fluences and pump wavelengths.

4 ACKNOWLEDGEMENTS

5 REFERENCES

[1] C.R. Phipps, J.R. Luke, G.G. McDuff, T. Lippert, SPIE **4760**, 833-842 (2002).

[2] L.S. Bennett, T. Lippert, H Furutani, H. Fukumura, H. Masuhara, Appl. Phys. A **63**, 327-332 (1996).

MICROSTRUCTURING OF GLASSY CARBON:
COMPARISON OF LASER MACHINING AND REACTIVE ION ETCHING

M. Kuhnke, C. David, T. Lippert, E.E. Ortelli (Dyconex), U.A. Paulus, G.G. Scherer, A. Wokaun

Reactive ion etching of glassy carbon can be performed with etch rates higher than 40 µm/h, but the aspect ratio is limited due to the degradation of the metal mask. Laser machining allows to fabricate channels with an aspect ratio of 5. Flowfield channels, i.e. 100 parallel channels per electrode with a depth of 250 µm and a width of 50 µm, were tested in a model of a micro fuel cell.

1   INTRODUCTION

Structuring of glassy carbon (GC) by various methods is studied at the PSI for several years. One possible application for micro structured GC are electrodes for micro fuel cells. Typical sizes of these structures are a depth of ≈ 200 µm and a width of ≈ 50 µm.

We are currently applying a direct laser structuring method and developing a process that combines the structuring of a metal mask by laser ablation with a sub-sequent reactive ion etching (RIE) step. Results from the metal film ablation experiments, optimization of the GC etching process and the test of laser-machined GC electrodes in a micro fuel cell (µFC) are presented.

2   LASER-RIE-PROCESS

The masks for the RIE process are prepared in several steps. The GC samples are coated with an adhesion promoting Cr layer of 20 nm and a mask layer of 400 nm Al on top of the Cr. The ablation characteristics for irradiation of 308 nm are studied by varying the fluence and the number of pulses. At low fluences, i.e. around 0.5 J cm^{-2}, melting and resolidification of the metal is observed without significant ablation. In the range of 1.0 to 2.0 J cm^{-2} the film is almost completely removed (Figure 1a). The number of Al particles in the ablated area decreases with increasing laser fluence, while an increasing ablation of the GC is also detected. At higher fluences a zone of redeposited Al is formed in the vicinity of the ablated spots.
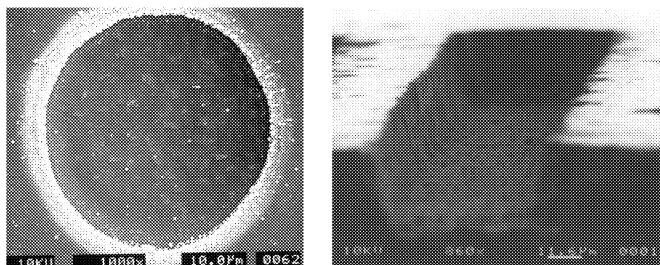
Fig. 1: (a) Laser-ablated Al/Cr film on GC; fluence 1.9 J cm^{-2}, 10 pulses; (b) 80 µm deep plasma etched GC channel.

Complete masks can be fabricated by a step and repeat ablation process of the metal films using a xyz stage. An Al/Cr mask with 1x1 mm^2 and a line width and distance of 50 µm was achieved.

Reactive ion etching of GC in an oxygen plasma produces tapered sidewalls but also flat bottoms (Figure 1b). A maximum etch rate of > 40 µm/h could be achieved by optimizing pressure and RF power (Figure 2).
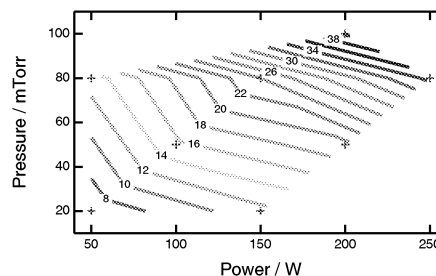
Fig. 2: GC etch rate [µm/h] in 2-D parameter space of pressure and power.

3   LASER-MACHINED MICRO ELECTRODE

The flow field of a µFC electrode was fabricated by laser ablation using a kHz-Nd:YAG at 355 nm (active area: 1 cm^2, see Figure 3b). Figure 3a shows a side view of the ≈ 250 µm deep channels with a spacing and width of 50 µm.
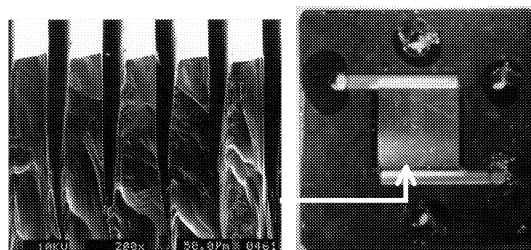
Fig. 3: (a) Laser-ablated flowfield channels in GC; (b) electrode with gas supply structures.

The electrodes were sputter-coated with 50 nm Pt as catalyst and tested with a Nafion 117 membrane (serving also as gasket). This concept allows us to omit gas diffusion electrodes and gaskets and simplifies the cell design. Max. power density: 2.5 mW/cm^2 (Figure 4).
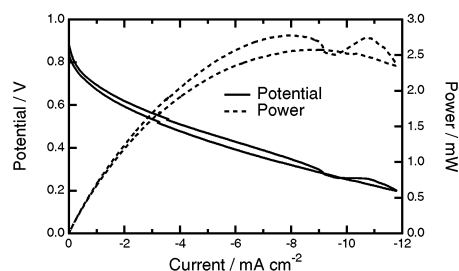
Fig. 4: U-I plot of µFC with laser-machined flowfield.

4   CONCLUSION

Metal masks for RIE of GC can be structured by laser ablation, but the mask performance during the RIE has to be improved. Laser machining is a suitable alternative method for fabricating high aspect ratio structures for µFCs, especially if high repetition lasers are applied.

LASER WRITING OF A 2D DATA MATRIX IN GLASS

Th. Dumont, P. Leyvraz (Frewitt SA), T. Lippert, A. Wokaun

The labeling of glass is an important processing step for the pharma industry that allows tracing and controlling these products. However, the conventional methods reveal several disadvantages such as "non-permanent" and "non-tamper-proof". Permanent laser marking of glass vials is a modern technique of writing product information directly on the surface. This case study investigated the feasibility to integrate this method within an industrial environment.

1   INTRODUCTION

Glass vials for pharmaceutical purposes have to be labeled to make them traceable and controllable for the company and along the distribution line. This is typically done by colored line codes or by printed labels. These techniques however have several disadvantages e.g. the ink and/or the glue of the label have limited or no adhesion on many surfaces such as silicone and they are not resistant to sterilization. By directly engraving the data matrix on the surface it is possible to mark almost any material using the appropriate laser parameters such as wavelength and laser energy. Experiments were performed with two types of glass (labeled "brown" and "clear") at two different wavelengths (266 and 355 nm) with different pulse numbers and fluences.

A 2D data matrix offers the possibility to store a certain amount of product information on a relatively small area. As an example, the applied 10x10 matrix corresponds to 6 digits. A 16x16 matrix contains already 24 digits.

There are basically two ways to write the matrix on the glass. One is using more than one laser mark (e.g. 9) to create one pixel of the whole matrix as shown in Figure 1. The other applies only one laser shot per pixel of the matrix as shown in Figure 2.
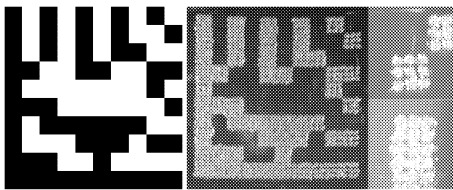
Fig. 1: 10x10 2D data matrix: bitmap (left), laser marking (middle), magnification (right).
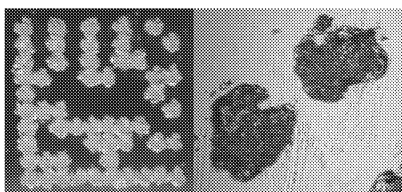
Fig. 2: 2D data matrix using large pixels.

Each method has its own advantages. The multi spot marking is less susceptible to errors by processing, e.g. the matrix is still readable with missing pixels. The disadvantage of this technique is the high number of laser marks, which have to be overcome by the appli-cation of high repetition rate lasers (e.g. kHz). The single mark method takes much less time since the number of marks is smaller, but higher laser fluences are necessary.

2   EXPERIMENTAL

The 3rd and 4th harmonics of a Nd: YAG laser was applied as irradiation source. The samples were mounted on a computerized XYZ stage and the ablation spots were characterized with a profilometer.

3   RESULTS AND DISCUSSION

The "brown" glass samples reveal light absorption to both irradiation wavelengths and can be marked at both wavelengths. The "clear", samples, however are highly transparent at 355 nm (90%). In this case rear-side ablation occurs. This phenomenon cannot be understood as "normal" ablation, i.e. as a consequence of homogeneous volume absorption of energy and evaporation of heated or decomposed material. Ablation of highly transparent materials can be mainly explained by scattering or absorption of radiation at singularities (impurities or other irregularities). These singularities are mainly concentrated at the surface. The threshold fluences for the rear side ablation are much lower than for front side ablation. This can be explained by the Fresnel theory:

"A wave is reflected at the front side with a phase shift of 180° thus leading to a destructive interference with the original wave. At the rear-side there is no phase shift thus leading to a constructive interference." This explains why the threshold fluence is lower for rear-side than for front-side ablation [1]. Although this phenomenon can be useful for some applications it is not desirable for marking closed vials as rear-side etching means in this case, etching at the inner side of the vial which can lead to chemical reactions with the content of the vial.

Rear side ablation does not occur at any fluence at 266 nm. The transparency at this wavelength is almost 0%, allowing direct front side ablation.

4   ACKNOWLEDGEMENTS

5   REFERENCES

[1]   J. Ihlemann Appl. Surf. Sci. **54,** 193-200 (1992).

LIST OF PROJECTS, TEACHING ACTIVITIES, CONTRIBUTIONS TO SCIENTIFIC JOURNALS, CONFERENCES, PATENT APPLICATIONS AND MEMBERSHIPS

PROJECT COLLABORATIONS WITH EXTERNAL PARTNERS

BBW

Projektleiter: P. Novák
CAMELiA (Calendar Life Mastering of Li-Ion Accumulator)
EU-Projekt

Projektleiter: P. Novák
LiBERAL (Lithium Battery Evaluation and Research – Accelerated Life Test Direction)
EU-Projekt

Projektleiter: P. Novák
SLiON (Solvent-Free Lithium Polymer Starter Battery)
EU-Projekt

BFE

Projektleiter: F.N. Büchi
PowerPac: Entwicklung eines mobilen 1 kW Brennstoffzellensystems
BFE and ETH Zürich

Projektleiter: G.G. Scherer
Polymer Elektrolyt Brennstoffzellen mit H_2 und Methanol als Brennstoff

EOARD

Projektleiter: T. Lippert
Polymers used as Fuel in Laser Plasma Thrusters in Small Satellites

EU AND INDUSTRY (CRAFT)

Projektleiter: P. Novák
High Performance Active Smart Card with Contactless Charging
EU-Projekt

INDUSTRY

Projektleiter: P. Novák
Entwicklung eines Batterieseparators sowie einer Brennstoffzellenmembran (PEM) auf Basis der keramischen Membranfolie der CREAVIS
CREAVIS Gesellschaft für Technologie und Innovation mbH, Marl, Germany

Projektleiter: P. Novák
Behandlung der Graphite für die negative Elektrode der Lithium-Ionentransferbatterie
TIMCAL AG, Bodio

Projektleiter: P. Novák
Elektrochemische Charakterisierung von Oxiden für Lithium-Ionen-Batterien
Ferro GmbH, Frankfurt (Main), Germany

Projektleiter: P. Novák
Entwicklung und Optimierung einer negativen Elektrode für Lithium-Ionen-Batterien
Ionity AG, Kamenz, Germany

Projektleiter: G.G. Scherer
Membranen für die Direkt Methanol Brennstoffzelle
Automobilindustrie

Projektleiter: G.G. Scherer
Membranentwicklung für Brennstoffzellen
Chemische Industrie

Projektleiter: G.G. Scherer
CO-Toleranz von Polymerelektrolyt Brennstoffzellen
Bosch AG

KTI

Projektleiter: R. Kötz
Optimized Electrochemical Capacitors

Projektleiter: R. Kötz
Synthesis of supported, nanosstructured, high porosity carbon as electrode material

Projektleiter: T. Lippert
Laser-Dünnglasbeschriftung: Methoden und Systeme

Projektleiter: B. Schnyder
Corrosion aspects of the EDM process

NATIONALFONDS

Projektleiter: T. Lippert
Application of Excimer Lamps for Polymer Processing and Catalysis

Projektleiter: R. Kötz
Scanning Probe Microscopy of the Solid Electrolyte Interphase (SEI)

Projektleiter: P. Novák
*Synthesis and Characterization of Advanced
Electroactive Materials for Electrodes of
Rechargeable Lithium-Ion Batteries*

Projektleiter: A. Wokaun, T. Lippert
*Laser Ablation as a Tool for Trace Analysis and High
Resolution Material Transport*

Projektleiter: A. Wokaun, T. Lippert
*Comparison of the Mechanisms of Laser Ablation and
Laser-Induced Material Transfer*

TEACHING ACTIVITIES

University Level Teaching

PD Dr. P. Novák, Prof. Dr. A. Wokaun
Elektrochemische Prozesse
ETH Zürich, WS 2002/2003.

Prof. Dr. A. Wokaun, Dr. J. Gass, Dr. G.G. Scherer
Technik erneuerbarer Energien, Teil 2
ETH Zürich, WS 2002/2003.

Contributions to Courses at Universities, FHL, and Other Institutes

Dr. F.N. Büchi
Brennstoffzellenstapel und Systeme
Beitrag zur Vorlesung "Technik erneuerbarer Energien
2", Prof. A. Wokaun, ETH Zürich, January 24, 2002.

Dr. F.N. Büchi
Brennstoffzellen: Saubere Energie für die Zukunft?
Volkshochschule der Region Zurzach, Villigen PSI,
November 7, 2002.

Dr. R. Kötz
*Elektrochemische Energiespeicherung –
Doppelschichtkondensatoren*
Beitrag zur Vorlesung "Technik erneuerbarer Energien
2", Prof. A. Wokaun, ETH Zürich, January 29, 2002.

Dr. T. Lippert
Beitrag zur Vorlesung "Physikalisch-chemische
Grundlagen der Energienutzung",
Prof. Dr. A. Wokaun, ETH Zürich, May 21, 2002.

PD Dr. P. Novák
*Elektrochemische Energiespeicherung
1. Grundlagen; 2. Batterien*
Beitrag zur Vorlesung "Technik erneuerbarer Energien
2", Prof. Dr. A. Wokaun, ETH Zürich, January 8 and
15, 2002.

Dr. G.G. Scherer
Brennstoffzellen
Beitrag zur Vorlesung "Technik erneuerbarer
Energien", Prof. Dr. A. Wokaun, ETH Zürich, January
22 and 29, 2002.

PUBLICATIONS

Peer Reviewed Papers

B. Andreaus, A.J. McEvoy[1], G.G. Scherer
*Analysis of Performance Losses in Polymer
Electrolyte Fuel Cells at High Current Densities by
Impedance Spectroscopy*
Electrochim. Acta **48**, 2223-2229 (2002).
[1] EPF Lausanne

C. Barbero[1], M.C. Miras[1], E.J. Calvo[1], R. Kötz,
O. Haas
*A probe beam deflection study of ion exchange at
poly(vinylferrocene) films in aqueous and nonaqueous
electrolytes*
Langmuir **18**, 2756-2764 (2002).
[1] Universidad Nacional de Rio Cuarto (UNRC),
Argentina

H.V. Brand[1], R.L. Rabie[1], D.J. Funk[1], I. Diaz-Acosta[2],
P. Pulay[2], T. Lippert
*Theoretical and experimental study of the vibrational
spectra of the a, b, and d phases of octahydro-1,3,5,7-
tetranitro-1,3,5,7-tetrazocine (HMX)*
J. Phys. Chem. B **106**, 10594-10604 (2002).
[1] Los Alamos National Laboratory, USA
[2] University of Arkansas, USA

A. Braun[1], M. Bärtsch, B. Schnyder, R. Kötz, O. Haas,
A. Wokaun
*Evolution of BET internal surface area in glassy
carbon powder during thermal oxidation*
Carbon **40,** 375-382 (2002).
[1] Lawrence Berkeley National Laboratory, CA, USA

E. Deiss, F. Holzer, O. Haas
*Modeling of an electrically rechargeable alkaline
Zn/air battery*
Electrochim. Acta **47**, 3995-4010 (2002).

J.-F. Drillet[1], A. Ee[1], J. Friedemann[1], R. Kötz,
B. Schnyder, V.M. Schmidt[1]
*Oxygen reduction at Pt and $Pt_{70}Ni_{30}$ in H_2SO_4 / CH_3OH
solution*
Electrochim. Acta **47**, 1983-1988 (2002).
[1] Fachhochschule Mannheim, Germany

P. Facci[1], D. Alliata[1], L. Andolfi, B. Schnyder, R. Kötz
*Formation and characterization of protein monolayers
on oxygen-exposing surfaces by multiple step self-
chemisorption*
Surf. Sci. **504**, 282-292 (2002).
[1] Università di Modena e Reggio Emilia, Italy

F. Gassmann, Th. Lippert, J. Wei, A. Wokaun
*Convection-induced absorption oscillations in a
cuvette after irradiation of a pentazadiene solution by
laser pulses*
J. Phys. Chem. A **106**, 4061-4067 (2002).

A.B. Geiger, A. Tsukada, E. Lehmann, P. Vontobel,
A. Wokaun, G.G. Scherer
*In situ investigation of two-phase flow patterns in flow
fields of polymer electrolyte fuel cells by neutron
radiography. I: Opportunities, limitations, and first
results*
Fuel Cells **2**, 92-98 (2002).

V.-M. Graubner[1], R. Jordan[1], O. Nuyken[1], Th. Lippert,
M. Hauer, B. Schnyder, A. Wokaun
*Incubation and ablation behavior of
poly(dimethylsiloxane) for 266 nm irradiation*
Appl. Surf. Sci. **197-198**, 786-790 (2002).
[1]　TU München, Garching, Germany

O. Haas, F. Holzer, S. Müller, J.M. McBreen[1],
X.Q. Yang[1], X. Sun[1], M. Balasubramanian[1]
*X-ray absorption and diffraction studies of
$La_{0.6}Ca_{0.4}CoO_3$ perovskite, a catalyst for bifunctional
oxygen electrodes*
Electrochim. Acta **47**, 3211-3217 (2002).
[1]　Brookhaven National Laboratory, Upton, USA

M. Hauer, T. Dickinson[1], S. Langford[1], Th. Lippert,
A. Wokaun
*Influence of the irradiation wavelength on the ablation
process of designed polymers*
Appl. Surf. Sci. **197-198**, 791-795 (2002).
[1]　Washington State University, Pullman, USA

M. Hauer, D.J. Funk[1], T. Lippert, A. Wokaun
*Laser ablation of a triazene polymer studied by ns-
interferometry and shadowgraphy*
SPIE Proc. **4760**, 259-268 (2002).
[1]　Los Alamos National Laboratory, USA

J. Huslage, T. Rager, B. Schnyder, A. Tsukada
*Radiation-grafted membrane/electrode assemblies
with improved interface*
Electrochim. Acta **48**, 247-254 (2002).

F. Joho, P. Novák, M.E. Spahr[1]
*Safety aspects of graphite negative electrode
materials for lithium-ion batteries*
J. Electrochem. Soc. **149**, A1020-A1024 (2002).
[1]　TIMCAL Group, Bodio

M. Koebel, G. Madia, F. Raimondi, A. Wokaun
*Enhanced reoxidation of vanadia by NO_2 in the fast
SCR reaction*
J. Catal. **209**, 159-165 (2002).

T. Lippert, C. David, M. Hauer, T. Masubuchi[1],
H. Masuhara[1], K. Nomura[1], O. Nuyken[2], C. Phipps[3],
J. Robert[2], T. Tada[1], K. Tomita[1], A. Wokaun
Novel applications for laser ablation of photopolymers
Appl. Surf. Sci. **186**, 14-23 (2002).
[1]　Osaka University, Japan
[2]　TU München, Garching, Germany
[3]　Photonic Associates, Santa Fe, NM, USA

T. Lippert, J.T. Dickinson[1], M. Hauer, G. Kopitkovas,
S.C. Langford[1], H. Masuhara[2], O. Nuyken[3],
J. Robert[3], H. Salmio, T. Tada[2], K. Tomita[2],
A. Wokaun
*Polymers designed for laser ablation-influence of
photochemical properties*
Appl. Surf. Sci. **197-198**, 746-756 (2002).
[1]　Washington State University, Pullman, USA
[2]　Osaka University, Japan
[3]　TU München, Garching, Germany

T. Lippert, M. Hauer, C.R. Phipps[1], A. Wokaun
*Polymers designed for laser applications:
Fundamentals and applications*
SPIE Proc. **4760**, 63-71 (2002).
[1]　Photonic Associates, Santa Fe, NM, USA

G. Madia, M. Elsener, M. Koebel, F. Raimondi,
A. Wokaun
*Thermal stability of vanadia-tungsta-titania catalysts in
the SCR process*
Appl. Catal. B: Environmental **39**, 181-190 (2002).

M.J. Montenegro, M. Döbeli[1], T. Lippert, S. Müller,
B. Schnyder, A. Weidenkaff[2], P.R. Willmott[3],
A. Wokaun
*Pulsed laser deposition of $La_{0.6}Ca_{0.4}CoO_3$ (LCCO)
films. A promising metal-oxide catalyst for air based
batteries*
Phys. Chem. Chem. Phys. **4**, 2799-2805 (2002).
[1]　ETH Zürich and PSI
[2]　University of Augsburg, Germany
[3]　University of Zürich and PSI

M.J. Montenegro, Th. Lippert, S. Müller,
A. Weidenkaff[1], P.R. Willmott[2], A. Wokaun
*Pulsed laser deposition of electrochemically active
perovskite films*
Appl. Surf. Sci. **197-198**, 505-511 (2002).
[1]　University of Augsburg, Germany
[2]　University of Zürich and PSI

U.A. Paulus, A. Wokaun, G.G. Scherer, T.J. Schmidt,
V. Stamenkovic[1], V. Radmilovic[1], N.M. Markovic[1],
P.N. Ross[1]
*Oxygen reduction on carbon-supported Pt-Ni and Pt-
Co alloy catalysts*
J. Phys. Chem. B **106**, 4181-4191 (2002).
[1]　Lawrence Berkeley National Laboratory, CA, USA

U.A. Paulus, A. Wokaun, G.G. Scherer, T.J. Schmidt,
V. Stamenkovic[1], N.M. Markovic[1], P.N. Ross[1]
*Oxygen reduction on high surface area Pt-based alloy
catalysts in comparison to well defined smooth bulk
alloy electrodes*
Electrochim. Acta **47**, 3787-3798 (2002).
[1]　Lawrence Berkeley National Laboratory, CA, USA

C.R. Phipps[1], J.R. Luke[2], G.G. McDuff[2], T. Lippert
Laser ablation powered mini-thruster
SPIE Proc. **4760**, 833-842 (2002).
[1] Photonic Associates, Santa Fe, NM, USA
[2] University of New Mexico, Albuquerque, USA

F. Raimondi, K. Geissler, J. Wambach, A. Wokaun
Hydrogen production by methanol reforming: Post-reaction characterisation of a Cu/ZnO/Al$_2$O$_3$ catalyst by XPS and TPD
Appl. Surf. Sci. **189**, 59-71 (2002).

R. Richner, S. Müller, M. Bärtschi, R. Kötz, A. Wokaun
Physically and chemically bonded carbonaceous material for double-layer capacitor applications
New Materials for Electrochemical Systems **5.3**, 297-304 (2002).

B. Schnyder, R. Kötz, D. Alliata[1], P. Facci[1]
Comparison of the self-chemisorption of azurin on gold and on oxygen-terminated surfaces
Surf. Interface Anal. **34**, 40-44 (2002).
[1] Università di Modena e Reggio Emilia, Italy

M.E. Spahr[1], H. Wilhelm[1], F. Joho, J.-C. Panitz, J. Wambach, P. Novák, N. Dupont-Pavlovsky[2]
Characterization and electrochemical properties of purely hexagonal graphite and the influence of surface modifications on its electrochemical lithium insertion properties
J. Electrochem. Soc. **149**, A960-A966 (2002).
[1] TIMCAL Group, Bodio
[2] University of Nancy I, France

J. Wambach, A. Wokaun, A. Hiltpold
Oxidation of stainless steel under dry and aqueous conditions: Oxidation behaviour and composition
Surf. Interface Anal. **34**, 164-170 (2002).

A. Weidenkaff[1], S.G. Ebbinghaus[1], T. Lippert, M.J. Montenegro, A. Reller[1]
Carbon nanotube-perovskite-composites as new electrode material
MRS Proc. **730**, V7.2.1-V7.2.5 (2002).
[1] University of Augsburg, Germany

A. Weidenkaff[1], S.G. Ebbinghaus[1], T. Lippert
Ln$_{1-x}$A$_x$CoO$_3$ (Ln = Er, La) (A= Ca, Sr) / carbon nanotube composite materials applied for rechargeable Zn/air batteries
Chem. Mat. **14**, 1797-1805 (2002).
[1] University of Augsburg, Germany

Other Papers

B. Andreaus, G.G. Scherer
Connaissances approfondies des caractéristiques courant-tension des piles à combustible à membrane de polymère (PEFC) par l'application de la spectroscopie d'impédance (EIS)
Actes du 15$^{\text{ème}}$ Forum sur les Impédances Electrochimiques, Paris, France, December 9, 45-54 (2002).

M.C. Baertsch, P. Novák
Treatment and characterization of carbon-based materials for rechargeable lithium-ion batteries
53$^{\text{rd}}$ ISE Meeting, Düsseldorf, Germany, (Symposium 8), Book of Abstracts, 261 (2002).

K. Boulouchos, P. Dietrich, G.G. Scherer
Antriebsstrategien für eine umweltfreundliche Mobilität
Automobiltechniche Zeitschrift **104**, 632-641 (2002).

F.N. Büchi, A. Tsukada, P. Rodatz[1], O. Garcia[1], M. Ruge[1], R. Kötz, M. Bärtschi, P. Dietrich
Fuel cell-supercap hybrid electric powertrain
Proc. Fuel Cell World Conference, Luzern, July, 1-5, 218-231 (2002).
[1] ETH Zürich

F.N. Büchi, M. Ruge[1]
Development of 200cm^2 active area PEFC-stacks for application in a vehicle powertrain
Proc. "Energy and Electrochemical Process for a Cleaner Environment" Symposium, of the 200$^{\text{th}}$ Meeting of the Electrochemical Soc., PV 2001-23, 165-173 (2002).
[1] ETH Zürich

H. Buqa, D. Goers, M.E. Spahr[1], P. Novák
The influence of graphite surface modification on the exfoliation during electrochemical lithium insertion
Advanced Batteries and Accumulators – 3$^{\text{rd}}$ International Conference, Brno, Czech Republic, Extended Abstracts, 22-1 – 22-4 (2002).
[1] TIMCAL Group, Bodio

A.B. Geiger, A. Tsukada, A. Wokaun, G.G. Scherer, E. Lehmann, P. Vontobel
In situ investigation of the two-phase flow patterns in flow fields of polymer electrolyte fuel cells by neutron radiography and locally resolved current measurements
Abstracts, 2002 Fuel Cell Seminar, Palm Springs, USA, November 18-21, 125 (2002).

D. Goers, H. Buqa, P. Novák
Electrochemical characterization of heat treated graphite
Chimia **56**, 377 (2002).

D. Goers, H. Buqa, P. Novák
Raman spectroscopic study of heat-treated graphites for lithium-ion batteries
9$^{\text{th}}$ Euroconference on Ionics, Rhodes, Greece, Book of Abstracts, 59, 2002.

F. Hajbolouri, B. Andreaus, G.G. Scherer, A. Wokaun
Temperature dependence of CO-poisoning in a polymer electrolyte fuel cell
Abstracts, 2002 Fuel Cell Seminar, Palm Springs, USA, November 18-21, 251 (2002).

R. Kötz, S. Müller, M. Bärtschi, B. Schnyder,
P. Dietrich, F. N. Büchi, A. Tsukada, G. G. Scherer,
P. Rodatz[1], O. Garcia[1], P. Barrade[2], V. Hermann[3],
R. Gallay[3]
Supercapacitors for peak-power demand in fuel-cell-driven cars
Advanced Batteries and Supercapacitors, G. Nazri, R. Koetz, B. Scrosati, P. A. Moro, E. S. Takeuchi, Edts., The Electrochemical Society, Inc., Pennington, NJ, USA, ECS Proc. PV 2001-21 (2002).
[1]   ETH Zürich
[2]   EPF Lausanne
[3]   montena components SA, Rossens

R. Kötz
Doppelschichtkondensatoren – Technik, Kosten, Perspektiven
Siebentes Kasseler Symposium Energie-Systemtechnik, Erneuerbare Energien und rationelle Energieverwendung, Energiespeicher und Energietransport, ISET e.V.,Tagungsband 138-149 (2002).

R. Kötz, M. Bärtschi, F. Büchi, R. Gallay[1], Ph. Dietrich
HY.POWER – A Fuel Cell Car Boosted with Supercapacitors
Proc. 12th International Seminar on Double Layer Capacitors and Similar Energy Storage Devices, Deerfield Beach, USA, December 9–11 (2002).
[1]   montena components SA, Rossens

P. Novák, J. Vetter
Structure and composition of the solid electrolyte interphase layer on carbon electrodes in lithium-ion batteries
43rd Battery Symposium in Japan, Book of Abstracts, Fukuoka, Japan, Abstract No. 1l07, 14-15 (2002).

U.A. Paulus, C. Draschil, T.J. Schmidt,
V. Stamenkovic[1], N.M. Markovic[1], P.N. Ross[1],
G.G. Scherer, A. Wokaun
Oxygen reduction activity of Pt and Pt-alloy catalysts: A comparison between kinetic measurements and polymer electrolyte fuel cell experiments
Abstracts, 2002 Fuel Cell Seminar, Palm Springs, USA, November 18–21, 742 (2002).
[1]   Lawrence Berkeley National Laboratory, CA, USA

A. Schneuwly[1], M. Bärtschi, V. Hermann[1],
G. Sartorelli[1], R. Gallay[1], R. Kötz
BOOSTCAP double-layer capacitors for peak power automotive applications
Advanced Automotive Batteries Conference, Las Vegas, USA, February (2002).
[1]   montena components SA, Rossens

M.E. Spahr[1], H. Wilhelm[1], D. Goers, F. Joho,
P. Novák
The role of graphite surface group chemistry on the graphite exfoliation during electrochemical lithium insertion
11th Int. Meeting on Lithium Batteries, Meeting Abstracts, Monterey CA, USA, Abstract No. 231 (2002).
[1]   TIMCAL Group, Bodio

J. Vetter, P. Novák
Novel alkyl methyl carbonate solvents for lithium-ion batteries
11th Int. Meeting on Lithium Batteries, Meeting Abstracts, Monterey CA, USA, Abstract No. 193 (2002).

A. Würsig, D. Goers, P. Novák
In situ investigation of interface reactions between different electrolyte solutions and electrode materials for lithium-ion batteries
Chimia **56**, 382 (2002).

TALKS

Invited Talks

F.N. Büchi
Locally resolved current measurements in PE fuel cells of technical size
Chemistry Department, Princeton University, NJ, USA, May, 17, 2002.

F.N. Büchi
Fuel cell-supercap hybrid electric powertrain
The Fuel Cell World, Luzern, July, 4, 2002.

F.N. Büchi
Series of 5 talks on state of PE fuel cell technology in Europe and research at PSI
Korea Institute of Science and Technology, Seoul, South Korea, August 26-29, 2002.

F.N. Büchi
Entwicklung eines PEM-Brennstoffzellensystems für einen hybriden Fahrzeugantrieb
-   Elektrotechnisches Institut, TU Karlsruhe, Germany, November 18, 2002.
-   Energiewirtschaftliches Seminar, TU München, Germany, December 2, 2002.

F.N. Büchi
HY.POWER – Ein Brennstoffzellenfahrzeug als Technologieplattform
Swiss Computer Graphics Association, Zürich, December 4, 2002.

B. Gupta[1], J. Hilborn[2], G.G. Scherer, N. Anjum[1]
Designing polymers & textiles for developing tailored materials
Paper in the International Conference on 'Polymers & Textiles in the New Millenium - An Integral Approach' , IIT New Delhi, India, February 15-16, 2002.
[1] Indian Intitute of Technology, New Dehli, India
[2] Uppsala University, Sweden

R. Kötz
Electrochemical double-layer capacitors: Fundamental principles and state of the art
GDCh-Kolloquium, Institut für Anorganische Chemie, Universität Regensburg, Germany, April 15, 2002.

R. Kötz
Supercapacitors – bringing dynamic to batteries and fuel cell systems
Battery and Fuel Cell Components Workshop, OMG, Hanau, Germany, August 13-16, 2002.

R. Kötz
Doppelschichtkondensatoren – Technik, Kosten, Perspektiven
Siebentes Kasseler Symposium Energie-Systemtechnik, Erneuerbare Energien und rationelle Energieverwendung, Energiespeicher und Energietransport. Institut für Solare Energieversorgungstechnik, Gesamthochschule, Kassel, Germany, November 14-15, 2002.

T. Lippert
Polymers designed for laser applications: Fundamentals and applications
– Plenary session talk at the SPIE Symposium on High power laser ablation, Taos, USA, April 2002,
– Los Alamos National Laboratory, USA, April 2002,
– Bundesanstalt für Materialforschung, Berlin, Germany, June 2002.

T. Lippert
Laser ablation applied for direct structuring, thin film deposition and emission spectroscopy
Lehrstuhl für Lasertechnik, Rheinisch Westfälische Hochschule Aachen, Germany, July 2002.

T. Lippert
Massgeschneiderte Polymere: Vom Laser-Mikro-Thruster zur nichtlinearen Optik
Brandenburgische Technische Universität Cottbus, Germany, July 2002.

T. Lippert
Laser Ablation Applied for Direct Structuring, Thin Film Deposition and Emission Spectroscopy
Brandenburgische Technische Universitaet Cottbus, July 2002.

P. Novák
Materials aspects of lithium-ion batteries
Colloquium of the Laboratory for Inorganic Chemistry, ETH Zürich, November 26, 2002.

P. Novák
Structure and composition of the solid electrolyte interphase layer on carbon electrodes in lithium-ion batteries
43rd Battery Symposium in Japan, Fukuoka, Japan, October 12, 2002.

P. Novák
Electrochemistry of graphite for lithium batteries
Ernest Orlando Lawrence Berkeley National Laboratory, Berkeley CA, USA, July 12, 2002.

G.G. Scherer
Brennstoffzellentechnologie – Eine kritische Einschätzung ihrer Möglichkeiten
Institut für Energiewirtschaft der Technischen Universität München, Germany, January 14, 2002.

G.G. Scherer
Polymerelektrolyt Brennstoffzellen – Forschungs- und Entwicklungsaktivitäten am Paul Scherrer Institut
BASF AG, Ludwigshafen, Germany, February 1, 2002.

G.G. Scherer, B. Andreaus, F. Büchi
Proton conducting polymers in fuel cells – humidification aspects
Max-Planck-Gesellschaft, International Workshop on Proton Transport and Proton Transfer, Schloss Ringberg, Germany, March 3-8, 2002.

G.G. Scherer
Brennstoffzellen – Entwicklungsstand und Herausforderungen
Celle a combustibile e turbine a gas, Elettricità Svizzera Italiana, Bellinzona, April 18, 2002.

G.G. Scherer, T.J. Schmidt, K. Simbeck, A. Geiger, T. Rager, F. Geiger, J. Huslage, H.-P. Brack, B. Gupta
Strahlengepfropfte Membranen für H_2- und Methanol Brennstoffzellen – Präparation, ex situ und in situ Charakterisierung
72. Seminar der Arbeits-Gemeinschaft Elektro-chemischer Forschungsinstitutionen e.V., "Grundlagenuntersuchungen und neue Entwicklungen von Brennstoffzellen-Membranen", Forschungs-zentrum Jülich, Germany, December 4, 2002.

T.J. Schmidt
Introduction to fuel cell technology
Vortrag im Rahmen der Lehrveranstaltung Energiesysteme, Georg-Simon-Ohm Fachhochschule Nürnberg, Germany, April 24, 2002.

Other Talks

B. Andreaus
– *Experimental evidence of humidification effects in PEFCs*
– *Modelling CO-tolerance on the basis of impedance spectroscopy*
Joint PSI-FZJ-ICL workshop on modelling of PEFCs, PSI Villigen, June 11-12, 2002.

M.C. Baertsch
Treatment and characterization of carbon-based materials for rechargeable lithium-ion batteries
53rd Annual Meeting of the ISE, Düsseldorf, Germany, September 15-20, 2002.

M. Bärtschi, R. Kötz, P. Dietrich
Supercapacitor Module for a Hybrid Drivetrain
53rd Annual Meeting of the ISE, Düsseldorf, Germany, September 15-20, 2002.

F.N. Büchi
Locally resolved current measurements in 200 cm^2 PEM fuel cells
201st Meeting of the Electrochemical Soc., Philadelphia, PA, USA, May 12-16, 2002.

H. Buqa
The influence of graphite surface modification on the exfoliation during electrochemical lithium insertion
3rd ABA International Conference, Brno, Czech Republic 2002.

A.B. Geiger
In situ diagnostic tools for mass transfer characterization
Joint PSI-FZJ-ICL workshop on modelling of PEFCs, PSI Villigen, June 11-12, 2002
D. Goers
Raman spectroscopic study of heat-treated graphites for lithium-ion batteries
9th Euroconference on Ionics, Rhodes, Greece, 2002.

R. Kötz, M. Bärtschi, F. Büchi, R. Gallay[1], Ph. Dietrich
HY.POWER – a fuel cell car boosted with supercapacitors
12th International Seminar on Double Layer Capacitors and Similar Energy Storage Devices, Deerfield Beach, USA, December 9–11, 2002.
[1]   montena components SA, Rossens

G. Kopitkovas, T. Lippert, C. David, A. Wokaun, J. Gobrecht
Fabrication of microoptical elements in quartz by laser induced backside wet etching
Micro- and Nanoengineering 2002 International Conference, Lugano, September 2002.

T. Lippert, M. Hauer, D. J. Funk[1], A. Wokaun
Laser ablation of a triazene polymer studied by ns-interferometry and shadowgraphy
SPIE Symposium on High power laser ablation, Taos, USA, April 2002.
[1]   Los Alamos National Laboratory, USA

T. Lippert, M.J. Montenegro, S. Mueller, A. Weidenkaff[1], P. Willmott[2], A. Wokaun
Analysis of the plasma produced by pulsed reactive crossed-beam laser ablation of $La_{0.6}Ca_{0.4}CoO_3$
E-MRS symposium physics and chemistry of advanced laser materials processing, Strasbourg France, June 2002.
[1]   University of Augsburg, Germany
[2]   University of Zürich and PSI

D. Schmid[1], M. Santis, M. Ruge[1], F.N. Büchi
Presentation of PowerPac Project
–   Fuel Cell 2002, Luzern, July 1-5, 2002;
–   REACH for process solutions, Basel, October 15-18, 2002.
[1]   ETH Zürich

T.J. Schmidt
Oxygen electrocatalyst for PEFC's
Joint PSI-FZJ-ICL workshop on modelling of PEFCs, PSI Villigen, June 11-12, 2002.

T.J. Schmidt, N. Lempola, U.A. Paulus, G.G. Scherer, A. Wokaun, N.M. Markovic[1], P.N. Ross[1]
Advances in oxygen reduction reaction electrocatalysis
4th Symposium on Electrocatalysis, Como, Italy, September 22-26, 2002.
[1]   Lawrence Berkeley National Laboratory, CA, USA

POSTERS

T. Akiyama[1], V. Auger[1], B. Ballesteros-Katemann[2], F. Campana, N. Eichenberger[3], M. Koudelka-Hep[1], N. F. de Rooij[1], W. Schuhmann[2], H. Siegenthaler[3]
Microfabricated scanning probes for electrolytic STM and SECM
53rd Annual Meeting of the ISE, Düsseldorf, Germany, September 15-20, 2002.
[1]   Universität Neuchâtel
[2]   Ruhr-Universität Bochum, Germany
[3]   Universität Bern

B. Andreaus, F. Hajbolouri, G.G. Scherer
Modelling the CO-tolerance of a polymer electrolyte fuel cell
53rd Annual Meeting of the International Society of Electrochemistry, Düsseldorf, Germany, September 15-20, 2002.

B. Andreaus, G.G. Scherer
Interprétation des caractéristiques courant-tension des piles à combustible à membranes de polymère par l'application de la spectroscopie d'impédance
15ème Forum sur les Impédances Electrochimiques, Paris, France, December 9, 2002.

F. Campana, R. Kötz, P. Novak, H. Siegenthaler[1], J. Vetter
In-situ SPM of the solid electrolyte interphase in lithium-ion batteries
Twannberg Workshop on Nanoscience 2002, September 30 – October 4, 2002.
[1]   Universität Bern

M. Hahn, R. Kötz, B. Schnyder, M. Bärtsch
Gas evolution upon self-discharge of double layer capacitors based on glassy carbon and sulphuric acid
53rd Annual Meeting of the ISE, Düsseldorf, Germany, September 15-20, 2002.

F. Hajbolouri, B. Andreaus, G.G. Scherer, A. Wokaun
Temperature dependence of CO-poisoning in a polymer electrolyte fuel cell
− 53rd Annual Meeting of the International Society of Electrochemistry, Düsseldorf, Germany, September 15-20, 2002;
− 2002 Fuel Cell Seminar, Palm Springs, USA, November 18-21, 2002;
− ETSF3, PSI Villigen, November 29, 2002.

F. Hajbolouri, B. Andreaus, G.G. Scherer, A. Wokaun
CO-tolerance in polymer electrolyte fuel cells
17. Tagessymposium, Elektrochemie, PSI, Villigen, September 11, 2002.

M. Hauer, J.T. Dickinson[1], D.J. Funk[2], S.C. Langford[1], T. Lippert, A. Wokaun
Indications for a photochemical ablation mechanism for a triazene polymer
XIXth IUPAC Symposium on Photochemistry, Budapest, Hungary, July 2002.
[1] Washington State University, Pullman, USA
[2] Los Alamos National Laboratory, USA

N. Lempola, T.J. Schmidt, G.G. Scherer, A. Wokaun
Development of catalyst for oxygen reduction reaction
4th International Conference on Electrocatalysis, Como, Italy, September 22-25, 2002.

T. Lippert, M. Hauer, D.J. Funk[1], A. Wokaun
Laser ablation of polymers studied by ns-interference and ns-shadowgraphy measurements
E-MRS symposium physics and chemsitry of advanced laser materials processing, Strasbourg France, June 2002.
[1] Los Alamos National Laboratory, USA

U.A. Paulus, C. Draschil, T.J. Schmidt, V. Stamenkovic[1], N.M. Markovic[1], P.N. Ross[1], G.G. Scherer, A. Wokaun
Oxygen reduction activity of Pt- and PtCo-alloy catalysts: A comparison between kinetic measurements and polymer electrolyte fuel cell experiments
8th Ulm ElectroChemical Talks (UECT), Neu-Ulm, Germany, June 20-21, 2002.
[1] Lawrence Berkeley National Laboratory, CA, USA

U.A. Paulus, E. Deiss, A. Wokaun, G.G. Scherer
Catalyst utilization at the electrode/polymer electrolyte interface: Development of a model system
8th Ulm ElectroChemical Talks (UECT), Neu-Ulm, Germany, June 20-21, 2002.

U.A. Paulus, C. Draschil, T.J. Schmidt, V. Stamenkovic[1], N.M. Markovic[1], P.N. Ross[1], A. Wokaun, G.G. Scherer
Oxygen reduction activity of Pt and Pt-alloy catalysts: A comparison between kinetic measurements and PEFC experiments
53rd Annual Meeting of the International Society of Electrochemistry jointly organized with GDCH-Fachgruppe Angewandte Elektrochemie, Düsseldorf, Germany, September 15-20, 2002.
[1] Lawrence Berkeley National Laboratory, CA, USA

U.A. Paulus, M. Kuhnke, E.E. Ortelli[1], E. Deiss, A. Wokaun, T. Lippert, G.G. Scherer
Catalyst utilization at the electrode/polymer electrolyte interface: Development of a model system and impact on the design of a miniaturized fuel cell
53rd Annual Meeting of the International Society of Electrochemistry jointly organized with GDCH-Fachgruppe Angewandte Elektrochemie, Düsseldorf, Germany, September 15-20, 2002.
[1] Dyconex AG, Bassersdorf

U.A. Paulus, C. Draschil, T.J. Schmidt[1], V. Stamenkovic[1], N.M. Markovic[1], P.N. Ross[1], A. Wokaun, G.G. Scherer
Oxygen reduction activity of Pt and Pt-alloy catalysts: A comparison between kinetic measurements and PEFC experiments
2002 Fuel Cell Seminar, Palm Springs, CA, USA, November 18-21, 2002.
[1] Lawrence Berkeley National Laboratory, CA, USA

F. Raimondi, B. Schnyder, R. Kötz, R. Schelldorfer, T. Jung, J. Wambach, A. Wokaun
Structural changes of model Cu/ZnO catalysts during exposure to methanol reforming conditions
Nano-7/ECOSS-21, Malmö, Sweden, June 24–28, 2002.

T.J. Schmidt, K. Simbeck, T. Rager, G.G. Scherer
Evaluation of radiation-grafted FEP membranes in H_2-O_2 PEFCs
Gordon Research Conference on Fuel Cells, Bristol, RI, USA, July 26 – August 2, 2002.

T.J. Schmidt, K. Simbeck, T. Rager, G.G. Scherer
Performance of potentially low-cost radiation grafted membranes in H_2-O_2 PEFC
17. Tagessymposium, Elektrochemie, PSI, Villigen, September 11, 2002.

T.J. Schmidt, K. Simbeck, T. Rager, G.G. Scherer
Performance of potentially low-cost radiation grafted membranes in H_2-O_2 PEFC
ETSF3, PSI Villigen, November 29, 2002.

B. Schnyder, T. Lippert, R. Kötz, A. Wokaun,
V.-M. Graubner[1], O. Nuyken[1]
*UV-irradiation induced modification of PDMS films
investigated by XPS and spectroscopic ellipsometry*
Nano-7/ECOSS-21; Malmö, Sweden, June 24–28,
2002.
[1] TU München, Germany

A. Tsukada, P. Rodatz[1], G. Paganelli[1], F.N. Büchi
*Efficiency improvements by pulsed hydrogen supply in
polymer electrolyte fuel cell systems*
Grove Fuel Cell Symposium: FUEL CELLS, Science
and Technology 2002, Amsterdam, The Netherlands,
September 25-26, 2002.
[1] ETH Zürich

PATENT APPLICATIONS

V. Hennige[1], G. Hörpel[1], Ch. Hying[1], P. Novák,
J. Vetter
*Separator mit asymetrischem Porengefüge für eine
elektrochemische Zelle*
Europäische Patentanmeldung, DE 10255121.9,
2002.
[1] CREAVIS GmbH, Marl, Germany

V. Hennige[1], G. Hörpel[1], Ch. Hying[1], P. Novák,
J. Vetter
*Langzeitstabiler Separator für eine elektrochemische
Zelle*
Europäische Patentanmeldung, DE 10255122.7,
2002.
[1] CREAVIS GmbH, Marl, Germany

J. Huslage, T. Rager
*Verfahren zur Herstellung von Propfcopolymeren
durch radikalische Polymerisation*
German Patent Application, DE 101 08 598 A1,
September 5, 2002.

M. Ruge[1], D. Schmid[1], F.N. Büchi
*Verfahren und Vorrichtung zur Befeuchtung der
Membran einer Brennstoffzelle*
Swiss Patent Application Nr. 2002 1031/02, June 17,
2002.
[1] ETH Zürich

CK Shin[1], G. Maier[1], G.G. Scherer
*A block copolymer for use as a solid polymer
electrolyte, an ion conductive membrane made from a
block copolymer and methods of making a block
copolymer*
Europäische Patentanmeldung, DE 10258175.4,
December 12, 2002
[1] TU München, Germany

MEMBERSHIPS IN EXTERNAL COMMITTEES

P. Novák
International Society of Electrochmistry
Member of Executive Committee (Treasurer) and
Council

G.G. Scherer
Neuartige Schichtstrukturen für Brennstoffzellen
Deutsche Forschungsgemeinschaft, Mitglied der
Prüfungsgruppe für das Schwerpunktprogramm

G.G. Scherer
European Fuel Cell Forum
Member, Advisory Board

G.G: Scherer
Fuel Cell Handbook
Advisory Board

G.G. Scherer
*Beirat Forschungsallianz Brennstoffzellen Baden
Württemberg, Germany*
Deputy Speaker

G.G. Scherer
*7th International Seminar on Electrochemical Science
and Technology (ISAEST VII)*
Member, Scientific Advisory Board

G.G. Scherer
*International Conference on 'Polymers & Textiles in
the New Millenium - An Integral Approach'*
Member, Scientific Advisory Board

G.G. Scherer
*Maturitätsprüfungskommission der Kantonsschulen
Baden und Wohlen*
Mitglied

THE LABORATORY FOR ELECTROCHEMISTRY

STRUCTURE

Laboratory for Electrochemistry

G.G. Scherer   (head)
I. Kalt   (secretary)

Fuel Cells
G.G. Scherer
Clean Energy Conversion
with high efficiency
Optimized components
and cells

Batteries
P. Novak
High energy density
Compact 4V cells

Capacitors
R. Kötz
High power density
complementary
storage device
High capacitance and
cycle life

Materials I
Th. Lippert
Design of functional materials
Fundamental under-standing
of interfacial processes

Materials II
H-P. Brack
Preparation &
characterization of functional
materials (polymers, polymer
membranes, sol-gel)

Fuel Cell Systems
F. Büchi
Optimisation of system
efficiency
Novel stack concepts

Interface Analysis
R. Kötz
In situ and ex situ
characterization of the
electrochemical interface

LEC-PERSONNEL

Staff

Andreaus Bernhard, Dr. (since July, 2002), **A**rcaro Manual (since March 2002), **B**ärtsch Martin, Dr., **B**ärtschi Martin, **B**rack Hans-Peter, Dr. (since May, 2002), **B**üchi Felix, Dr., **B**uqa Hilmi, Dr. (since January, 2002), **D**eiss Erich, Dr., **G**eiger Friederike, **G**ubler Lorenz, Dr. (since November, 2002), **H**ahn Matthias, Dr., **H**ottinger Peter, **K**aiser Hermann, **K**alt Isabella, **K**ötz Rüdiger, Dr., **L**ippert Thomas, Dr., **M**army Christian, **N**ovák Petr, Dr., **P**anozzo Roberto, **P**eter Sandra (since January, 2002), **R**ager Timo, Dr. (until October, 2002), **R**ichner Roy, Dr., **S**auter Jean-Claude, **S**cheifele Werner, **S**cherer Günther G., Dr., **S**chmidt Thomas, Dr. (until September, 2002), **S**chnyder Bernhard, Dr., **S**teiger Beat, Dr., **S**tössel-Sittig Caroline Dr. (since May, 2002), **T**sukada Akinori, **V**etter Jens, Dr., **W**ambach Jörg, Dr.

PhD Students

Andreaus Bernhard (until June, 2002), **C**ampana Flavio, **D**umont Thomas, **G**eiger Arne (until November, 2002), **G**oers Dietrich, **H**ajbolouri Faegheh, **H**auerc Marc, **K**opitkovas Giedrius, **K**ramer Denis (since June, 2002), **K**uhn Holger (since June, 2002), **K**uhnke Markus, **L**empola Nina, **M**ontenegro Macarena, **P**aulus Ursula (until September, 2002), **P**iotto Piotto Andrea, **R**aimondi Fabio (until November 2002), **S**antis Marco (since May, 2002), **S**laski Michal (since November, 2002), **S**teuernagel Leif (until October, 2002), **W**immer Jean, **W**ürsig Andreas (since January, 2002)

HABILITATION

THOMAS LIPPERT, DR.

ETH Zürich, May 13, 2002

Work on:

*Photopolymers designed for laser ablation, ablation mechanisms and applications*

AWARDS

L. Gubler
Operating polymer electrolyte fuel cells with reformed fuel
ETH-Medaille
Doktorarbeit, ETH Zürich, 2002.

D. Schmid[1], M. Santis, M. Ruge[1], F.N. Büchi
PowerPac Projekt
2. Platz, Internationaler Umweltpreis REACH 2002.
[1] ETH Zürich

THESE PHD STUDENTS FROM LEC GRADUATED IN 2002

Dr. Bernhard Andreaus

Title of thesis:

Die Polymer-Elektrolyt Brennstoffzelle: Charakterisierung ausgewählter Phänomene durch elektrochemische Impedanzspektroskopie

Advisor at university:	Prof. M. Grätzel, EPFL
	Dr. A. McEvoy, EPFL
Advisor at PSI:	Prof. A. Wokaun
	Dr. G.G. Scherer
Date of oral examen:	June 10, 2002
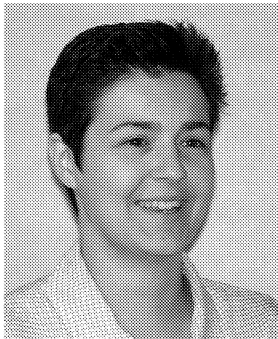
Dr. Ursula Agnes Paulus

Title of thesis:

Electrocatalysis for Polymer Electrolyte Fuel Cells: Metal Alloys and Model Systems

Advisor at PSI	Prof. A. Wokaun
	Dr. G.G. Scherer
Date of oral examen:	September 25, 2002
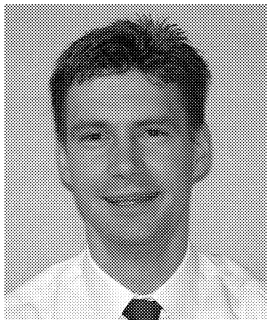
Dr. Arne Björn Geiger

Title of thesis:

Characterization and development of direct dethanol fuel cells

Adviser at PSI	Prof. A. Wokaun
	Dr. G.G. Scherer
Date of oral examen:	October 30, 2002
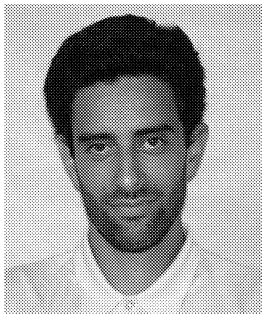
Dr. Fabio Raimondi

Title of thesis:

Structural Modifications of Cu/ZnO-based Commercial and Model Catalysts during Methanol Reforming

Adviser at PSI	Prof. A. Wokaun
	Dr. J. Wambach
Date of oral examen:	December 17, 2002

DIPLOMA THESES, SUMMER STUDENTS

F. Campana
In situ STM-Untersuchungen an polykristallinen Pt-Electroden
Universität Bern, December 14, 2001.

S.A. Freunberger
Wasserhaushalt und Leistungsverhalten von Polymer-Elektrolyt Brennstoffzellen technischer Relevanz
Technische Universität Wien, AT, April – October 2002.

M. Gisiger
Optimierung der Betriebsparameter von Direktmethanol-Brennstoffzellen
Fachhochschule beider Basel FHBB, February 2002.

R. Picenoni
Charakterisierung neuartiger Polymermembranen für Direktmethanol-Brennstoffzellen
Fachhochschule beider Basel FHBB, February 2002.

K. Simbeck
Charakterisierung von strahlengepfropften protonen-leitenden Membranen in H_2/O_2-Polymerelektrolyt-Brennstoffzellen
Georg Simon-Ohm Fachhochschule Nürnberg, DE, November 2001 – April 2002.

A. Vigueras-Rodriguez
Modelling of Supercapacitor Behaviour
Universidad Polytechnica De Cartagena, ES, July – October, 2002

D. Stuber
Einfluss der Flussfeldgeometrie von Kleinzellen ($30cm^2$) auf das Leistungsverhalten von DMFC
Kantonsschule Zug, July, 2002

S.Reich
Proton Conducting Membranes
Technische Universität Clausthal, DE, August – October, 2002

L. Hardwick
In situ Spectroelectrochemical Characterization of the Electrode/Electrolyte Interfaces in Lithium-Ion Batteries (Raman Microscopy)
University of Southampton, UK, August – December, 2002

SEMINAR, INVITED SPEAKERS

Dr. Martin Ruge, ETH Zürich
Methodisches Vorgehen im Entwicklungsprozess
March 18, 2002.

Dr. Albert Rössler, ETH Zürich
Blue Jeans und Elektrochemie? – Umweltfreundliches Färben von Textilien mit Hilfe elektrochemischer Verfahren
September 30, 2002.

Dr. Carsten J. Winnewisser, Centre Suisse de Electronique et de Microtechnique (CSEM), Zürich
Polymer Optoelectronics at CSEM
November 11, 2002.

Dr. Hermann Pütter, BASF Ludwigshafen, DE
Green is not enough – Umwelt und chemische Innovationen: Beispiele aus der Elektrochemie
November 28, 2002.

CONFERENCES – WORKSHOPS

Celebratory-Colloquium 60th Birthday of Dr. Otto Haas
January 23, 2002
Organisers: G.G. Scherer, A. Wokaun

With contributions from:

Prof. Dr. Meinrad Eberle, PSI
Prof. Dr. Peter Suter, Thal,
Dr. Peter Kesselring, Urdorf,
Prof. Dr. Louis Schlapbach, EMPA Dübendorf,
Prof. Dr. Ulrich Stimming, Technische Universität München, DE
Prof. Dr. Alexander Wokaun, PSI

Modelling of Polymer Electrolyte Fuel Cells
Joint Workshop: PSI – Research Center, Jülich (FZJ), DE – Imperial College, London, UK
June 11 & 12, 2002
Organiser: G.G. Scherer

With contributions from:

Dr. Bernhard Andreaus, PSI
Dr. Eckhard Spohr, Forschungszentrum Jülich, DE
Dr. Thomas Schmidt, PSI
Dr. Anthony Kucernak, Imperial College, London, GB
Prof. Enn Lust, University of Tartu, EE
Prof. Dr. Alexei Kornyshev, Forschungszentrum Jülich, DE
Mr. Stefan Salchenegger, Montanuniversität Leoben, AT
Mr. Wilhelm Brandstetter, Montanuniversität Leoben, AT
Dr. Andrei Kulikovsky, Forschungszentrum Jülich, DE
Dr. Arne Geiger, PSI
Dr. Felix Büchi, PSI
Dr. Ioannis Mantzaras, PSI
Dr. Günther G. Scherer, PSI

Carbons for Electrochemical Applications
17th One-Day-Symposium
September 11, 2002
Organisers: G.G. Scherer, R. Kötz

With contributions from:

Prof. Dr. Jürgen O. Besenhard, Technical University of Graz, AT
Dr. Francis Fischer, ex Timcal, Sins
Dr. Andreas Züttel, University of Fribourg
Dr. Thomas Lehmann, Infracor GmbH, Marl, DE
Dr. Michael E. Spahr, Timcal SA, Bodio
Dr. Margriet Reimerink, Norit, Amersfoort, NL
Dr. Joachim Köhler, OMG AG, Hanau, DE
Dr. Norbert Berg, SGL Technologies GmbH, Meitingen, DE

Fuel Cells and Combustion Engines in Competition for the Future
ETSF 3, November 29, 2002
Organisers: A. Wokaun, P. Dietrich, K. Boulouchos, G.G. Scherer

With contributions from:

Prof. Dr. Alexander Wokaun, PSI
Mr. Hans-Ulrich Schärer, Bundesamt für Energie BFE, Bern
Mr. Jörg Schindler, L-B-Systemtechnik GmbH, Ottobrunn, DE
Prof. Dr. Michael Bargende, Universität Stuttgart, DE
Dr. Philipp Dietrich, PSI
Mr. Hermann Kabs, Siemens AG, Erlangen, DE
Prof. Dr. Konstantinos Boulouchos, ETH Zürich and PSI
Prof. Dr. Eberhard Jochem, CEPE-ETH Zürich and FH-ISI Karlsruhe, DE
Prof. Dr. Ralph Eichler, PSI

REVIEW ACTIVITIES OF THE LABORATORY
FOR FOLLOWING JOURNALS

Analytical and **B**ioanalytical Chemistry, **A**pplied Surface Science, **C**hemical Communications, **C**hemistry of Materials, **E**lectrochemica Acta, **E**lectrochemical and Solid State Letters, **E**lectrochemistry Communications, **J**ournal of Materials Chemistry, **J**ournal of Materials Research, **J**ournal of Electrochemical Society, **J**ournal of Physical Chemistry, **J**ournal of Power Sources, **J**ournal of Solid State Electrochemistry, **L**angmuir, **M**acromolecular Materials and Engineering, **M**icroelectronic Engineering, **N**ature Materials, **P**hysChemComm, **P**hysical Chemistry Chemical Physics, **P**olymer, **P**olymer International, **P**rogress in Surface Science, **S**olid State Ionics.

REVIEW ACTIVITIES OF THE LABORATORY
FOR THE FOLLOWING ORGANISATIONS

Alexander von Humboldt-Stiftung, DE, **A**lliance for Global Sustainability, **D**eutsche Forschungsgemeinschaft, **M**istra (Swedish Environmental Research Fund), **P**aul Scherrer Institut (Forschungskommission), **R**oyal Society of Chemistry, UK, **S**imon Fraser University, CA.

CO-REFEREE'S REPORT FOR DISSERTATIONS

Bernhard **A**ndreaus, EPF Lausanne, Arne **G**eiger ETH Zürich, Ursula **P**aulus ETH Zürich, Roland **W**idmer, University of Bern.

PAUL SCHERRER INSTITUT

PSI

GENERAL ENERGY
LABORATORY FOR ELECTROCHEMISTRY